République Algérienne Démocratique et Populaire

Ministère de l'Enseignement Supérieur et de la Recherche Scientifique

Université Ibn Khaldoun de Tiaret

Faculté des Sciences Appliquées

Département de Génie Mécanique

Laboratoire de Recherche des Technologies Industrielles

THÈSE

Pour l'obtention du diplôme de
Doctorat 3ème cycle LMD

Domaine : Sciences et Technologie
Filière : Génie Mécanique
Spécialité : Énergétique

Thème

Etude numérique de la convection mixte dans les enceintes lors de l'écoulement d'un nanofluide

Présenté par :

M. SALEH Mo'men Sami Mohammad

Soutenue publiquement le 08/06/2023, devant le Jury composé de :

MM.

HADDOUCHE Kamel	Professeur (Université de Tiaret)	Président
KHERRIS Sahraoui	Professeur (Université de Tissemsilt)	Encadrant
MEKROUSSI Said	Professeur (Université de Tiaret)	Co-encadrant
SAD CHEMLOUL Nord-Eddine	Professeur (Université de Tiaret)	Examinateur
BEN MOUSSA Hocine	Professeur (Université de Batna)	Examinateur
BOUALI Belkacem	MCA (Université de Laghouat)	Examinateur

Année universitaire : 2022 – 2023

People's Democratic Republic of Algeria

Ministry of Higher Education and Scientific Research

Ibn Khaldun University of Tiaret

Faculty of Applied Sciences

Department of Mechanical Engineering

Research Laboratory of Industrial Technologies

THESIS

For the 3ʳᵈ cycle LMD Doctoral degree

Domain: Sciences and Technology
Major: Mechanical Engineering
Specialty: Energy

Thème

Numerical study of mixed convection in enclosures during the flow of a nanofluid

Presented by:

Mr. Mo'men Sami Mohammad Saleh

Publicly defended on 08/06/2023, in front of the Jury composed of:

Mrs.

Kamel Haddouche	Professor (University of Tiaret)	President
Sahraoui Kherris	Professor (University of Tissemsilt)	Supervisor
Said Mekroussi	Professor (University of Tiaret)	Co-supervisor
Nord-Eddine Sad Chemloul	Professor (University of Tiaret)	Examiner
Hocine Ben Moussa	Professor (University of Batna)	Examiner
Belkacem Bouali	Lecturer (University of Laghouat)	Examiner

Academic year: 2022 – 2023

Dedication

To my parents, who have always believed in me,

To my partner, who has been my rock throughout this journey,

To my friends, who have cheered me on every step of the way,

This thesis is for you.

Mo'men Sami Mohammad Saleh

Acknowledgments

I would like to express my sincere gratitude to my Supervisor Sahraoui Kherris for his invaluable guidance and support throughout my Ph.D. program. His expertise and encouragement helped me to complete this research and write this thesis.

I am deeply grateful to my Co-supervisor Said Mekroussi for his unwavering support and guidance throughout my Ph.D. program. His expertise and patience have been invaluable to me and have played a crucial role in the success of this thesis.

I extend my sincere thanks to all my esteemed Professors in the Department of Mechanical Engineering who spared no effort in directing me and providing me with what I needed throughout the study days in terms of books from their abundant libraries.

I would like to extend my sincere thanks to my esteemed Professors of the Jury for their kindness to me in accepting the discussion of this dissertation.

I would like to thank everyone who helped me and assisted me in the completion of this dissertation.

Summary

Chapter I: Bibliographic review

Chapter II: Generality on the thermal properties of nanofluids

Chapter III: Mathematical formulation of convective flow of nanofluids

Chapter IV: Results and discussion

List of figures

Chapter I: Bibliographic review

Chapter II: Generality on the thermal properties of nanofluids

Chapter III: Mathematical formulation of convective flows of nanofluids

Chapter IV: Results and discussion

List of tables

General introduction

"The beginning is always difficult"

General introduction

In light of technological and industrial development, which are developing significantly and continuously, heat transfer has become of great scientific and practical importance because it is involved in many fields despite its presence in several forms (conduction, convection, and radiation). Convection is the most targeted type because it has many forms (natural, forced, mixed convection) and it is of vital importance in areas of application such as air conditioning and heating in housing, refrigeration in thermophones, mechanical or electronic systems, fluid heating systems that include solar collectors, drying of agricultural food products, and heat exchangers; this heat transfer mode is related to fluids and gases.

Due to temperature variations caused by heat transfer between the wall and fluid; this last may move as a result of changes in its density. Forced convection occurs when an external force, such as fans or pumps, causes the fluid to move. In specialized engineering, the convective heat transfer may be increased by tweaking the shape, adding fins, using surface roughness, and modifying the physical characteristics of a fluid utilized in the cooling process researchers have given particular attention to the fundamental issue of heat transfer by natural, forced, and mixed convection in a cavity due to the prevalence of such challenges in several applications. Long-term usage of electronic devices causes components to overheat, degrade, or even explode and catch fire. Batteries, light-emitting diodes (LEDs), and microprocessors create heat during operation. In addition to lost energy, overheating may degrade the effectiveness and longevity of the devices. This made the necessity for increased fluid heat transmission, creating a new class of fluids known as nanofluids, which are solutions comprising nanoparticles suspended in a base fluid that may be employed in various industrial applications due to their qualities that increase thermal performances.

Objective of study:

This thesis aims to study and to model the heat transfer inside a nanofluid-filled cavity in order to cool the electronic components. Our study focused on explaining the effect of several parameters on heat tranfer, such as nanoparticles type and their volume fraction, Aspect Ratios of cavity, Richardson number, Grashof number, and the thermal amplitude. The numerical modeling of heat transmission in nanofluid-filled cavity was examined by altering a number of the aforementioned parameters with a sinusoidal temperature to identify the ideal size cavity and the

best nanofluid as a way to increase the heat transfer between the nanofluid (coolant) and the cavity walls in order to maintain the temperature of the electronic components.

Structure of the thesis:

This thesis is structured in four chapters:

❶ **The first chapter** will present various previous research studies over the years that examined convection heat transfer within cavities filled with different fluids and boundary conditions.

❶ **For the second chapter**, the types of nanofluids and their preparation techniques will be reported, as well as numerous models, which are created to calculate the thermophysical properties of multiple nanofluids.

❸ **The third chapter** including the mathematical formulation of convective flow of nanofluids. The fluid flow equations (continuity, momentum, and energy) and the accompanying assumptions are presented. Also, this chapter describes the numerical approach used for simulation (Finite Volume Method), the mesh choice, and the thermophysical properties of nanoparticles and base fluids used in the numerical simulation. The Ansys Workbench Fluent codes used in numerical simulation calculations are briefly discussed at the end of the chapter.

❹ **The fourth chapter** includes the results of this study; firstly, the chapter had the test of mesh, and secondly, validations of the developed code have been successfully carried out, and then the case of mixed convection flow is investigated in a cavity filled with several fluids to determine the current lines and isotherms, as well as the Nüsselt number for the different volume fraction of nanoparticles, Aspect Ratios, Richardson number, Grashof number, and the temperature amplitude.

The thesis is finished by summarizing the broad conclusions drawn from the instances examined and providing perspectives for the remaining work.
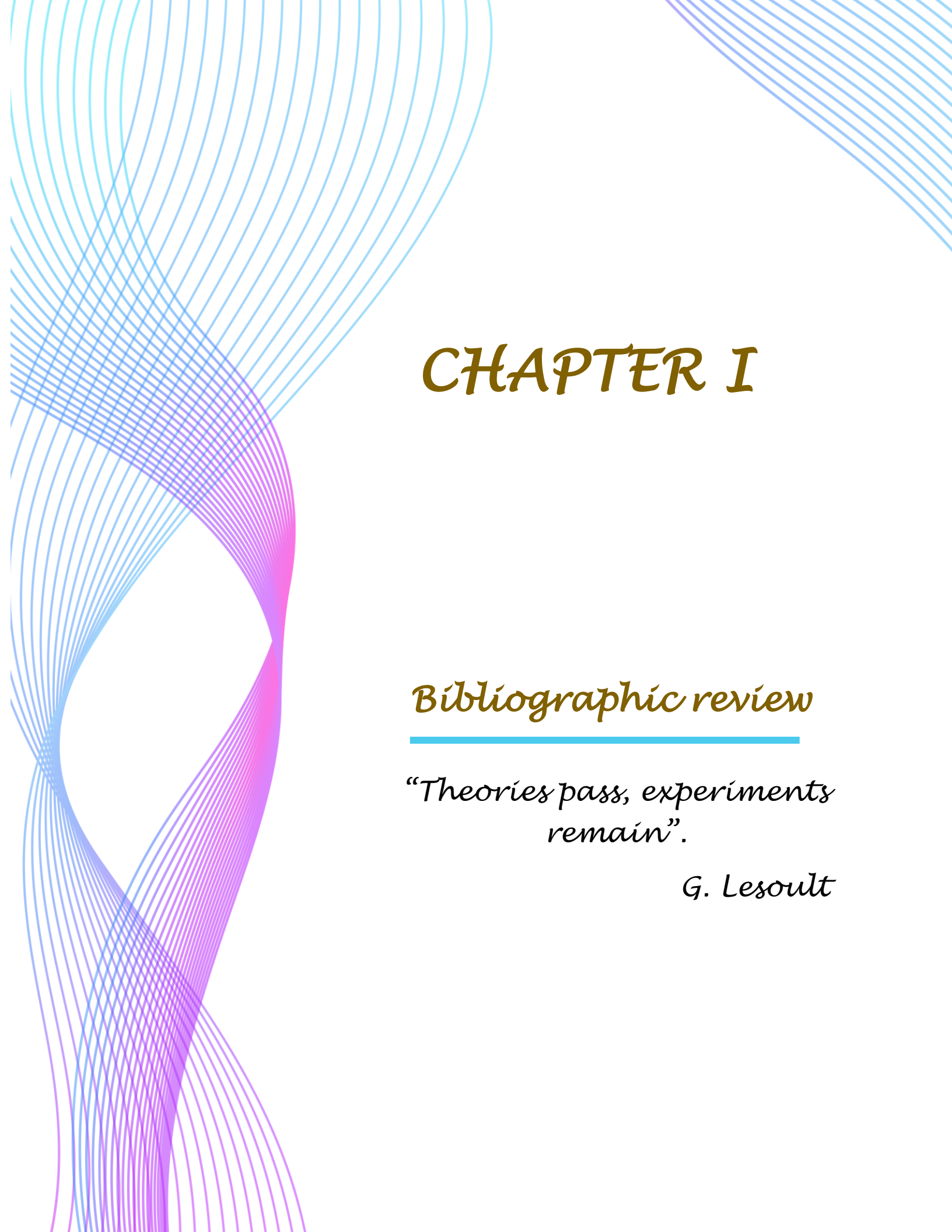
CHAPTER I

Bibliographic review

"*Theories pass, experiments remain*".

G. Lesoult

CHAPTER I

Bibliographic review

I.1. Introduction

The main problem of heat transfer by natural, forced, and mixed convection in a cavity has received significant attention from researchers because such problems are common in many engineering applications such as cooling electronic components, drying, heat transfer in solar ponds, etc. The necessity to improve heat transmission has led to the creation of a new class of fluids known as nanofluids, which are solutions comprising nanoparticles suspended in a base fluid that may be employed due to their qualities that increase thermal performances.

This chapter will present various previous research studies over the years that examined convection heat transfer within cavities filled with different fluids and boundary conditions.

I.2. Bibliographic synthesis on mixed convection in a cavity

The lid-driven cavity problem reveals many details about fundamental fluid physics. It has produced tremendous data and results because it is often used in numerical measurement. However, many questions remain and need to be further investigated. Due to the importance of cavities in many different industrial applications, the scenario of stability and transition in constrained systems remains a significant concern.

The current development of nanoscience is due to the presentation of the specific properties of matter with nanoscale dimensions. This has sparked new fields of study in a large number of laboratories, and this has enabled the development of nanofluids with original properties in heat transfer. The development of nanoparticles and their addition to pure fluids as nanofluids has improved heat transfer if it is related to cooling or heating in many engineering fields. There are many previous studies and different research work due to the different thermal conditions.

In this part, we provide theoretical and experimental studies of heat transfer by convection in nanofluids from their discovery to this day. Also, researchers paid great attention to nanofluids in the latter part of the twentieth century, which is illustrated in Figure I.1 as the number of published annual research is constantly increasing.
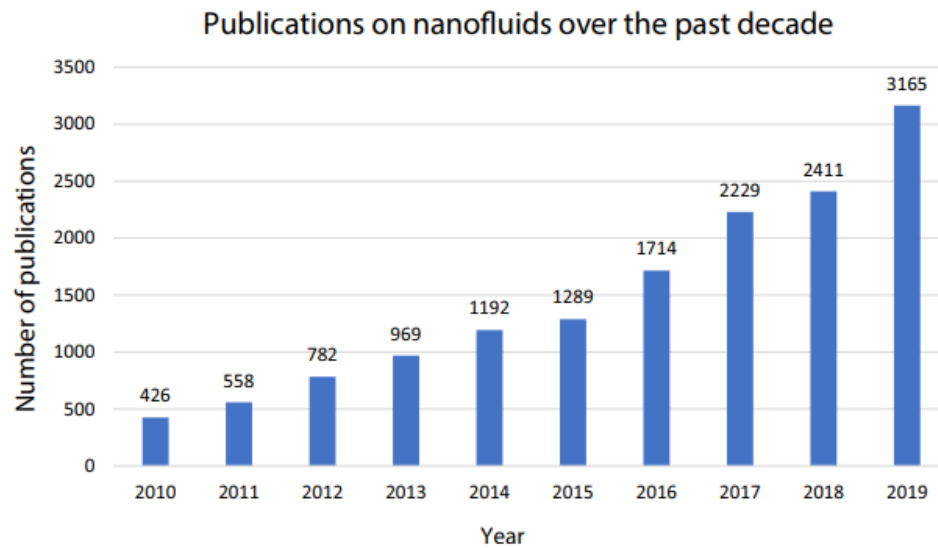
Figure I.1: Publications on nanofluids over the past decade **[1]**.

The topic of nanoparticles has been the focus of several studies and academic publications. In their investigations on the thermal conductivity of different minerals and liquids. In their research work on the thermal conductivity of various minerals and fluids, **Choi & al. [2]** introduced the term "nanofluid" to describe the effect particle size and shape have on the conductivity of a liquid-particle system. Later, in their publication Choi & al. asserted in their article **[3]** claimed that the thermal conductivity of the liquid may be improved by up to 150%, even at a nanotube concentration in the oil of less than 1% by volume. In different circumstances, **Eastman & al. [4]** heat conductivity may be improved by using copper nanoparticles with a diameter of 10 nm; many experimental and computational investigations have analyzed the impact of introducing nanoparticles to conventional fluids on thermal conductivity **[5-13]** and convective heat transfer **[14-20]**. Using nanofluids as a heat transfer fluid in heat exchangers by adding nanoparticles to the base liquid increases the viscosity of the final mixture, which may prove the system natural convection**.** In light of the prohibitive costs associated with conducting experiments, we have focused our attention here on the convective heat transfer mechanism as reported by numerical studies. When natural and forced convection are combined, a phenomenon known as "mixed convection" results. This convection is characterized by a combination of wall movement and buoyant force. Several different businesses, like as the food, glass, and electronics industries, rely on this kind of mixed convection for their production processes (cooling electronic equipment)

[21-31]. It has been conducting much research on fluid nanoparticles in recent years to help understand all the mechanisms and special cases by the nanofluid to become more efficient heat transfer and different geometrical and boundary conditions, as well as a moveable wall containing nanofluid, have been used to investigate the mixed convection heat transfer occurring inside the enclosures by various scientists have looked at how to increase convective heat transmission, but their findings have varied in various forms in cavities using nanofluids such as square enclosure **[32, 33]**, and triangular cavity **[34, 35]**. The enclosures are filled with various working fluids to research flow heat transfer and mixed convection fluid. Because of its increased thermophysical characteristics, nanofluid has sparked much attention in recent years. Researchers have employed many forms of nanofluids such as: Fe_3O_4 **[36-39]**, Al_2O_3 **[40-42]**, Cu **[43-46]**, TiO_2 **[47-49]**, Ag **[50-52]**, CuO **[53-55]**.

I.2.1.   Square lid-driven cavity

Several researchers have carried out numerical investigations of mixed convection inside cavities of various shapes, boundary conditions, and sizes of solid nanoparticles, as example: **A. Arefmanesh & al. [56]** studied the effects of uncertainty in Al_2O_3-water nanofluid effective dynamic viscosity on laminar mixed convection fluid flow and heat transfer in a square cavity. The enclosure right and left vertical walls and horizontal top wall are kept at (T_c). The horizontal wall moves from left to right at a constant speed and a higher temperature than the rest of the walls. For both viscosity models, the average Nüsselt number of the hot wall rises as the volume fraction of nanoparticles increases. Convective heat transmission around a heated square cylinder was studied by **Rosdzimin & al. [57]** in an enclosed, lid-driven cavity; the inner square of the square cavity was maintained at a higher temperature than the other square walls. According to the result, the Reynolds and Richardson numbers have an impact on the Nüsselt number. **H. Nemati & al. [58]** studied mixed convection flows using nanofluids using the Lattice Boltzmann Method in a lid-driven cavity; the nanofluid was comprised of water and Cu, CuO or Al_2O_3 nanoparticles filling the cavity. As the Reynolds number rises, the solid concentration effect decreases. The effects of Reynolds number and solid volume percentage on hydrodynamic and thermal properties are studied for diverse nanofluids. Using changing thermal conductivity and viscosity, **Sheikhzadeh & al. [59]** examined mixed convection in a nanofluid filled lid-driven enclosure. A water-based nanofluid

containing Al_2O_3 nanoparticles was used to fill the container. **Abdelkader & al. [60]** investigated mixed convection in a square cavity within a combination of several kinds of nanoparticles and water. The cavity top and lower walls are thermally insulated, while the remaining walls are movable and differentially heated, from the result the (Nu_{avg}) number increases as the nanoparticle volume fraction rise and the (Ri) number decreases. **E. Büyüküt & al. [61]** investigated the impact of several nanofluid thermal conductivity models on mixed convection flow and heat transmission in a lid-driven enclosure heated from the left vertical cooled from the top wall. Multiple triangular cylinders are heated in a square cavity with a moving lid, **Z. Boulahia & al. [62]** examined the issue of mixed convection of a nanofluid. The left and right walls are chilled at a constant temperature (T_c), while the above and bottom walls are thermally insulated. In four different lid-driven cases, **M. Mastiani & al. [63]** investigates the laminar mixed convection flow of Cu-water nanofluid at the density maximum of water. In a lid-driven square cavity that contains nanofluids and is simultaneously heated by two heat sources installed on the two vertical walls at a constant heat flux, **l. Zeghbid & al. [64]** provide a numerical study of two-dimensional laminar mixed convection. On the movable wall of the cavity and the bottom wall, respectively, the local cold temperature (T_c) is maintained. Nanofluid heat transfer in a lid-driven porous medium square enclosure with numerous pairs of heat sources and sinks has been numerically modelled by **Jahirul & al. [65]**. **Serna & al. [66]** investigated the flow problem in the heated lid-driven filled with nanofluid and in the presence of a pulsating flow by using model unsteady and viscous. **F. Talebi & al. [67]** performed a numerical simulation of mixed convection in a square cavity with a cap moving uniformly in the horizontal plane, where the upper and lower walls were isolated while the left wall had a higher temperature than the right. **S. M. Sebdani & al**. **[68]** investigated the impact of modifying nanofluid characteristics on heat transfer by mixed convection in a square chamber with a heat source on the bottom wall and movement of cold side walls. **A. J. Chamkha & al. [69]** researched the problem of steady laminar mixed convective flow and heat transfer of a nanofluid in single and double-lid driven cavities was considered. The bottom and top walls were kept at a constant temperature considering that the top wall is the hot wall and the left and right walls are isolated. **M. A. Mansour & al. [70]** presented in his research study a numerical study of mixed convection in a square cavity that was heated by a source of heat present in his bottom wall while the other left and right and top walls were preserved for cooling. In a square cavity with inlet and outlet ports, **M. Shahi & al. [71]** conducted a numerical examination of mixed convection

fluxes via a copper-water nanofluid. **F. Garoosi & al. [72]** conducted a numerical study related to mixed convection load in a horizontally heated square cavity of Al_2O_3-water nanofluids. **Hajialigol & al. [73]** has done a numerical study of a mixed thermal load in a driven enclosure, where the horizontal walls of the enclosure were isolated and the moving vertical walls were kept at a constant temperature where his study was divided into two cases: the first case shows that the left wall, the cold wall moved upward, while the hot wall, which is the right wall, move downward. As for the second case, it shows that the cold wall moves to the bottom, while the hot wall moves upward taking into account that the moving walls have the same speed and gravitational force parallel to the moving walls. In a lid-driven square cavity filled with nanofluids, **Z. Said & al. [74]** investigated the impact of laminar mixed convection; insulation is present on the cavity bottom and the top wall is set at a constant velocity, while the vertical walls are kept at various temperatures. **Z. Boulahia & al. [75]** investigated the effect of three triangular heating blocks inside a lid-driven square cavity filled with nanofluids on mixed convection. **M. S. Rahman & al. [76]** have done a numerical study of mixed convection within a lid-driven square enclosure filled with water and copper nanoparticles where the horizontal wall is thermally insulated. **F. Selimefendigil & al. [77]** investigated the mixed convection of an oscillating lid-driven cavity filled with nanofluid under the influence of an inclined uniform magnetic field, where the cavity is heated from below and chilled from above, with adiabatic side walls. The top wall velocity fluctuates sinusoidally, while the cavity other walls are subjected to no-slip boundary requirements. Two-dimensional mixed convection was studied numerically by **H. F. Oztop & al. [78]** a vertical two-sided lid driven differentially heated square cavity in a steady-state. Top and bottom walls are thermally insulated while left and right movable walls are maintained at different temperatures at all times. Three cases were evaluated based on the orientation of the sliding barriers. **B. Sharma & al. [79]** explored the heat transport of Cu-water nanofluids in a square cavity using laminar flow. Different length heaters with isothermal boundary conditions are installed symmetrically on two neighboring sides to heat the cavity. The movable lid is cold, and the rest of the borders are insulated. A thermally conductive solid cylinder is inserted in the cavity middle. **M. K. Bora & al. [80]** performed numerical analysis in a lid-driven cavity utilizing silver Ag-water nanofluid while preserving diverse shapes of conducting and insulating cylinders at the center. A bottom-mounted heater provides isothermal heating to the cavity. The right and left walls are insulated, while the top cold wall is moving. **N. Muhammad & al. [81]** studied the mixed convective flow of Ag–Ethylene

Glycol nanofluids inside a square cavity where it heated from center and the bottom and all of the side walls have lower temperatures; the side walls moving upward and downward. **S. Hussain & al. [82]** investigated in their study the effect of using fins and inclined magnetic fields inside lid-driven and double lid-driven cavities filled with nanofluids where they cared about the length and distance of fins. **A. Karim & al. [83]** investigated the effects of the periodicity of sinusoidal boundary condition for unsteady mixed convection heat transfer characteristics of an Ag–water nanofluid confined within a square shape lid-driven cavity. **B. Abbou & al. [84]** have investigated the effect of Aspect Ratio (AR) and non-uniform temperature on mixed convection in an enclosure.

In a lid-driven inclined square enclosure with nanofluid within, stable laminar mixed convection flow has been numerically modeled by **E. Abu-Nada & al. [85]**; the top and bottom walls of the enclosure are kept at consistent temperatures with the top surface moving at a constant speed as the hot wall. The left and right sides of the enclosure are kept insulated. In a study by **M. Alinia & al. [86]** numerical simulations were used to investigate the convection of a nanofluid in an inclined chamber. The top and lower insulated walls are sliding lids, while the left and right walls are kept at differing temperatures. **A. A. Abbasian Arani & al. [87]** explored the mixed convection numerically in a square cavity driven by a double lid with different inclination degrees and discrete heat sources. The moving walls on the right and at the top are cold. The bottom and left walls bottom halves are adiabatic, while the other halves are maintained at high temperatures. **A. Fereidoon & al. [88]** examined mixed convection flows in a double lid-driven square cavity with varying inclination degrees on the top and bottom walls, which slide in opposing directions at a constant speed. In the presence of a vertical magnetic field, **GH. R. Kefayati [89]** investigated laminar mixed convection of non-Newtonian nanofluids in a square lid-driven cavity. **M. Jafari & al. [90, 91]** examined the influence of mixed convection heat transfer in a hollow with a corrugated wall and a lid-driven flow. The vertical sides are insulated, and the lid is maintained at a constant temperature (T_h) higher than the wavy bottom wall (T_c). An investigation of the incompressible flow, the mixed convection in a horizontal lid-driven cavity is done by **S. Parvin & al. [92]**. The cavity has two fully insulated vertical walls, and the bottom wall is wave-shaped and has a temperature that is greater than the top sliding lid. In a nanofluid-filled vertical triangular wavy enclosure, constant laminar combined convection flow has been numerically modeled by **R. Nasrin & al. [93]**; a triangular wavy pattern is seen on the cavity left and right vertical walls.

The horizontal walls at the top and bottom are mechanically propelled. The bottom and top surfaces move at the same constant speed in the right and left directions, respectively. They keep their temperature constant at a level below both vertical walls. The mixed convection flow and heat transfer in a lid-driven cavity with a wavy bottom surface were studied numerically by **L. K. Saha & al. [94]**. The top wall of the cavity moves at a constant speed of unity, but the other walls do not slide. It is necessary to insulate the cavity vertical walls while keeping the top surface at a constant temperature that is greater than that of the wavering bottom. Using a Buongiorno model, **F. Garoosi & al. [95]** examined the mixed convection heat transfer of a nanofluid in a lid-driven cavity flow. Inside the hollow are a number of pairs of heater and coolers (HACs) with isothermal walls made of T_h and T_c ($T_h > T_c$). Nanofluid flow and heat transfer in a lid-driven cavity with a heated rectangular obstruction were studied by **M. Hemmat Esfe & al. [96]**, the thermal conductivity and effective viscosity of the nanofluid were shown to be temperature and nanoparticle concentration-dependent.

I.2.2.   Rectangular lid-driven cavity

Hakan [97] performed an investigation on the coupled convection that occurs in a porous lid driven hot cavity while simultaneously moving the top cold wall from left to right at a constant velocity. He showed the heating source should be positioned on the left perpendicular wall for the most efficient transmission of heat. In order to explore the mixed convection in a lid-driven rectangular cavity exposed to uniform heat flux along with its vertical short sides, **H. El Harfi & al. [98]** utilized Cu-H_2O nanofluids. It was determined that forced convection by a lid and natural convection by buoyancy-driven processes, respectively, dominate heat transfer for low and high values of Richardson numbers. Cu-nanoparticles may also improve heat transmission by acting as a lid and degrade it by acting as buoyancy-driven objects, respectively, when added to pure water. **H. Salahi & al. [99]** and **A. Karimipour & al. [100]** investigated the laminar mixed convection in 2D inclined lid-driven rectangular filled with nanofluids. The two sides are insulated, the top moving compartment lid is hot, and the bottom is cold. The effect of two movable barriers on mixed convection was investigated by **Sheikhzadeh & al. [101]** who used two different levels of the enclosure: fist condition, where the left vertical wall (cold wall) shifted upward, whereas second condition enclosure right vertical wall (hot wall) shifted downward, the enclosure left wall slid

lower while its right wall moved upward. **A Karimipour & al. [102]** examined the impact of the periodic mixed convection inside a rectangular enclosure with different AR. The temperature of the cavity bottom wall is considered to be higher than that of the top lid, which oscillates horizontally with the velocity indicated by sinusoidal function. **M. Mahmoodi [103]** examined the mixed convection in rectangular lid-driven enclosures. The enclosure left and right vertical walls as well as its top horizontal wall are kept at a constant frigid temperature (T_c). The enclosure bottom horizontal wall, which travels from left to right, is maintained at (T_h) constant, with $T_h > T_c$. **GH. R. Kefayati & al. [104]** have completed a 2D simulation of mixed convection in an enclosure with differentially heated sidewalls in the presence of a uniform magnetic field while the enclosure is filled with a viscoplastic fluid for various AR of the enclosure. The identical Bingham model was used to simulate the viscoplastic fluid without any restrictions. A rectangular enclosure with moveable walls on both sides was employed by **R. Bidgoli & al. [105]** where the Hamilton-Crosser and the Jang & al. models were used, respectively, to determine the thermal conductivity and effective viscosity of nanofluids. **D. Chatterjee & al. [106]** examined the effect of rotating circular cylinders on mixed convection inside a rectangular enclosure filled with nanofluids. In a lid-driven enclosure filled with nanofluids, where the top wall moves at a constant speed or with a temporally sinusoidal function and the other walls are stationary, **M. V. Ardalan & al. [107]** studied the unsteady physics of laminar mixed convection. The vertical walls are assumed adiabatic, whereas the horizontal top and bottom walls are maintained at low and high temperatures, respectively. In three-three square blocks inside porous rectangular cavity filled with nanofluids was examined by **M. H. Kabir & al. [108].** The temperature of the enclosure top and bottom walls is kept constant at (T_c). The walls on the left and right are maintained at room temperature. The interior of the enclosure is a three-square heating block.

I.2.3. Additional lid-driven cavity geometries

To better understand the convective recirculation and flow mechanisms brought on by a nanofluid, **M. M. Billah & al. [109]** examined numerically a lid-driven triangular enclosure with a partly heated bottom side. **M. M. Rahman & al. [110]** used numerical modeling in triangular inclined lid-driven enclosure to study how a nanofluid caused convective recirculation and flow. **K. Javaherdeh & al. [111]** have modeled stable laminar mixed convection flow in a lid-driven

triangular enclosure containing a nanofluid-filled triangular heat source. The left and right enclosure walls are kept at constant temperatures, while the top enclosure wall, which moves at a constant speed, is insulated. **M. M. Rahman & al. [112]** investigated the mixed convection in a triangular enclosure driven by an inclined lid and containing nanofluids. The enclosure is heated at the base surface while also being cooled at the inclined surface. The vertical wall is moving at a constant pace and is adiabatic. Mixed convection was studied numerically by **F. Selimefendigil & al. [113]** in a lid-driven chamber filled with nanofluids and including internal heat generation and a partially flexible wall. **I. Zahan & al. [114]** studied the effects of Joule heating and Magneto Hydro Dynamic (MHD) in a lid-driven triangular cavity. The cavity bottom wall is undulated in a sinusoidal pattern and cooled isothermally. The cavity left vertical wall is heated while the sloped side is insulated. In a trapezoidal enclosure filled with porous media, **Al-Rashed & al. [115]** investigated the flow field and heat transfer of a nanofluid with changing characteristics. In two separate lid-driven trapezoidal cavities, one with a heated wall on the squabby base and the other with a heated wall on the long base, **M. H. Hasib & al. [116]** evaluated the impact of the cavity tilt angle on mixed convection heat transfer while a continuous high temperature is offered at the bottom surface of the chamber; the top wall is kept at an isothermal cold temperature that is travelling in its own plane at a constant pace. **A. Aghaei & al. [117]** investigated how a magnetic field affected the flow field, heat transfer, and entropy formation of nanofluid mixed convection in a trapezoidal enclosure where the bottom wall is hot and the side walls are insulated while the top lid is cold and moving to the right or left. **S. E. Ahmed & al. [118]** investigated the laminar two-dimensional magnetohydrodynamic mixed-convection flow in trapezoidal enclosures filled with micropolar nanofluids. The temperature of the trapezoidal enclosure left and right inclined vertical sidewalls was kept low while a portion of the bottom wall is heated uniformly; the horizontal top wall is deemed adiabatic and travels at a uniform lid-driven velocity. An external magnetic field is applied at various orientation angles on the enclosure left sidewall. **Cho & al. [119]** studied the heat transfer properties of nanofluids contained in a lid-driven cavity with mixed convection heat transmission; left and right walls are believed to be wavy while the above and below walls are assumed to be flat. Additional assumptions include a steady heat flux on the left-wavy wall, a low temperature on the right-wavy wall, and horizontal movement on both walls.

I.2.4. Experimental studies on mixed convection with nanofluids

The number of experimental studies was disproportionate to that of work carried out numerically. This comes down to the cost and difficulty of handling. The mixed convection of Al_2O_3-water nanofluids was investigated in an experiment by **R. Ben Mansour & al. [120]** who heated the outside surface of a copper tube at a constant rate. There is a discussion of how the concentration of nanoparticles and the strength of the applied power influence the development of the thermal field in laminar flow; coefficient of heat transfer in experiments is shown to decrease somewhat when the particle volume concentration increases from 0% to 4%. **G. G. Momin [121]** did two experiments: the first one was to study how Al_2O_3-water nanofluid moved around inside an angled copper tube. Under laminar flow conditions, the impacts of nanoparticle fraction and the effects of different power sources on the growth of the thermal field are analyzed and discussed. In a second experiment, Al_2O_3–Cu/water hybrid nanofluid is used to show a fully developed laminar convective heat flow through a uniformly heated circular tube. In the first study, it was found that when the particle volume concentration went from 0% to 4%, the experimental heat transfer coefficient went down a little. Also, the results of the friction factor between 0.1% Al_2O_3-Cu/water hybrid nanofluids and 0.1% Al_2O_3/water nanofluids is somewhat greater. **S. Aberoumand & al. [122]** evaluated the convective heat transfer increase of Ag-Heat Transfer Oil nanofluids flow within curved tubes, which has been empirically tested in the thermal entry zone. As a boundary condition, the temperature of the tube wall is made to remain constant 91 °C. In order to study the impact of employing nanofluids as well as the impact of altering geometry on heat transfer, experiments were conducted for pure fluid flow within straight and curved tubes. The findings reveal that the Nüsselt number increases and convection heat transfer coefficient were measured to be 57% and 33%, respectively. **E. Manay & al. [123]** investigated experimentally the characteristics of mixed convection heat transfer of nanofluids in circular microchannels with 500 µm diameter filled with water-based SiO_2 nanofluids. The nanofluid volumetric particle ratios were chosen to be 0.2% and 0.4%. For all fluid, thermal conductivity and viscosity were characterized between the temperatures of 20 °C and 60 °C. The overall heat transmission was improved by 4–13% by raising the test section inclination angle. The overall heat transfer increased from 12 to 14% for a 0.2 vol percent and from 29 to 32% for a 0.4 vol percent by adding nanosized SiO_2 particles to the water. Mixed convection was investigated by **A. Rostamzadeh & al. [124]**,

for a vertical W-shaped copper tube filled with Al_2O_3-water nanofluid. Many different combinations of Reynolds number, temperature, and particle volume fraction were tested. When the Reynolds number is raised, heat transfer coefficient increases slightly. **A. D. Abdulsahi & al. [125]** conducted an experiment to study the mixed convection in a square enclosure divided into two layers. Al_2O_3–water nanofluid (upper layer) and superposed porous medium (lower layer) were used in the experiments, which had an adiabatic rotating cylinder at their core for the tests. The top and lower walls were considered to be adiabatic while the right wall was heated and the left wall cooled throughout the experiment. The findings showed that as the temperature differential increases, so does the flow intensity.

The Table I.1 shows the geometries used in the previous studies from the literature, with the used solution methods and the most important variable parameters that the researchers used in their studies with the most important results obtained.

Table I.1: Summary of previous works related to cavities.

Ref.	Geometry	Type of fluid and parameter range	Method	Results
[56]		Al_2O_3 - Water $Gr=10^4$ $Ri=0.01\text{-}100$	FVM	• For both viscosity models, the average Nüsselt number of the hot wall rises as the volume fraction of nanoparticles increases.
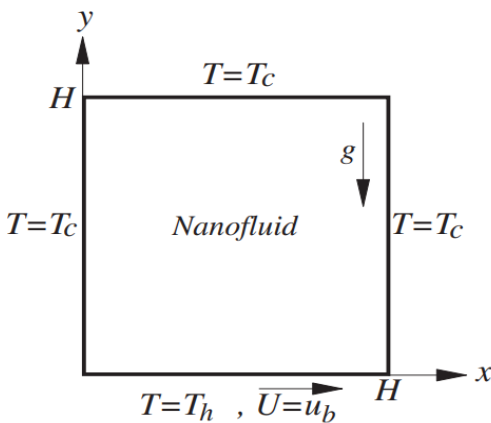
[57]

T=T$_{COLD}$, u=0.1 ,v=0

T=T$_{HOT}$, u=0,v=0

T=T$_{COLD}$, u=0 ,v=0

T=T$_{COLD}$, u=0 ,v=0

T=T$_{COLD}$, u=0 ,v=0
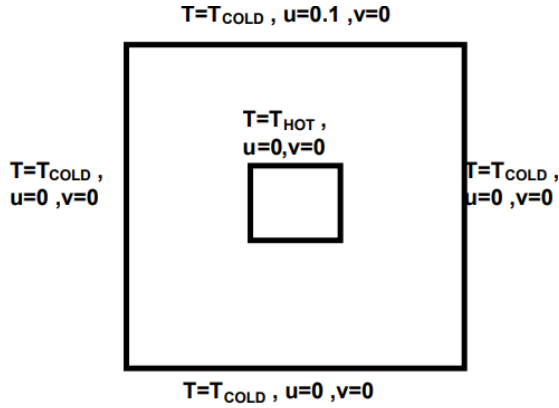
Air
$100 \leq Re \leq 1000$
$0.01 \leq Ri \leq 1$
$Pr = 0.71$

LBM

- The Reynolds and Richardson numbers have an impact on the Nüsselt number.

[58]

$\frac{\partial T}{\partial y} = 0$

U

$T=T_h$

g

H $T=T_c$

y

W

x

$\frac{\partial T}{\partial y} = 0$
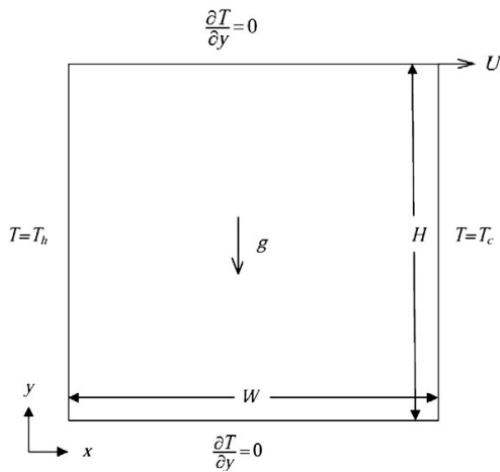
$\begin{pmatrix} CuO, \\ Cu, \\ Al_2O_3 \end{pmatrix} - H_2O$
$Ra = 10^4$
$Re = 1, 10, 100$
$\varphi = 0, 0.01, 0.03, 0.05$

LBM

- For Al2O3, CuO and Cu, the effects of solid volume fraction increase sequentially.
As the Reynolds number rises, the solid concentration effect decreases.

[59]

Adiabatic U_P

T_h T_c

Adiabatic
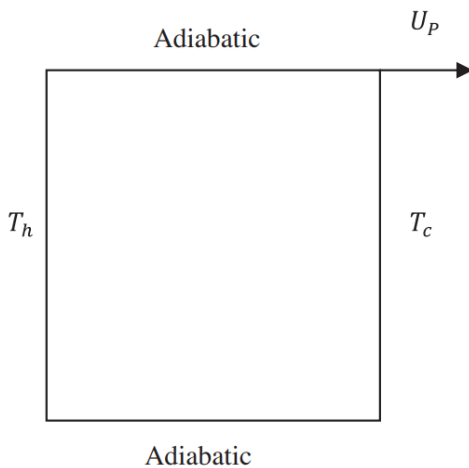
$Al_2O_3 - H_2O$
$Pr = 6.2$
$Ri = 0.01 - 100$
$\varphi = 0 - 0.06$
$Gr = 10^4$

FVM

- Using different models for thermal conductivity and viscosity, the average Nüsselt number for a constant solid volume fraction varies.
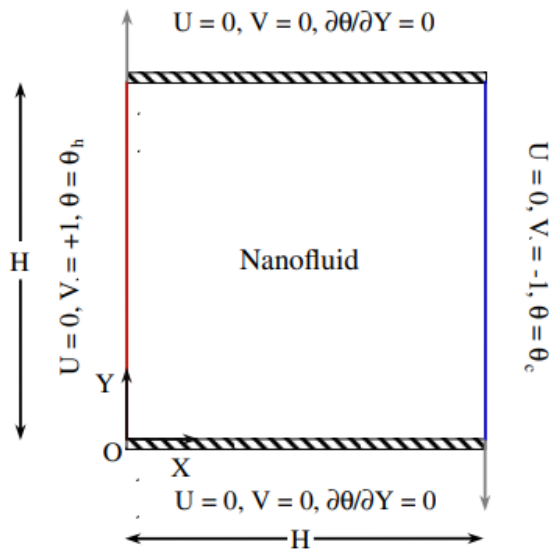
[60]		$Ri = 0.01 - 100$ $\varphi = 0 - 10\%$	LBM	• The Nu_{avg} number increases as the nanoparticle volume fraction rise and the Ri number decreases.
[61]		Al_2O_3 with Ethylene Glycol-water mixture $\varphi = 0 - 0.08$ $Gr = 10^4$ $Ri = 0.1 - 10$	FEM	• The Pak and Cho model produces much higher average Nüsselt values than the other models.
[62]		$Cu - H_2O$ $0.1 \leq Ri \leq 100$ $0 \leq \varphi \leq 0.05$ $Pr = 6.2$	FVM	• Size and quantity of heated triangular cylinders both have an impact on the heat transfer rate. The Nu_{avg} number increases as φ rise and the Ri decreases.
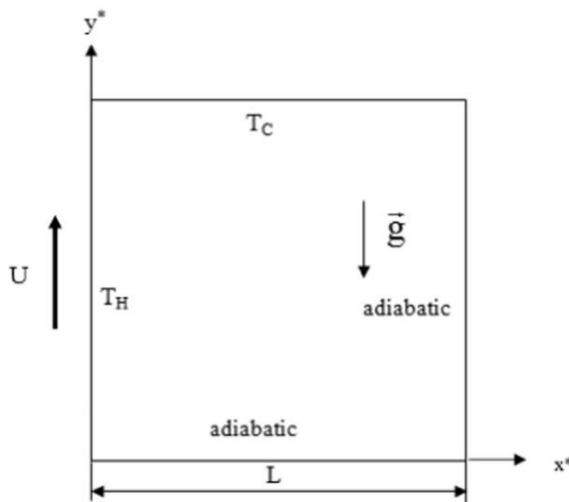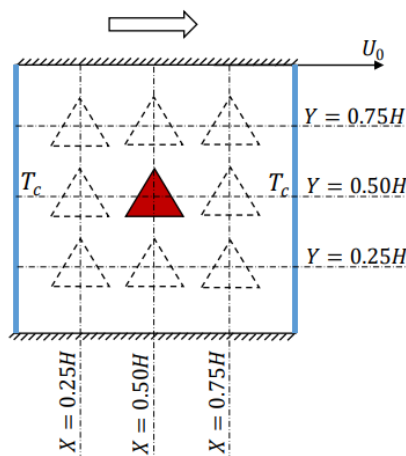
[63]
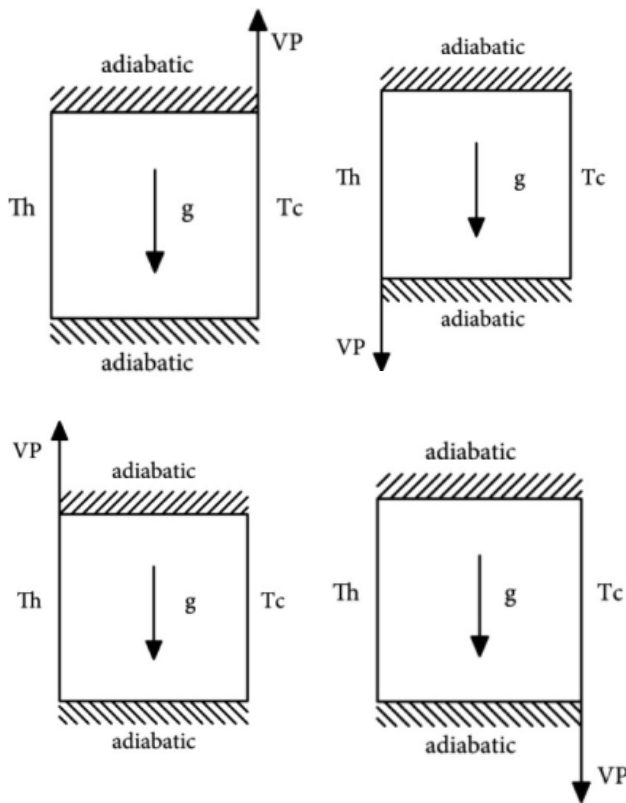
$Cu - H_2O$
$\varphi = 0 - 0.05$
$Ri = 0.01 - 100$
$Pr = 6.2$

FVM

- As the nanoparticle volume fraction increases, so does the Nu_{avg} number. The Boussinesq approximation allows for the highest Nu_{avg} number to be obtained when the shear-driven force is in balance with the buoyancy force.

[64]
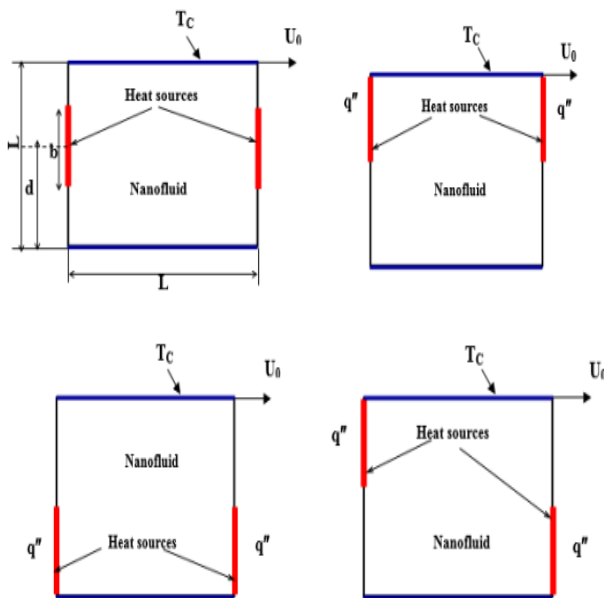
$Re = 1 - 500$
$Ra = 10^3 - 10^4$
$\begin{pmatrix} Ag, \\ Cu, \\ Al_2O_3, \\ TiO_2 \end{pmatrix} - H_2O$
$\varphi = 0 - 0.1$
$Pr = 6.2$

FVM

- The solid volume fraction and Rayleigh number of nanofluids both contribute to a rise in the Nu_{avg} number.

[65]
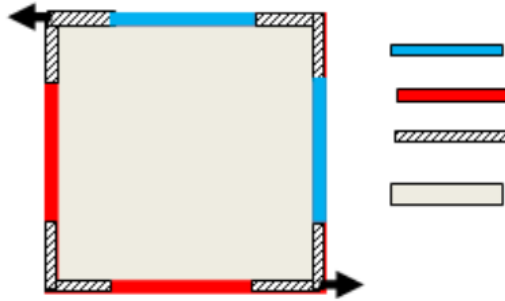
$Cu - H_2O$

$\varphi = 5\%$

$Pr = 6.2$

$10^3 \leq Gr \leq 10^6$

$1 \leq Re \leq 100$

$10^{-5} \leq Da \leq 10^{-2}$

FEM

- The increase in the velocity of the fluid flow is aided by the addition of Cu nanoparticles, resulting in an increase in heat transfer rate.

[66]
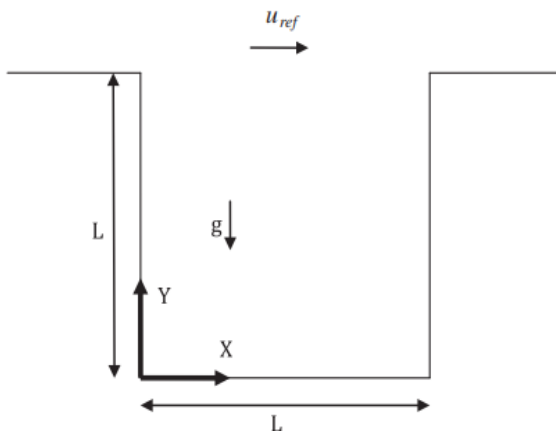
$CuO - H_2O$

$Pr = 3.93$

$Ri = 11.82$

$Re = 50$

NSM

- The time-averaged Nüsselt number in the cavity is increased by increasing sinusoidal velocity waves at the lid-driven.

[67]
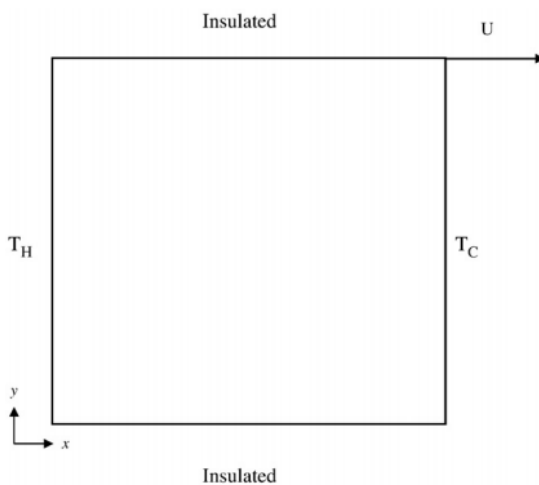
$Cu - H_2O$

$\varphi = 1 - 0.05$

$Ra = 10^4 - 10^6$

$Re = 1 - 100$

FVM

- At a certain number of Reynolds and Rayleigh numbers, the size of the nanoparticles has a positive effect on heat transfer.

[68]
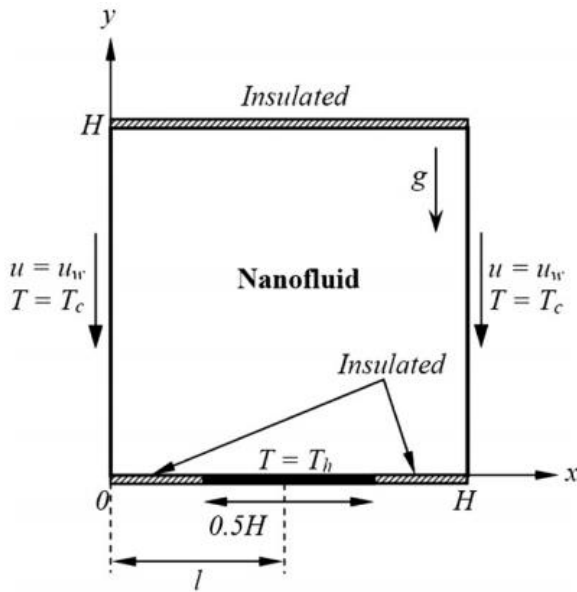
$Al_2O_3 - H_2O$

$Re = 10 - 100$

$Ra = 10^3 - 10^5$

$\varphi = 0.01 - 0.09$

FVM

- The Nu_{avg} value rises as the heat source moves closer to the left wall.

  The rate of heat transmission increases as the Rayleigh number rises while the Reynolds number stays the same.

[69]
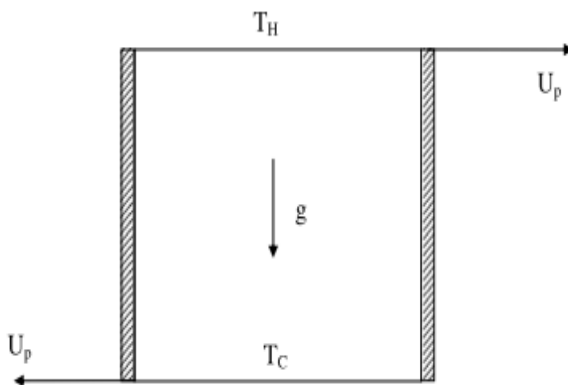
$Al_2O_3 - H_2O$

$\varphi = 0 - 0.1$

$Ri = 0.001 - 10$

FVM

- Significant heat transfer enhancement can be obtained due to the presence of nanoparticles and this was accentuated by increasing the nanoparticle volume fractions at moderate and large Richardson numbers using both nanofluid models for both single, and double-lid cavity configurations.

[70]
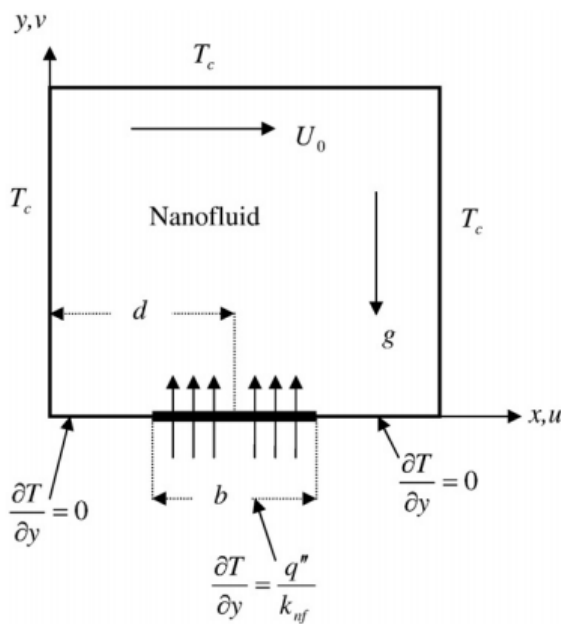
$\begin{pmatrix} Ag, \\ Cu, \\ TiO_2, \\ Al_2O_3 \end{pmatrix} - H_2O$

$0 \leq \varphi \leq 0.2$

$1 \leq Re \leq 100$

$0.2 \leq B \leq 0.8$

$0.2 \leq D \leq 0.8$

FVM

- The average number of Nüsselt increased due to the decrease in the fluid activity and its temperature due to the increase in the volume of nanoparticles.
It has also been observed that when adding nanoparticles of alumina Al_2O_3 to the base liquid, this gives greater values to the number of Nüsselt unlike adding nanoparticles of titanium oxide TiO_2.

[71]
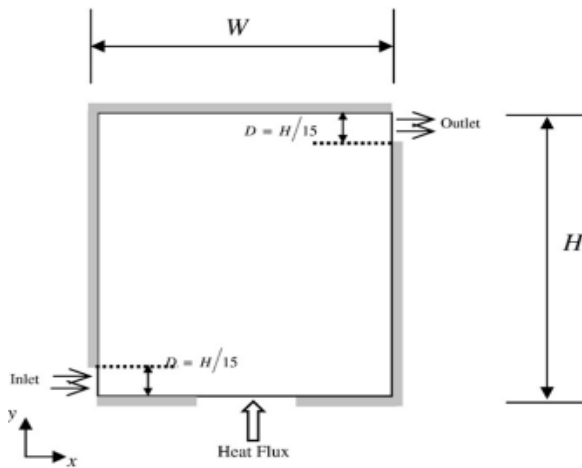
$Cu - H_2O$

$50 \leq Re \leq 1000$

$0 \leq \varphi \leq 0.05$

$0 \leq Ri \leq 10$

FVM

- The increase in solid concentration leads to an increase in the average Nüsselt number.
The increase in Re decreases the average temperature for the same Ri.
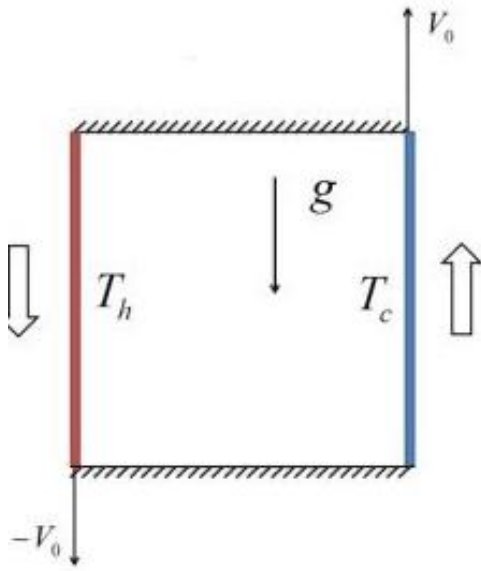
| [72] | | $Al_2O_3-H_2O$ $0 \le \varphi \le 0.05$ $0.01 \le Ri \le 10^3$ $10^2 \le Gr \le 10^4$ $25nm \le dp \le 145nm$ | FVM | • The heat transfer rate increases as the Grashof number rises and the Richardson number decreases. For all Richardson numbers with Grashof number $Gr = 10^2$, by increasing the volume fraction of nanoparticles, the heat transfer is enhanced. On the other hand, at Grashof number $Gr=10^4$ for each Ri, there is an optimum volume fraction of nanoparticles, where the maximum heat transfer occurs. |
| [73] | | $Cu-Water$ $0.25 \le AR \le 4$ $Gr = 10^4$ $Ri = 0.1, 1, 10$ | FVM | • The difference in the mean Nu on the hot wall as a linear temperature indicator in both cases was due to the increase in the size of the nanoparticles. The direction of the movable wall has a major impact on the temperature gradient. |
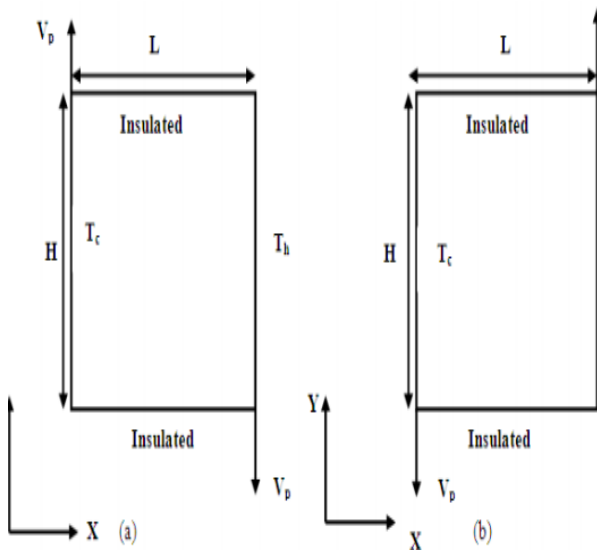
[74]
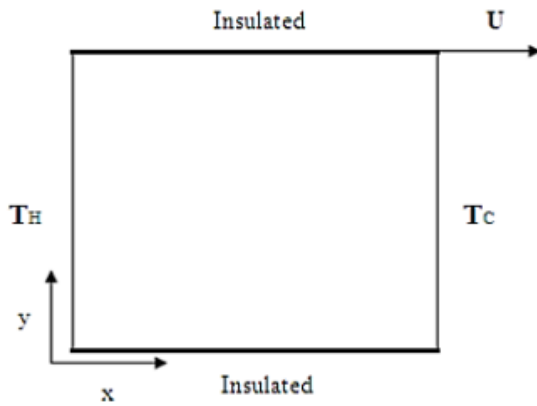
$$\begin{pmatrix} Al_2O_3, \\ CuO, \\ SiO_2, \\ TiO_2 \end{pmatrix} - H_2O$$

$1600 \leq Re \leq 700$

$0 \leq \varphi \leq 0.04$

$10^4 \leq Ra \leq 10^6$

$dp = 25, 40, 60nm$

FVM

- Nüsselt number rises with an increase in volume percentage, while it falls with an increase in nanoparticle diameter. Higher Nüsselt numbers are also a consequence of a larger differential between the hot and cold walls.

[75]
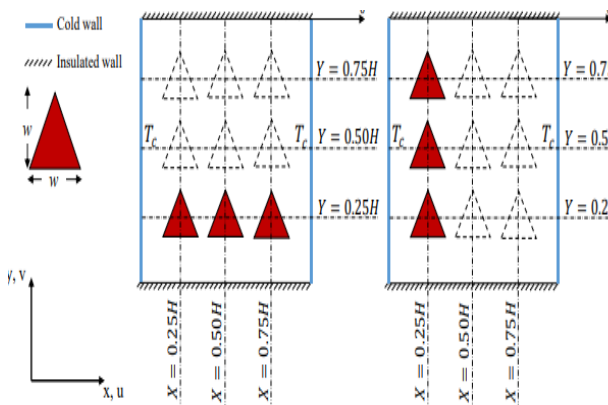
$Cu - H_2O$

$0 \leq \varphi \leq 0.05$

$0.1 \leq Ri \leq 100$

$Pr = 6.2$

FVM

- The average Nüsselt number rises as the Richardson number is decreased and the volume fraction of nanoparticles is raised.

[76]
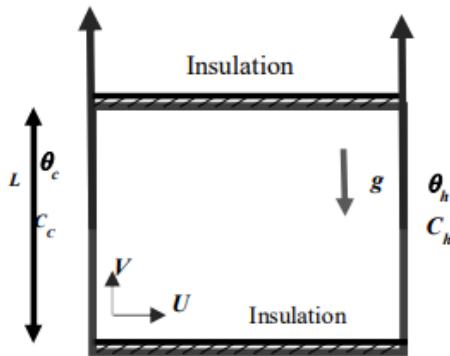
$Cu - H_2O$

$Ri = 0.1 - 10$

$\varphi = 0.02$

FEM

- When Ri is increased from 0.1 to 10, the rate of heat and mass transfer increases by roughly 6% for water, but by around 34% for nanofluids.

[77]
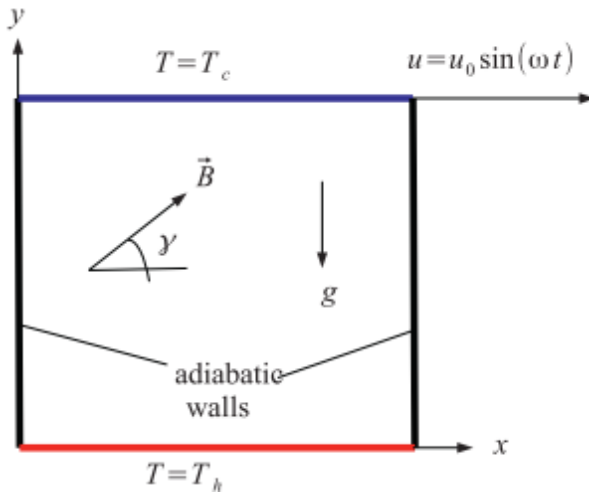
$Cu - H_2O$

$0.1 \leq Ri \leq 100$

$0 \leq Ri \leq 60$

$0 \leq \gamma \leq 90°$

$0 \leq \varphi \leq 0.04$

$0.001 \leq St \leq 1$

FEM

- For high Strouhal, Hartmann St, and Richardson numbers, the heat transfer process becomes inefficient. When the solid volume fraction of nanoparticles is 0.04 compared to the base fluid, an average heat transfer enhancement of 28.96% is produced.

[78]
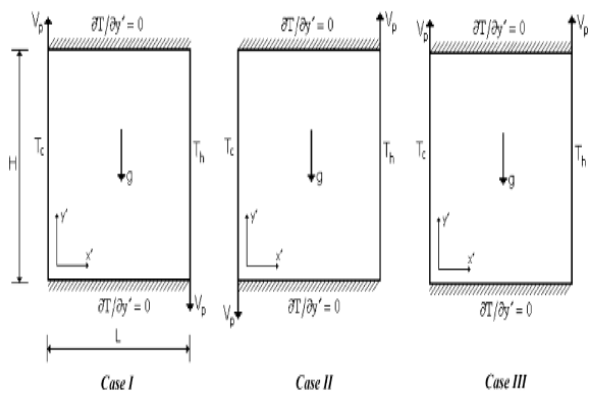
Air

$0.01 \leq Ri \leq 100$

$Pr = 0.7$

FVM

- It is discovered that the fluid flow and heat transfer in the cavitation are affected by both the Richardson number and the direction of the moving walls.

[80]
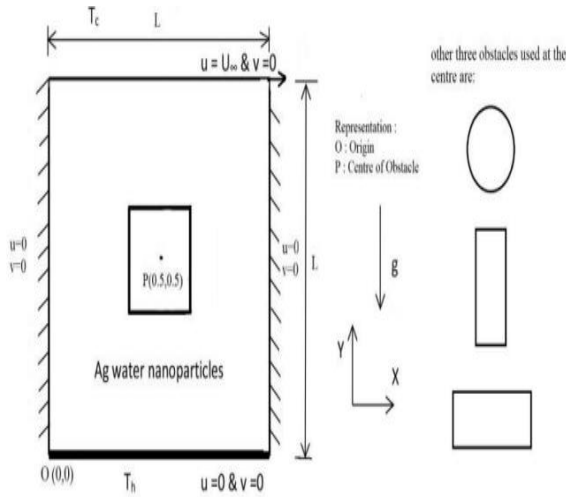
$Ag - H_2O$
$Ri = 0.01 - 10$
$0 \le \varphi \le 0.08$
$Gr = 10^4$
$Pr = 6.2$

FVM

- Nüsselt number rises as the proportion volume of nanoparticles increases, while Ri has the opposite impact on Nu.
For all Richardson numbers, minor variations in flow and thermal field are found with changes in the thermal boundary conditions (insulation and conduction) of a centrally located solid cylinder.

[81]
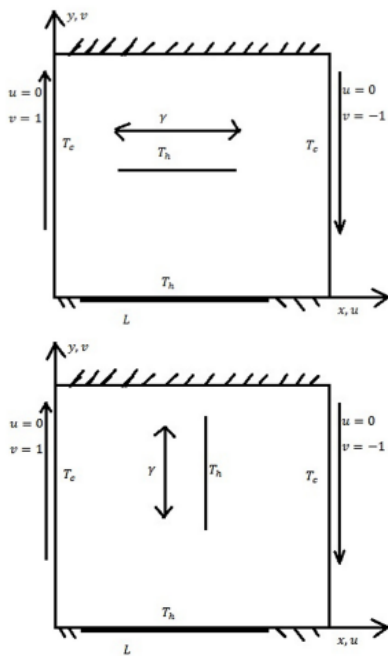
$C_2H_6O_2 - Ag$
$\varphi = 0.06$
$Re = 100$
$Pr = 7$
$Ri = 1, 5, 10, 20, 100$

FVM

- When a horizontal heater is put in the middle of the cavity, heat transmission in contained nanofluid in an enclosure is improved in the case of Cattaneo-Christov heat flux.
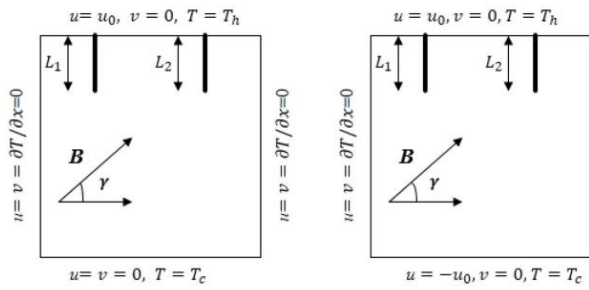
[82]	$u = u_0,\ v = 0,\ T = T_h$ ... $u = v = \partial T/\partial x = 0$ ... B ... γ ... $u = v = 0,\ T = T_c$ ... $u = -u_0, v = 0, T = T_c$	$Cu - H_2O$ $0.25 \leq L_1$ $L_2 \leq 0.5$ $0 \leq Ha \leq 100$ $0^\circ \leq \gamma \leq 90^\circ$ $Ri = 0.01 - 0.1$ $N = 2 - 5$	FEM	• Inferring from the existence of fins against their absence, fluid flow and heat transmission are drastically altered. Distances between adiabatic fins of 0.3 m provide for the lowest possible convective heat transmission.
[83]	L ... $u=U_0$ ... $T=T_c$ ... Adiabatic wall ... L ... g ... Ag-water nanofluids ... $T= T_c + (T_h-T_c)\,\sin(N\pi x/L)$	$Al_2O_3 - H_2O$ $Gr = 10^5 - 10^7$ $N = 1 - 6$ $\tau = 0.1,\ 1$	FEM	• The Grashof number and the sinusoidal even and odd frequency have a large impact on the streamlines and isotherms inside the cavity.
[84]	y ... $\dfrac{\partial T}{\partial y} = 0, U = 0$ ... H ... U_0 ... T_c ... T_c ... U_0 ... T_H or $T_H = T_c + (1 - \cos(2\pi x))/2$ ... L ... x	Air $AR = 0.25 - 5$ $Pr = 0.71$ $Gr = 10^4$	FVM	• The localized thermal exchange rate was sinusoidal and produced by uneven heating (Ri = 1 and 100), with the lowest quantities at the margins and the highest amounts in the bottom center.
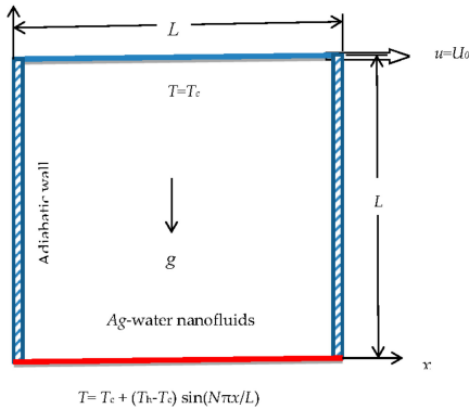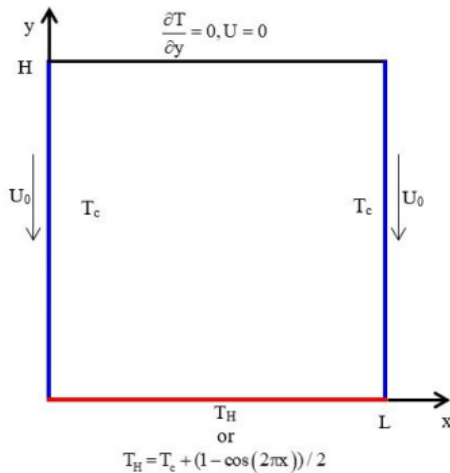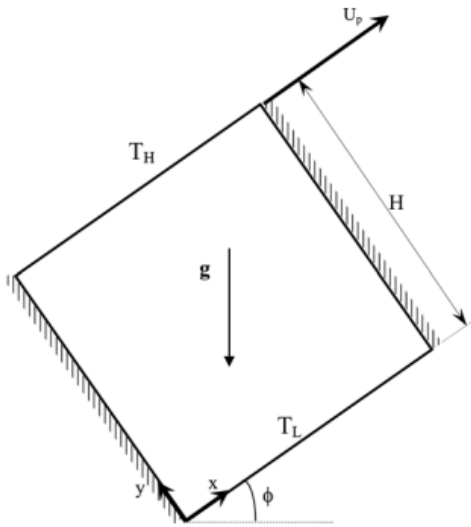
[85]		$Al_2O_3 - H_2O$ $\varphi = 0-10\%$ $\gamma = 0-90°$ $Ri = 0.001-10$ $Gr = 100$	FVM	• The enclosure inclination for moderate and high Richardson values emphasizes the presence of nanoparticles that increase the rate of heat transmission.
[86]		$SiO_2 - H_2O$ $\gamma = -60° - +60°$ $Ri = 0.01-100$ $Gr = 10^4$ $\varphi = 0-8\%$	FVM	• Adding nanoparticles to the cavity significantly improves heat transmission and alters the flow pattern. As the Richardson number rises, inclination angle impact becomes more visible.
[87]		$Al_2O_3 - H_2O$ $\gamma° = -90° - 90°$ $Ri = 0.1-10$ $Re = 1-100$ $\varphi = 0-6\%$	/	• In an improve of the volume fraction, heat transmission increases with increasing Richardson and Reynolds.
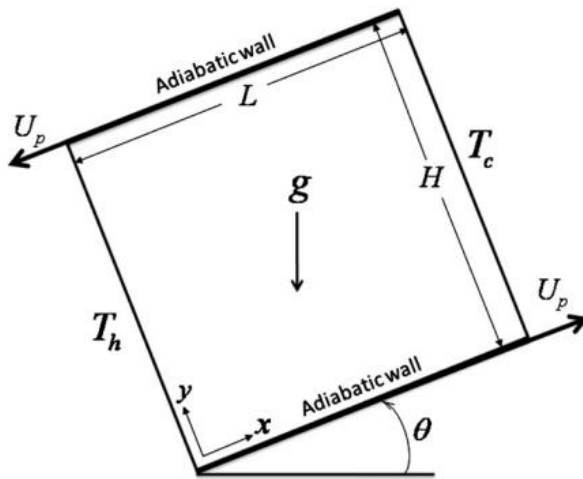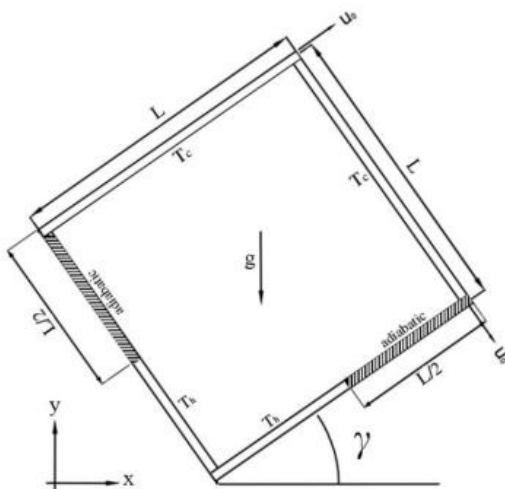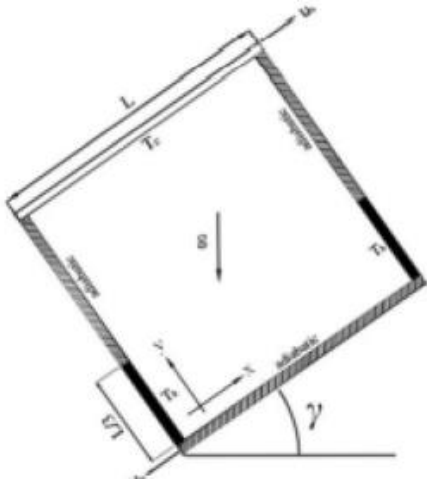
Ref	Figure	Parameters	Method	Findings
[88]		$Al_2O_3 - H_2O$ $\gamma^\circ = -90^\circ - 90^\circ$ $Ri = 0.1 - 10$ $Re = 1 - 100$ $\varphi = 0 - 6\%$ $d_p = 15nm$	FVM	• At a fixed Reynolds number, the heat transmission rises with the solid volume fraction.
[89]		$Cu - H_2O$ $Ri = 0.0001 - 1$ $n = 0.2 - 1$ $\varphi = 0 - 9\%$	LBM	• Increased Richardson number reduces heat transmission. The MHD reduces heat transmission in general and modifies the strength of the influence that nanoparticles have on an increase in heat transfer.
[90, 91]		$\begin{pmatrix} CuO, \\ Cu, \\ Al_2O_3 \end{pmatrix} - H_2O$ $Ri = 0 - 0.05$ $A = 0.05 - 0.25$ $Re = 25$	LBM	• The average Nüsselt number decreases as the amplitude of the wavy wall increases for large Richardson numbers.
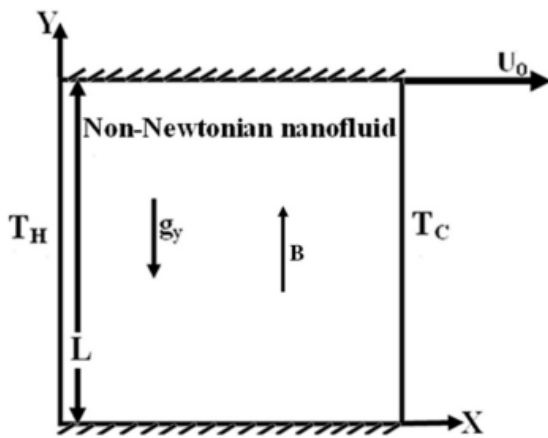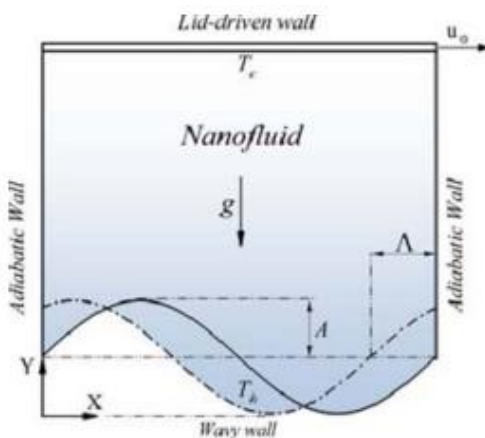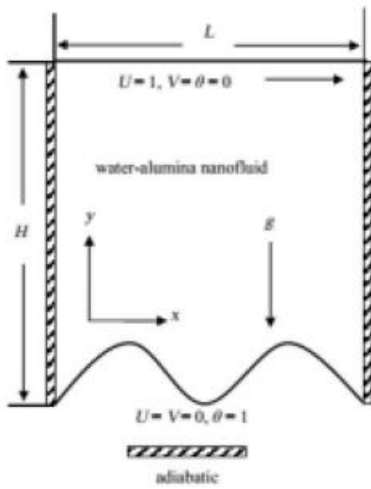
[92]		$Al_2O_3 - H_2O$ $\varphi = 5\%$ $Ra = 10^4$ $Re = 100$ $Pr = 6.2$	FEM	• At a greater amplitude of the wavy bottom surface, the lid-driven cavity filled with nanofluid may be seen as an efficient heat transmission mechanism.
[93]		$CuO - H_2O$ $\varphi = 1\% - 10\%$ $Re = 10 - 300$ $Pr = 7$ $Ri = 0.1 - 10$	FEM	• The rate of heat transmission is increased by decreasing the Ri number, increasing the Re number, and raising the solid volume fraction.
[94]		Air $Pr = 0.7$ $Re = 100 - 5000$ $Gr = 10^3 - 10^6$	FEM	• Wavy surface amplitudes and greater Grashof numbers make the lid-driven cavity an efficient heat transfer mechanism.
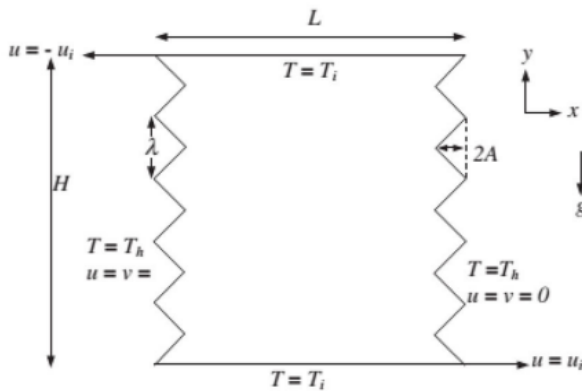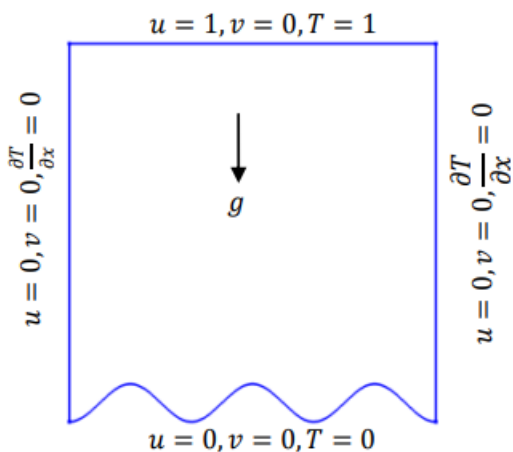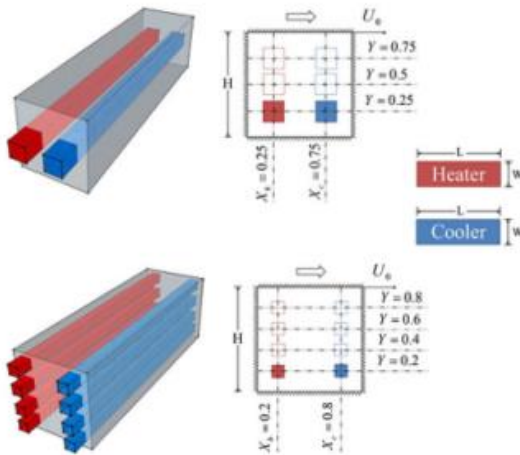
[95]		$Al_2O_3 - H_2O$ $Ri = 0.01 - 100$ $Re = 10 - 10^3$ $d_p = 25 - 145nm$ $\varphi = 0 - 0.05$ $Gr = 10^4$	FVM	• By switching the heater and cooler from horizontal to a vertical configuration, the rate of heat transfer is boosted.
[96]		$Al_2O_3 - H_2O$ $\varphi = 0 - 5\%$ $Ri = 0.01 - 100$ $d_p = 20 - 80nm$ $Gr = 10^4$	FVM	• As the Richardson number and nanoparticle diameter is increased, so does the average Nüsselt number for the total solid volume fraction.
[99]		$Cu - H_2O$ $Pr = 6$ $Re = 408.21$ $Ar = 10$ $Ri = 0.1 - 10$ $Ra = 10^5 - 10^7$ $\gamma = 0° - 20°$ $\varphi = 0.05 - 0.08$	FVM	• For the forced convection-dominated case (Ri = 0.1), the Nu$_{avg}$ grows with cavity inclination just a little, but for the natural convection-dominated case (Ri = 10), it increases with inclination considerably more significantly.
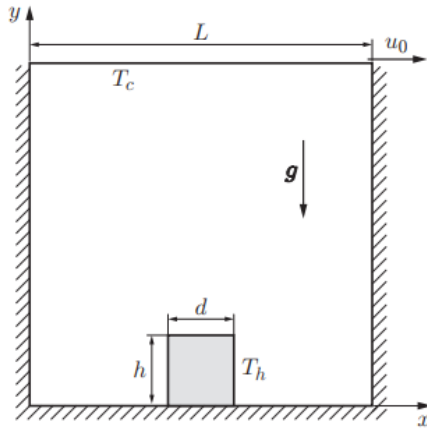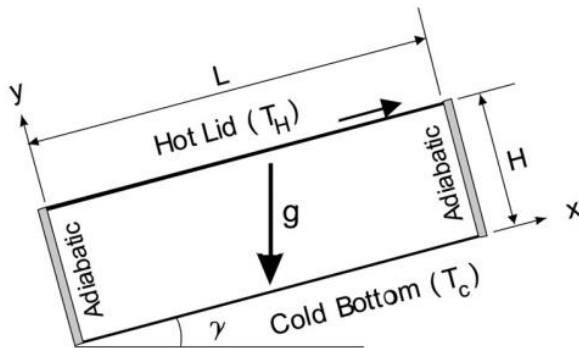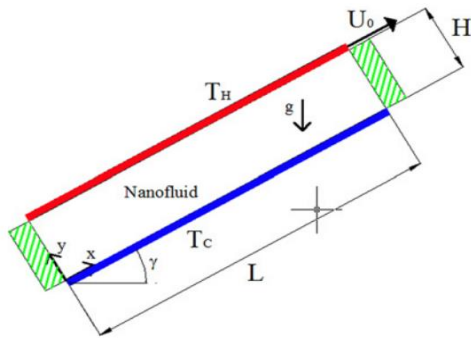
[100]		$Cu - H_2O$ $Ar = 5$ $\gamma = 0° - 90°$ $\varphi = 0 - 0.04$ $Ri = 0.1 - 10$ $Re = 100$	FVM	• At larger values of inclination angle and nanoparticles volume fraction gives achieved an increases Nu.
[102]		$Cu - H_2O$ $\varphi = 0 - 4\%$ $Ri = 0.1 - 10$ $Gr = 10^4$ $Pr = 6.2$ $Ar = 3$	FVM	• In a stable oscillation condition, the largest Richardson number corresponded to lower values of fluctuation amplitude of the average Nüsselt number.
[103]		$Al_2O_3 - H_2O$ $\varphi = 0 - 0.1$ $Ri = 0.1 - 10$ $Gr = 10^4$ $Ar = 0.5 - 2$ $Pr = 6.8$	FVM	• The average Nüsselt number of enclosure hot wall rose with increasing nanoparticle volume percentage for all aspect ratios and Richardson values.
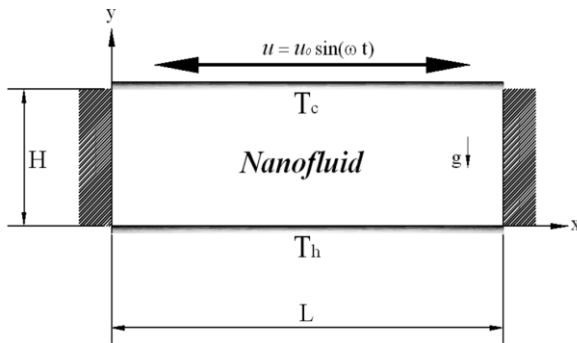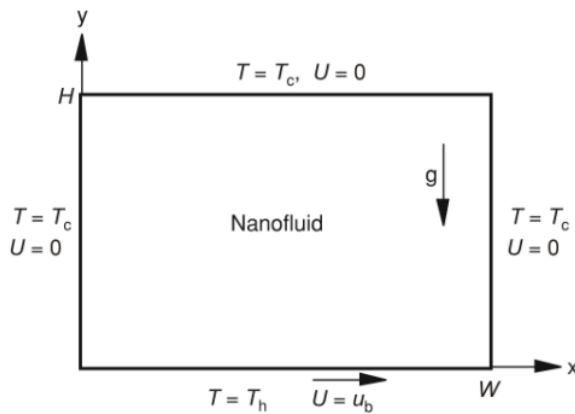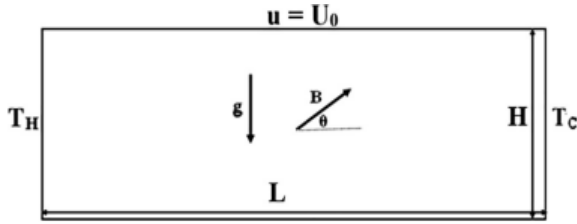
[104]		*Viscoplastic fluid* $Ha = 0 - 5$ $Bn = 1 - 10$ $AR = 0.5 - 4$ $Re = 100 - 1000$	LBM	• An increase in the Bingham number Bn reduces heat transmission while increasing the size of the unyielding section. The increase in AR modifies the size and placement of the unyielding/ yielding zones.
[105]		$Al_2O_3 - H_2O$ $Re = 100$ $Ar = 2$ $d_P = 80nm$ $Ri = 0.1 - 100$	FVM	• Heat transfer rate increased with rising velocity in every instance (except from those with extremely low Ri numbers), and it also increased significantly with increasing Nu number as a result.
[106]		$Cu - H_2O$ $0 \leq \Omega \leq 5$ $1 \leq Ri \leq 10$ $\varphi = 0 - 0.2$	FVM	• The cylinder spinning speed, the intensity of the mixed convection, and the concentration of nanoparticles all have a significant impact on heat transmission.
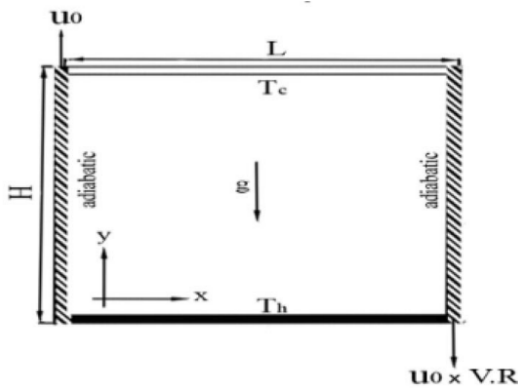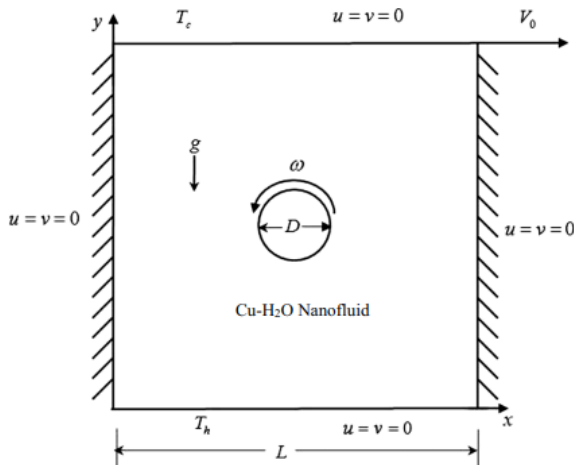
[107]

(a)
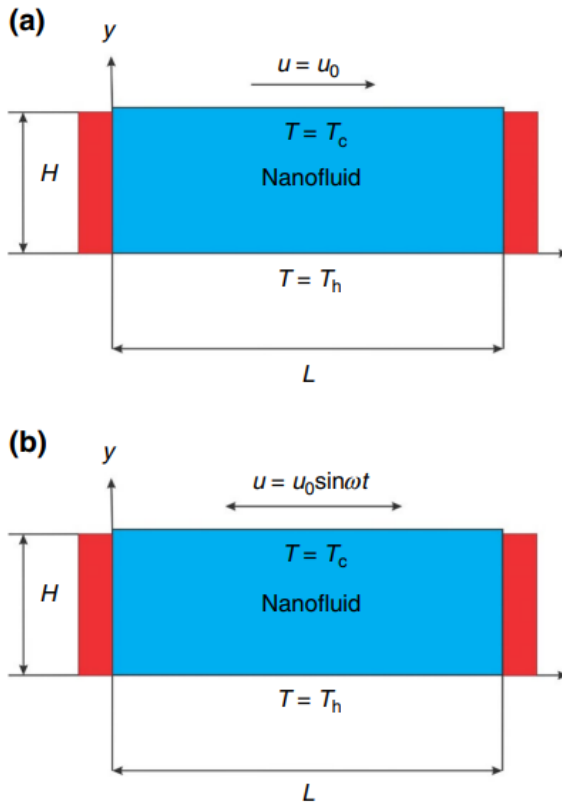
$Cu - H_2O$
$Pr = 6.2$
$Gr = 10^4$
$Ri = 0.1, 10$
$\varphi = 0 - 0.04$

LBM

- Low-frequency oscillations are amplified by the sinusoidal lid wall motion. When the non-dimensional frequency increases, the Nüsselt number decreased.

(b)

[108]
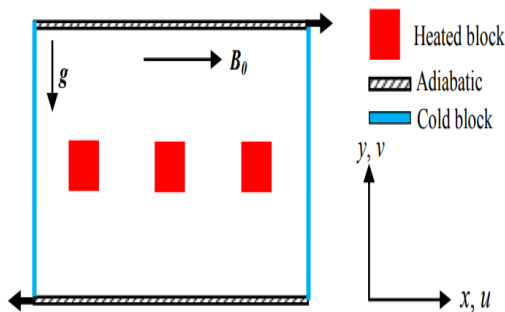
$Cu - H_2O$
$Pr = 6.2$
$Ri = 0.1 - 10$
$Ha = 25$
$Da = 10^{-5} - 10^{-2}$

FEM

- The rate of heat transmission increases as the Darcy and Richardson numbers rise. A suitable control parameter for heat transfer in fluid flow through a porous media in an enclosure is the Darcy number.
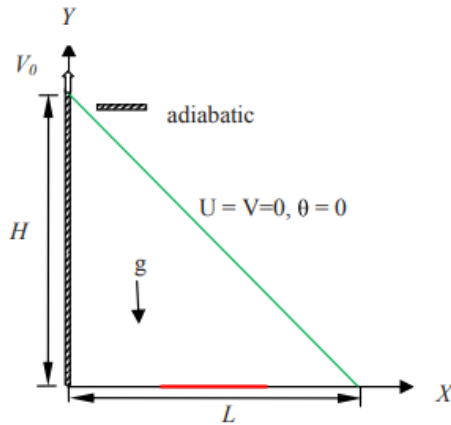
[109]		$Cu - H_2O$ $Ri = 0.1 - 10$ $Pr = 6.2$	FEM	• Maximum heat transfer was observed when the length of the heating source was minimal, making it an appropriate regulating parameter for both ways of using base fluid and nanofluid inside the enclosure.
[110]		$Cu - H_2O$ $\varphi = 0 - 10\%$ $Pr = 6.2$ $\gamma = 60°$ $Ri = 0.1 - 5$ $Re = 100$	FEM	• The fluid flow and heat transfer in the enclosure during the three convective regimes were significantly impacted by the solid volume percentage.
[111]		$TiO_2 - H_2O$ $\varphi = 0.01 - 0.05$ $d_p = 10 - 100nm$ $Ri = 0.01 - 10$	FDM	• The increase in heat transmission when nanoparticles are present at different Richardson numbers (small, medium, and large).
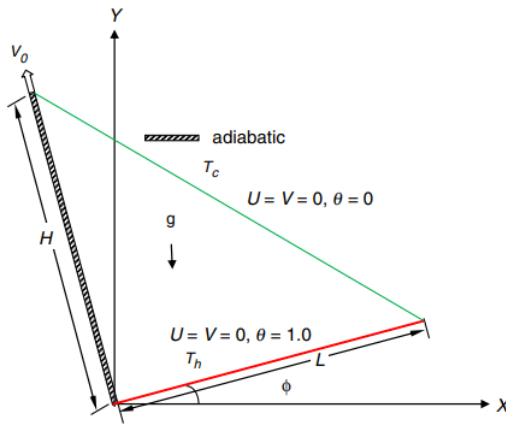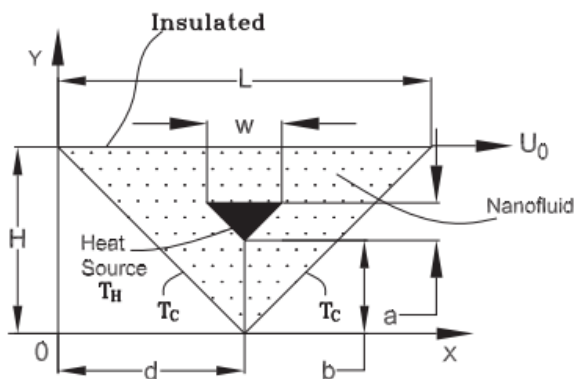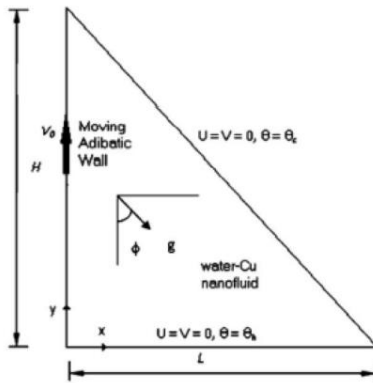
[112]		$Cu - H_2O$ $\gamma = 0° - 270°$ $Re = 100$ $Pr = 6.2$ $Ri = 0.1 - 10$	FEM	• When the tilt angle is larger, the average Nüsselt number increases slowly; but when the tilt angle is lower, it increases considerably more quickly.
[113]		$CuO - H_2O$ $Ra = 10^4 - 10^8$ $\varphi = 0 - 0.04$ $Ri = 0.05 - 50$	ALE	• Local and average heat transmission increase as the inclined wall elastic modulus and nanoparticle volume fraction increase.
[114]		$Cu - TiO_2 - H_2O$ $0.5 \leq Ri \leq 10$ $0 \leq Ha \leq 50$ $0 \leq N \leq 3$ $Pr = 6.2$	FEM	• Increasing the wave number from 0 to 3 improves heat transmission rate.
[115]		$Cu - H_2O$ $\gamma = 30° - 60°$ $Re = 10 - 1000$ $Da = 10^{-2} - 10^{-4}$ $\varphi = 0 - 4\%$	FVM	• Limiting convection and motion, a drop in the Da number causes a decrease in the nanofluid velocity and local Nu.
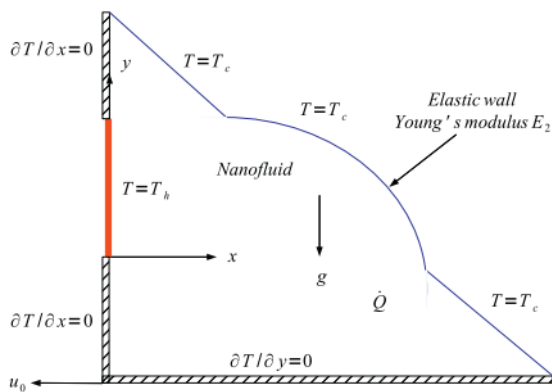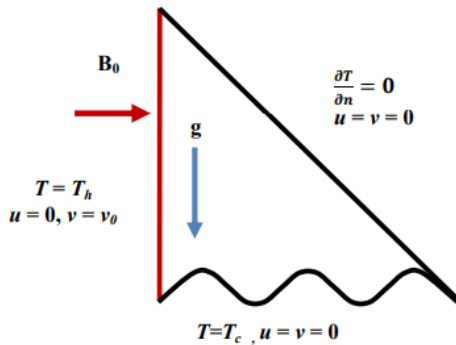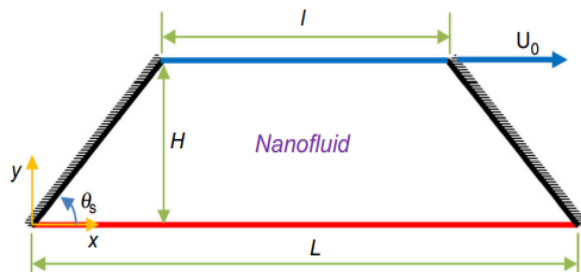
[116]
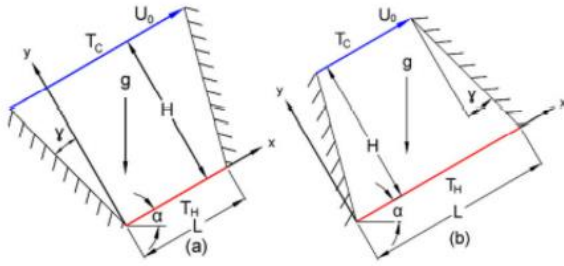
$Al_2O_3 - H_2O$

$Re = 0.1 - 10^4$

$Gr = 0.01 - 10^8$

$\gamma = 0° - 45°$

FEM

- Scientists have shown that the parameters of mixed convection heat transfer from the heated bottom wall of trapezoidal cavities are affected by the mechanical action of the sliding lid and by the buoyancy-driven flow.

[117]
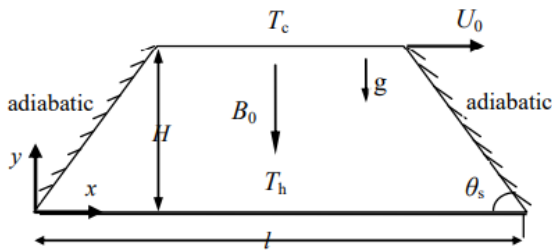
$Cu - H_2O$

$Re = 3 - 1000$

$\gamma = 15° - 60°$

$\varphi = 0 - 0.04$

$Ha = 25 - 100$

FVM

- In all Reynolds numbers and the solid volume percentage, the average Nüsselt number decreased as the Hartmann number Ha increased. The Hartmann number and entropy generation are inversely related.

[118]
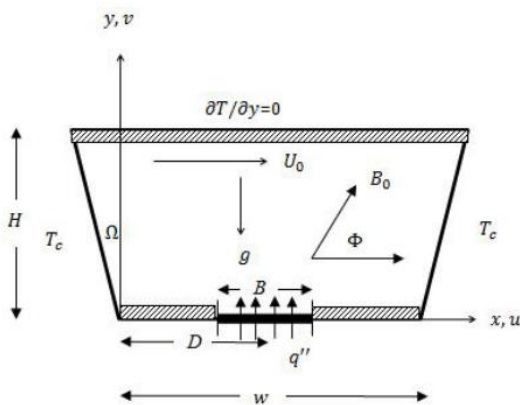
$\begin{pmatrix} Cu, \\ Al_2O_3, \\ Ag, \\ TiO_2 \end{pmatrix} - H_2O$

$Re = 10$

$0 \le \varphi \le 0.02$

$0.04 \le Ri \le 100$

$0 \le Ha \le 50$

FVM

- The average Nüsselt number rises as the solid volume percentage rises, and when Ri decreases.

[119]
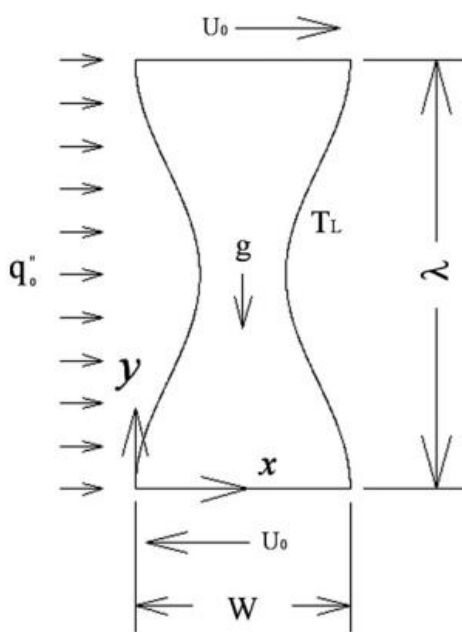
$$\begin{pmatrix} Cu, \\ TiO_2, \\ Al_2O_3 \end{pmatrix} - H_2O$$

$$Ri = 0.01 - 10$$

$$Gr = 10 - 10^4$$

FVM

- The Cu-Water nanofluid has the best heat transmission properties of the three nanofluids.

I.3. Conclusion

According to our knowledge, and after studying the mentioned literature and clarifying all the different physical and geometrical properties that the researchers gave in their previous research mentioned in Table I.1, the following points can be summarized:

1. The use of nanofluids gives higher rates of heat transfer.
2. The rise in heat transfer outweighed the rise in viscosity, which caused a decrease in pressure and strength.
3. Increasing the rate of heat transfer and decreasing pressure by increasing the concentration of nanoparticles.
4. The increase in Rayleigh number improves heat transfer.

After summarizing all the previous points from the previous studies, the following problem was raised:

Electronic devices suffer from high temperatures due to prolonged use, which can slow down or damage their components or even explode and set their contents on fire. Some devices, including batteries, light-emitting diodes (LEDs) and computer microprocessors, generate heat during operation. Overheating can reduce the efficiency and life of devices and waste energy. As far as we know, all devices have a variable temperature, which depends on the ambient temperature

and the time of use. While the researchers did considerable observation and investigation, they presented, generally, their results at a constant temperature, which goes against the scientific logic since the temperature of anybody fluctuates with time and distance. Therefore, this study was proposed to answer many questions, including:

1. Is there a difference between heat transfer at constant temperature and variable temperature?
2. Does the Aspect Ratio affect heat transfer?
3. Does using base fluids other than water in nanofluids give higher heat transfer?
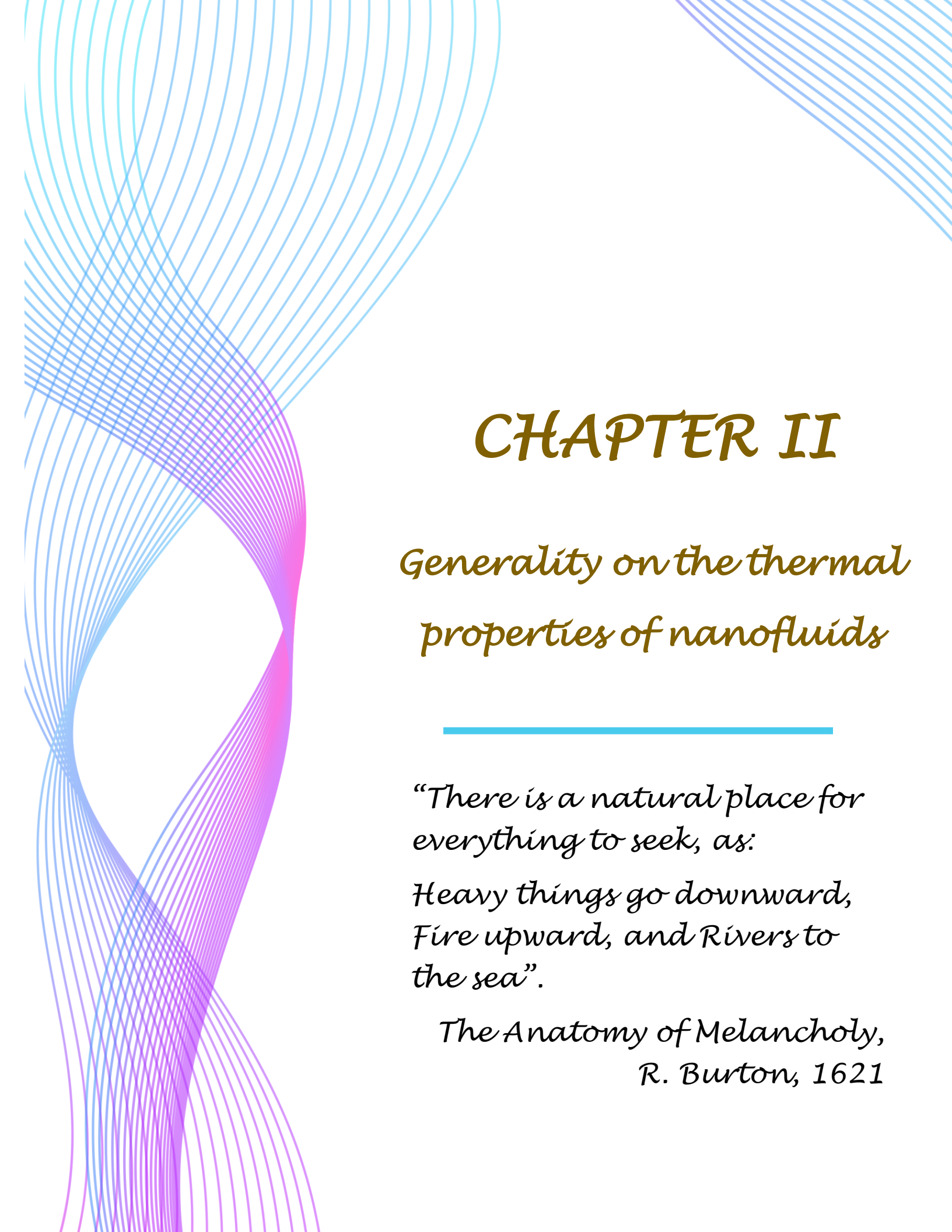
CHAPTER II

Generality on the thermal properties of nanofluids

"There is a natural place for everything to seek, as:

Heavy things go downward, Fire upward, and Rivers to the sea".

The Anatomy of Melancholy,
R. Burton, 1621

CHAPIER II

Generality on the thermal properties of nanofluids

II.1. Introduction

In recent years, high-speed advances in nanotechnology and heat transfer have created a new class of fluids known as nanofluids. These last consist of a basic fluid with suspended nanoparticles composed of metal or metal oxide for enhancing conduction and convection, and allowing for more heat transmission. Since discovering their unique thermal characteristics, nanofluids has generated significant attention.

In this chapter, the types of nanofluids and their preparation techniques will be reported, as well as numerous models, which are created to calculate the thermophysical properties of multiple nanofluids.

II.2. Types of nanofluids

In 1995, **Choi [2]** made the original suggestion that adding nanoparticles may improve the thermodynamic characteristics of thermo-fluids. Since then, research into creating nanofluids with unique thermophysical characteristics, including thermal conductivity, thermal diffusivity, and viscosity, has increased significantly **[126-130]**.

According to studies, adding small concentrations of nanoparticles to a base fluid improves the thermal properties; there is a wide range of nanoparticles: pure metal nanoparticles (Cu, Ag …), metal oxide nanoparticles (CuO, Fe_3O_4, Al_2O_3 …), and carbon nanoparticles (graphite, diamond). These nanoparticles have been integrated into fluids like water, Ethylene-Glycol, oil, and Ionic liquid.

II.2.1. Single-material nanofluids

The initial proposal for single-material nanofluids suggested by **Choi [2]** uses just one sort of nanoparticle to make the suspension, by a variety of preparation methods, where the single-material nanofluids may take on a variety of shapes, including pure metal, oxide metal, carbon and carbides.

Additionally, carbon atoms may create a range of bonds or allotropes of carbon may be created by the many ways in which carbon atoms can connect. Diamond, graphite, and amorphous carbon are

examples of typical carbon allotropes. Allotropes may have a wide range of carbon morphologies and topologies, including crystalline (i.e., diamond, carbon nanotubes, and graphite sheets).

A few nanometers to several hundred micrometers is the diameter range of carbon nanotubes. Single-Walled Carbon NanoTubes (SWCNT) are nanotubes made up of a single graphene layer that is wrapped around the tube itself. They may also be composed of many layers of graphene, in which case they are known as: "Multi-Walled Carbon NanoTubes" (MWCNT). Diamond molecular structures, carbon nanotube and a graphite are seen in the following figure.
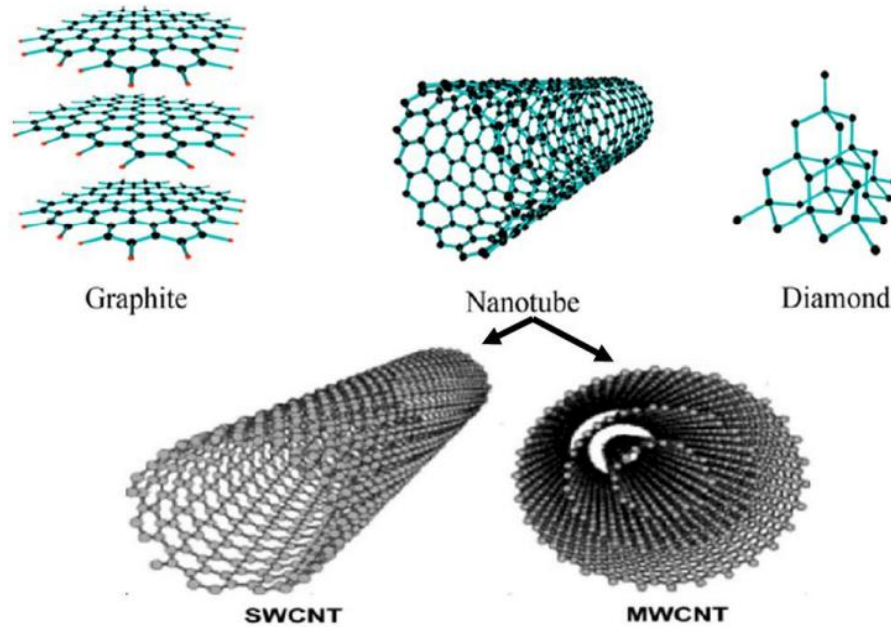
Figure II.1: Graphite, carbon nanotube and diamond molecular structures **[131].**

There are several investigations on carbon nanotube-based nanofluids, where **Z. Han [132]** showed in his study that thermal conductivity has increased by more than 200% for volume fractions of less than 1 %.

According to research by **Y. Wang & al. [133]**, the high temperature and uniform dispersion in a reactive environment impede the production of nanofluids derived from carbon nanotubes. To solve this dispersal issue, the nanotube surfaces are functionalized. The result obtained by **S. Berber & al. [134]** show that carbon nanotubes have the maximum thermal conductivity: k = 6600 W/m.K at ambient temperature aimed at an adiabatic nanotube.

II.2.2. Hybrid nanofluids

A developing class of nanofluids, hybrid nanofluids consists of more than one kind of nanoparticles floating in a pure fluid. Can produce hybrid nanoparticles using either physical or chemical processes. A few examples of hybrid nanofluids are: Alumina-graphene/H_2O, Ag-MgO/H_2O, etc.

One of the first researchers to start researching hybrid nanoparticles CNT, Cu, and Au nanoparticles dispersed in water and their hybrids (CNT-Au/H_2O and CNT Cu/H_2O) were studied by **Jana & al. [135]**; the findings demonstrated that the Cu/H_2O nanofluid had the best thermal conductivity of all the tested samples and rose linearly as particle concentration increased.

II.3. Preparation of a nanofluid

The production of high-quality nanofluid relies heavily on uniform dispersion and stable suspension of nanoparticles in the host liquid.

The characteristics of nanofluids can only be studied and used if the dispersion and suspension are stables. The solution to dispersing nanoparticles before they agglomerate is the key to making stable nanofluids. It has proven possible to create nanofluids using both physical and chemical methods. Scientists are also developing different methods to fabricate fluids at the nanoscale.

II.3.1. One-step method

The one-step procedure involves directly creating nanoparticles using the physical vapor deposition (PVD) technique or the liquid chemical method, followed by synthesizing nanofluids. Also, desiccating storage, transportation, and discontinuous dispersion of nanoparticles are avoided with the method, which minimizes nanoparticle buildup and increases fluid stability. Nanoparticle synthesis and dispersion into the base fluid happen concurrently in a single step. For instance, when a thin layer of base fluid forms on a container because of the spinning of a disk by the effect of centrifugal force, raw materials are heated to cause them to evaporate, and the vapor is condensed into nanoparticles when it comes into contact with the cold base fluid film, resulting in the formation of nanofluid.

The following figure shows the one-step vapor deposition method for preparation of a nanofluid.
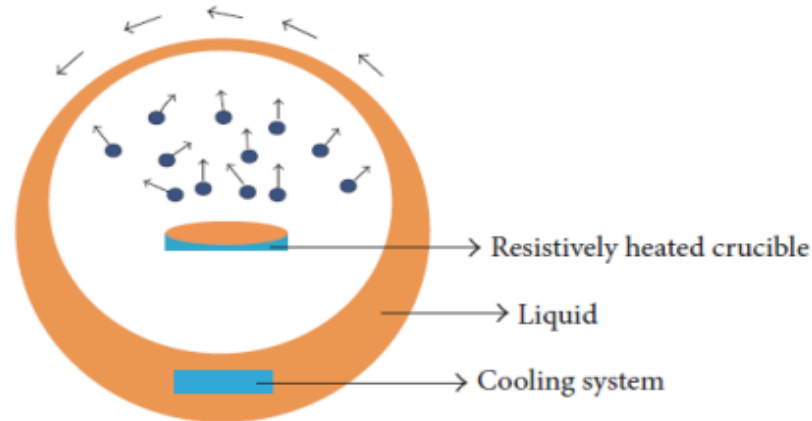
Figure II.2: A one-step vapor deposition method for preparation of a nanofluid **[136]**.

II.3.2. Two-steps method

The most popular approach for creating nanofluids is the two-steps procedure (Figure II.3); in this process, nanoparticles, nanofibers, nanotubes or other nanomaterials are first employed to create dry powders by chemical or physical means. Then, the nanosized powder will be distributed into a base fluid with vigorous magnetic force agitation, ultrasonic agitation, high-shear mixing, homogenizing, and ball milling. Because commercial production levels of nanopowder synthesis methods have already been reached; the two-step process is the most cost-effective way to generate nanofluids on a large scale. Nanoparticles prefer to agglomerate because of their large surface area and surface characteristics.
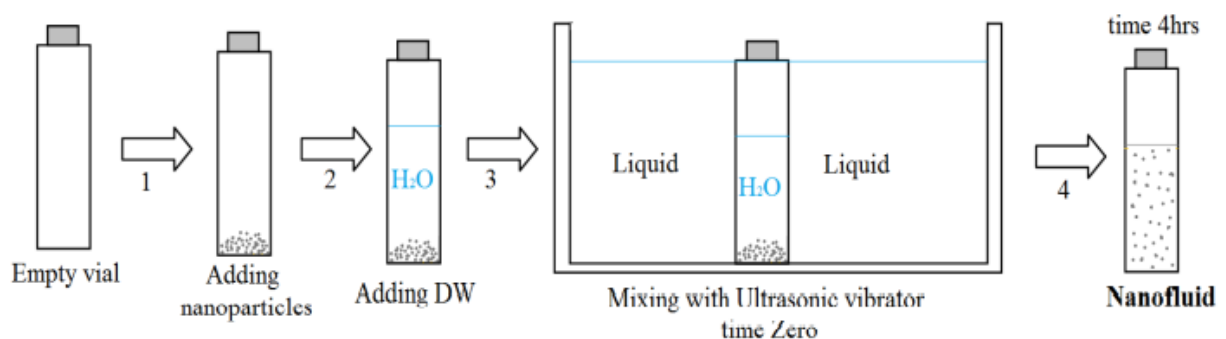
Figure II.3: A two-steps process for creating nanofluids **[136]**.

II.4. Thermophysical properties of nanofluids

The following figure shows the thermal characteristics of common heat transfer fluids like Ethylene-Glycol, motor oils, and water are much worse than those of solids. It shows the difference between the solids and base fluids in thermal conductivities. It also clarifies why a nanofluid-containing particulate diamond is superior to other nanofluids, making it especially intriguing. Diamond has the maximum thermal conductivity of any solids because of its robust carbon-carbon (C-C) covalent bonds and low phonon scattering **[137]**. In contrast, metal elements such as silver (Ag) have a high heat conductivity, nevertheless, the high conductivity of it makes unsuitable for many applications. Low-volume (small-size) diamonds in host fluids or compounds have a variable thermal conductivity **[138]**.
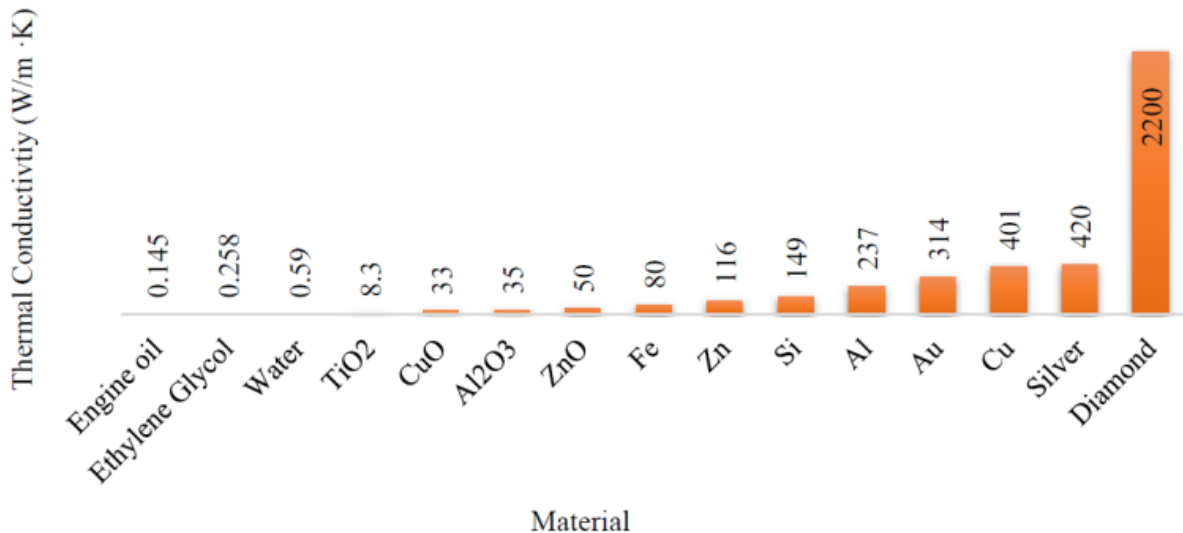
Figure II.4: Various thermal conductivities for base fluids and solids at 25 °C **[138]**.

II.4.1. Volume fraction

The volume fraction is the most critical property for a nanofluid since it is used as a starting point for calculating all the others properties. The value of the volume fraction is changed between 0 (pure base fluid) and 1. The following relationship gives the volume fraction:

$$\varphi = \frac{V_s}{V_T}$$

(I.1)

The value of the base fluid and the caliber of the nanoparticles dispersed in it have an imperative impact on nanofluids physical thermal characteristics. Also, affecting the nanofluid physical characteristics are the particles shapes and sizes, the fluid temperature, and the concentration of suspended particles. The thermophysical characteristics of nanofluids are shown in the following figure, which will be discussed in greater depth below.
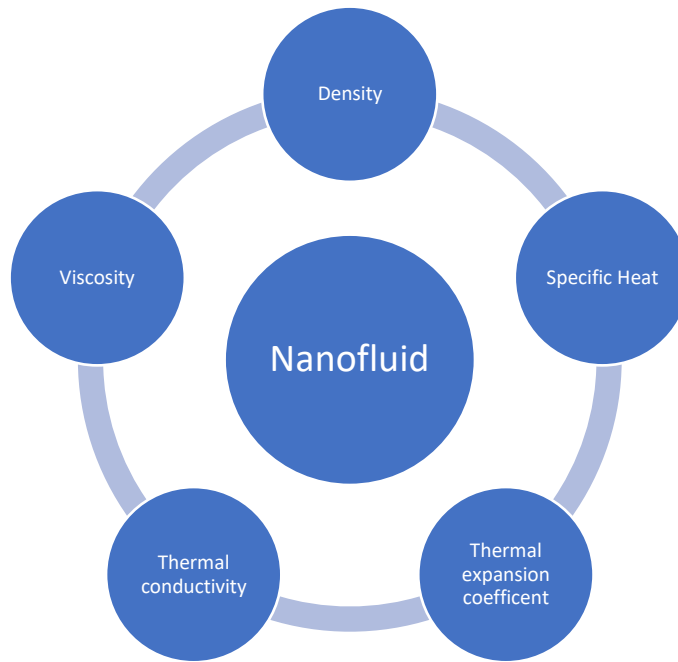
Figure II.5: Thermophysical characteristics of nanofluids.

II.4.2. Density

One of the less investigated thermophysical characteristics of nanofluids is density. Determining density is crucial for estimating the nanofluid capacity for heat transmission, even if it has no direct bearing on thermal performance. The flow characteristics of nanofluids are governed by density, which is significant. Pressure drop, Nüsselt number, and Reynolds number are all influenced by the density of the nanofluid. Nanomaterials distributed in a base fluid make up a nanofluid. Because the distributed nanomaterial weighs more than the base fluid, the base fluid density is eventually increased. This rise in density directly impacts the entire functionality of the nanofluid. The density of a fully homogenous nanofluid is calculated (with excellent nanoparticle dispersion in the fluid) in terms of (φ) at a certain temperature (T).

The mixing rule developed by Pak and Cho serves as the primary method for calculating the density of nanofluid **[139]** as:

$$\rho_{nf} = (1-\varphi)\rho_f + \varphi\rho_s$$ (I.2)

The density of the nanofluid has often been calculated using this equation. It provided accurate forecasts for alumina nanofluids **[140, 141]**. When the temperature is greater and the concentration is lower, it is more suited for estimating the density of nanofluids **[142]**. Another research stated using this equation that there was consistency between experimental and theoretical values for alumina nanofluids **[143]**. However, ZnO nanofluids were discovered to be in disagreement. This shows that the equation is incompatible with nanofluids other than those based on alumina. **Teng and Hung [142]** also offer the following equation based on the same method:

$$\rho_{nf} = \frac{(1-\varphi)\rho_f\rho_f + \varphi\rho_s\rho_s}{(1-\varphi)\rho_f + \varphi\rho_s}$$ (I.3)

Additionally, **Khanafer and Vafai [144]** provided the following equation for estimating the density of alumina nanofluids using experimental data from **Ho & al. [141]**:

$$\rho_{nf} = 1001.064 + 2738.6191\varphi - 0.2095T$$ (I.4)

The equation demonstrates the relationship between the density of nanofluid and concentrations between 0 and 4 vol%, and temperatures between 5 °C and 40 °C.

II.4.3. Specific heat

A nanofluid capacity for heat transmission depends on its specific heat; therefore, understanding it is equally crucial. Its specific heat must be determined to calculate a nanofluid thermal conductivity. A solid specific heat is often lower than a liquid. This is due to the fact that liquids are better at absorbing heat than solids. Therefore, the heat specific of liquids must be adversely affected by including solid particles. Nanofluids are complicated and may act differently because they include solid nanoparticles distributed throughout. It is still unknown, however, exactly how the addition of the nanoparticles influenced the specific heat.

The relationships shown below are useful for calculating a nanofluid specific heat. Many researchers, such as **Pak and Cho [139]**, used:

$$\left(\rho C_p \right)_{nf} = (1 - \varphi)\left(\rho C_p \right)_f + \varphi \left(\rho C_p \right)_s \qquad (\text{I.5})$$

Others, such as **Xuan and Roetzel [145]** employed:

$$\left(\rho C_p \right)_{nf} = (1 - \varphi)\left(\rho C_p \right)_f + \varphi \left(\rho C_p \right)_s \qquad (\text{I.6})$$

II.4.4. Coefficient of thermal expansion

A material coefficient of thermal expansion describes how quickly its dimensions change when its temperature rises or falls. There are linear, area, and volume expansion coefficients that may be derived from the various measures of size change. The change in density brought on by temperature in fluid incompressible (density unaffected by pressure) is referred to as the coefficient of thermal expansion **[146]**.

The value of the thermal coefficient expansion for nanofluids can be determined as follows:

$$\left(\rho \beta \right)_{nf} = (1 - \varphi)\left(\rho \beta \right)_f + \varphi \left(\rho \beta \right)_s \qquad (\text{I.7})$$

According to **Kim & al. [147]**, a fluid thermal expansion coefficient is substantially higher than that of solid nanoparticles; Equation (II.7) was streamlined to the following form:

$$\left(\rho \beta \right)_{nf} = (1 - \varphi)\left(\rho \beta \right)_f \qquad (\text{I.8})$$

II.4.5. Thermal conductivity of nanofluids

In general, thermal conductivity is a significant necessity; still, it is especially significant in our study because it is a key part of how heat moves from one place to another. It can show how well fluid or solid moves heat because conductivity depends on temperature. The thermal conductivity of the nanofluid changed not only with the temperature but also with the volume fraction. From the resolution of the energy equation, many thermal conductivity calculation models have been made to estimate the conductivity of nanofluids, which are made up of very regular parts. The following models are used to determine a nanofluid thermal conductivity.

II.4.5.1. Maxwell model [148]

One scientist that is interested in determining the thermal conductivity of a fluid containing

suspended spherical particles is Maxwell. He used the assumption that the fluid includes many spherical particles. He reasoned that there must be many particles in the fluid, each having an equal diameter. The particles are separated by a sufficient distance leading to the absence of mutual interaction between them; consequently, the medium is strongly dilated (no contact between the particles). Maxwell equation is given by:

$$\frac{k_{nf}}{k_f} = \frac{\left(k_s + 2k_f\right) - 2\varphi\left(k_f - k_s\right)}{\left(k_f + 2k_s\right) + 2\varphi\left(k_f - k_s\right)}$$

(I.9)

II.4.5.2. Hamilton-Crosser model [149]

The Maxwell model limit was solved using the Hamilton and Crosser model. The latter only applies to spherical particles, rendering the model ineffective for describing the behavior under study. Due to the concept of the geometric property known as sphericity, this typical was created to increase the efficiency of calculating the thermal conductivity of nanofluid regardless of the nanoparticle shape. The ratio of the surface of a sphere with the same volume as a nanoparticle to that surface is how this factor is defined. The following expression provides the model of thermal conductivity is as follows:

$$k_{nf} = \frac{k_s + (n-1)k_f - (n-1)(k_f - k_s)\varphi}{k_s + (n-1)k_f + (k_f - k_s)\varphi} k_f$$

(I.10)

Where:

n= $3/\psi$ (empirical form)

n=3 (spherical particles)

n=6 (cylindrical particles).

Similarities exist between the Maxwell and Hamilton-Crosser models for $\psi=1$ (spherical particles).

II.4.5.3. Yu and Choi model [150]

Yu and Choi presented a new phrase for estimating thermal conductivity. They suggested modeling nanofluids as basic liquid and solid particles separated by a nanometric layer, which serves as a thermal link between the fluid and the particles. Additionally, they presumptively believed that the liquid thermal conductivity is lower than that of the nanoscale layer.

$$k_{nf} = \frac{k_s + 2k_f + 2\varphi(k_s - k_f)(1+\beta)^3}{k_s + 2k_f - 2\varphi(k_s - k_f)(1+\beta)^3} k_f \qquad (\text{I.11})$$

II.4.5.4. Bruggeman model [151]

The model provided by Bruggeman seems to reflect certain experimental results more closely than previous models in the situation of spherical nanoparticles with no constraint on the concentrations of nanoparticles.

$$k_{nf} = \frac{(3\varphi - 1)\dfrac{k_s}{k_f} + \left[3((1-\varphi) + \sqrt{\Delta})\right]}{4} k_f \qquad (\text{I.12})$$

Modeling the thermal conductivity behavior is done by providing mathematical correlations. Some of the mathematical relationships for thermal conductivity are included in the following table.

Table II.1: Mathematical correlations for thermal conductivity (k_{nf}) of nanofluids in several literatures.

Investigator	Correlation	Comments
S. K. Gupte & al. [152]	$k_{nf} = k_f(0.0556Pe + 0.1649Pe^2 - 0.0391Pe^3 + 0.0034.$	Translational motion effects of nanoparticles.
J. Avsec & al. [153]	$k_{nf} = \left[\dfrac{k_s + (n-1)k_f - (n-1)\alpha_e(k_f - k_s)}{k_s + (n-1)k_f + (n-1)\alpha_e(k_f - k_s)}\right]k_f$	Based on statistical nanomechanics and taking into account the thickness of the fluid layer.
W. Evans & al. [154]	$k_{nf} = \left(1 + 3\varphi\dfrac{\gamma - 1}{\gamma + 2}\right)k_f$	At a low particle fraction
S. Pil Jang & al. [155]	$k_{nf} = k_f(1-\varphi) + \beta k_s\varphi + \varphi h\delta_T$	Depends on the degree to which the base fluids and particles transmit heat. Nanoparticles may collide with one another and undergo nano-convection.

M. H. Esfe & al. [156]	$\dfrac{k_{nf}}{k_f} = 0.4 + 0.0332\varphi + 0.00101T + 0.000619T + 0.0687\varphi^3$ $+ 0.0148\varphi^5 - 0.00218\varphi^6 - 0.0419\varphi^4 - 0.0604\varphi^2$	For MgO/Water-EG nanofluid.
X. Li & al. [157]	$k_{nf} = (4.583 + 12.71\varphi)k_f$	For SiC/EG nanofluid.

II.4.5.5. Factors that impact thermal conductivity

The following figure depicts a few parameters that influence thermal conductivity.
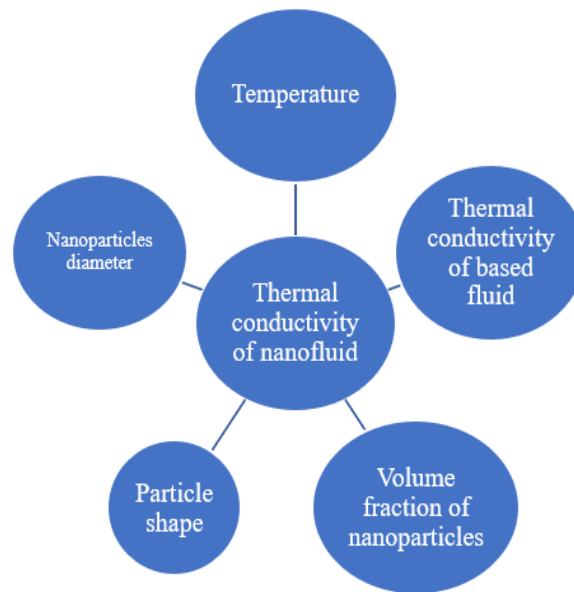
Figure II.6: A few factors that have an impact on the thermal conductivity.

a. Influence of nanoparticle and temperature size on thermal conductivity

The temperature has a huge impact on how the thermal conductivity of nanofluids improved. The thermal conductivity of Al_2O_3-Ethylene Glycol dioxide was investigated in the work by **Patel & al. [158]**, for volume fractions of 1% and 3%, and for particle sizes of 11 and 150 nm. Figure (II.7) shows an rise in the surface area to volume ratio, the thermal conductivity increases with temperature and also diminutions with nanoparticle size, allowing for more effective heat transmission to the base liquid with smaller nanoparticle sizes. Additionally, the thermal conductivity has risen due to greater Brownian motion with smaller nanoparticles.
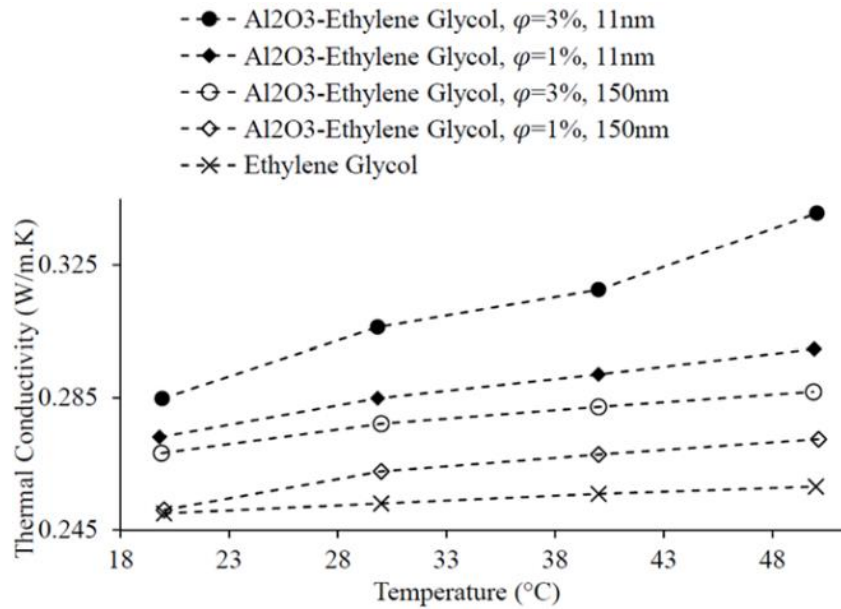
Figure II.7: Thermal conductivity of an Al$_2$O$_3$-Ethylene Glycol nanofluid varies with temperature and is characterized by particles with a diameter of 150 nm **[161]**.

The thermal conductivity of Al$_2$O$_3$-H$_2$O nanofluid was examined in another work by **Chun & al. [159]** between 294 K and 344 K, and it was discovered that the conductivity improved with temperature. Using a 0.00026% volume fraction of nanoparticles, **Paul & al. [160]** investigated the temperature dependence of Au–H$_2$O nanofluid thermal conductivity as a nanoparticle size. According to their findings, decreasing the nanoparticle size enhanced the conductivity, as seen in the following figure.
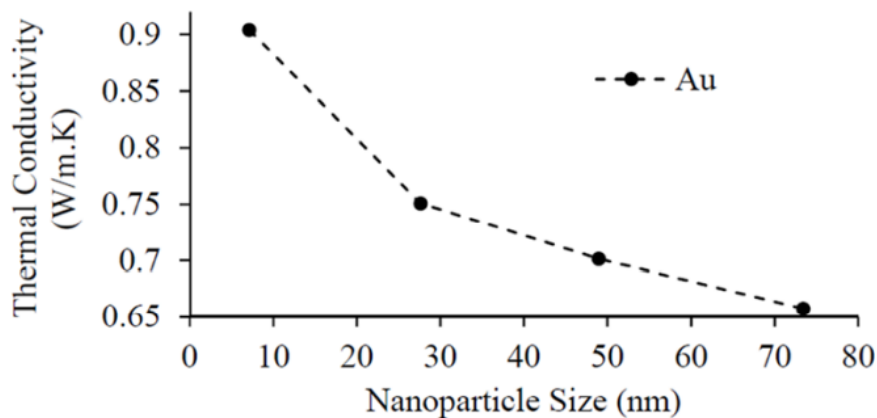
Figure II.8: Thermal conductivity of the Au-H$_2$O nanofluid varies with temperature and nanoparticle size **[161]**.

b. Influence of the volume fraction of nanoparticle on thermal conductivity

The effect of the volume percentage of nanoparticles on the thermal conductivity of different nanofluids has been investigated by several scientists. At different temperatures of nanofluid, the following figure illustrates the change in the conductivity ratio with volume fraction. The bulk of the research investigations underlined the fact that growing amounts of solid nanoparticles improve nanofluids capacity to transfer heat. While most investigations discovered that the connection was linear, others discovered that it was nonlinear. This phenomenon may be related to the relations within the system particles (**Choi & al. [162]**) or the buildup of nanoparticles in liquids, as indicated in **[163]**.
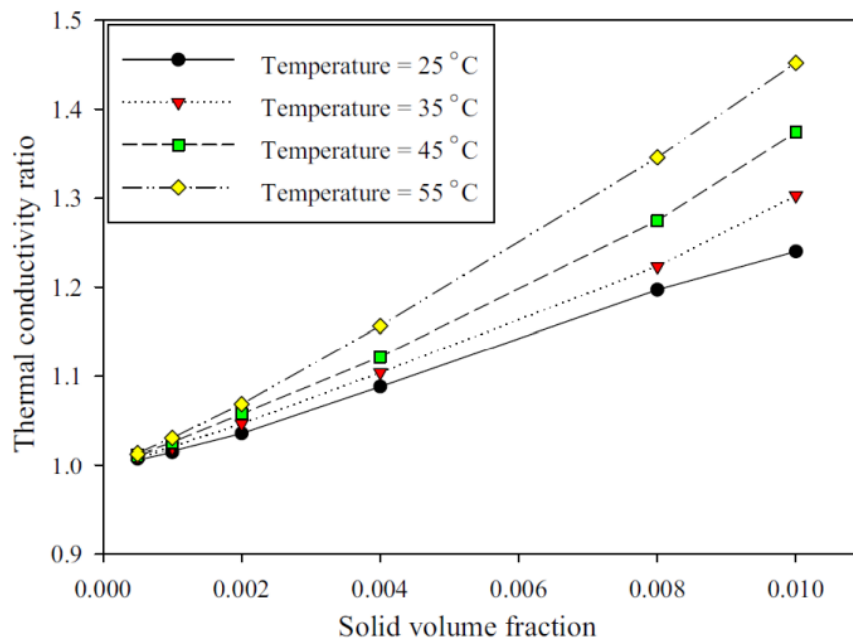
Figure II.9: Thermal conductivity ratio using volume fraction at different temperatures **[164]**.

c. Influence of the base fluid on thermal conductivity

There have been numerous research looking at how fundamental fluids affect nanoparticles, yet the outcomes of each study have varied. According to certain study's findings **[165-167]**, the thermal conductivity improvement was inversely related to the pure fluid thermal conductivity. A study by **Wang & al. [168]** shows that the thermal conductivity of CuO and Al_2O_3 nanoparticle suspensions in various base liquids, including EG, EO, H_2O, and VPO, EG had the maximum

thermal conductivity ratio of the other base liquids studied. They discovered that while the thermal conductivity of the base liquid drops, nanofluids thermal conductivity rises. Although, other researchers **[169]** found the contrary. The findings of **Chopkar & al. [170]**,which were based on improving the thermal conductivity of nanofluids, are in opposition to the results shown above. It utilizes base fluids with high conductivity.

Furthermore, a recent study reported in **[171]** by selecting three nanoliquids for their experiment, including (35% BG-0.5% SiC), (water-0.5% SiC), and (0.5% SiC-35% EG), to find the most pure fluids to utilize for solar PV applications. These liquids were tested at temperatures ranging from 25 to 60 °C. Finally, they found no appreciable differences in the three nanoparticles thermal conductivity as shown in the following figure.
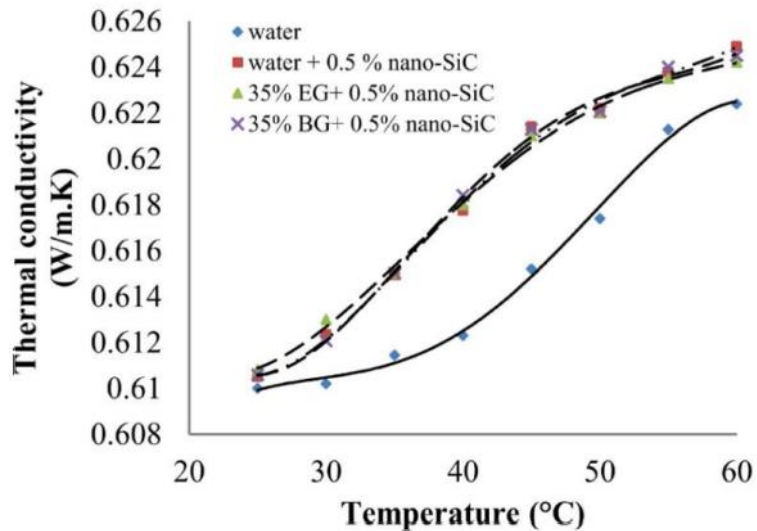
Figure II.10: Thermal conductivity of various nanofluids and the effect of the base fluid **[171]**.

Another research **[172]** investigated experimentally how base fluids affected the thermophysical characteristics of SiO2 nanofluids. In terms of volume, Ethylene-Glycol and water ratios were 40:40 and 60:40, respectively. By dispersing SiO_2 nanoparticles in (EG) and (W) combined in "60:40" (60EGW) and "40:60" (40EGW) ratios by size, they created nanofluids. The stability of nanofluids using zeta potential, electrical conductivity, and pH values was investigated. According to the experimental findings, the thermal conductivity of SiO2 molecules improved by 34% and 32% when used with the two pure fluids. Additionally, it has discovered that nanofluids based on 40EGW had a greater thermal conductivity.
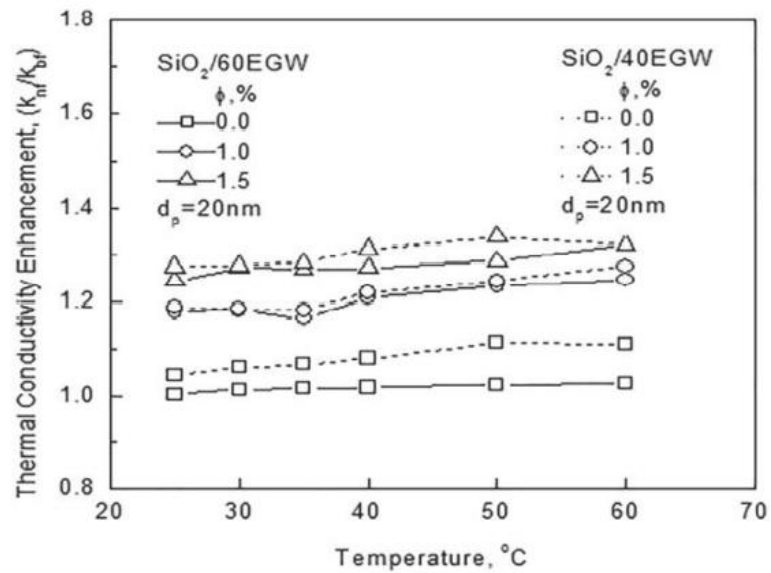
Figure II.11: Comparison of SiO$_2$/40EGW and SiO$_2$/60EGW nanofluids for improving thermal conductivity **[172]**.

d. Influence of particle shape on thermal conductivity

Scientists examined how the morphologies of nanoparticles affected thermal conductivity and found that although volume ratios had a better thermal conductivity; nanofluids containing nanoparticles have a larger surface area.
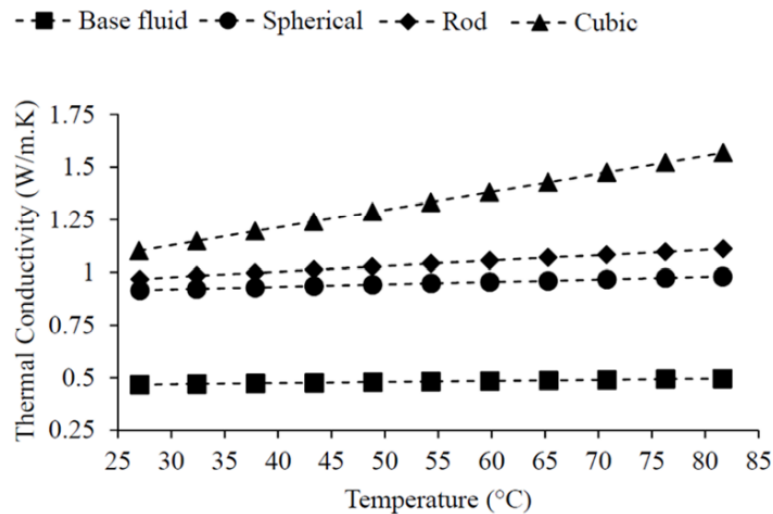
Figure II.12: Influence of nanoparticle shape on the thermal conductivity of a nanofluid composed of TiO$_2$ and water at a concentration of 2.5% **[161]**.

Maheshwari & al. [173] used spherical nanoparticles (22.9 nm), cubic nanoparticles (51.87 nm), and rod nanoparticles to study TiO_2-H_2O (43.08 nm) nanofluid thermal conductivity. They discovered that the thermal conductivity of the nanofluid with cubic nanoparticles was the greatest and that of the nanofluid with spherical nanoparticles was the lowest, as shown in Figure II.12. They verified that using round nanoparticles stabilizes the atoms and lessens the blocking issue.

II.4.6. Dynamic viscosity

A fluid ability to resist deformation while in motion is known as viscosity. So, the viscosity is an indicator of a fluid internal friction. The fluid that has significant internal friction is extremely viscous. The quality of the nanoparticle dispersion in the pure fluid and the temperature significantly impact the viscosity dynamic of the nanofluid, which can be computed from the nanofluid volume fraction and the base fluid dynamic viscosity.

There are many mathematical models for calculating the dynamic viscosity of a nanofluid, and some of them can be extracted as follows.

II.4.6.1. Einstein model [174]

This model gives the dynamic viscosity of a nanofluid made up of a dilute suspension of rigid fine particles.

$$\mu_{nf} = (1 - 2.5\varphi)\mu_f \qquad\qquad (\text{ I.13})$$

Since its experimental validation, Einstein's formula has been accepted as adequate for spherical particle suspensions at low volume concentrations (usually less than 1%). As a point of emphasis, the impacts of inter-particles interaction and particles size are not taken into account by this model.

II.4.6.2. Brinkmann model [175]

By adding a concentration of nanofluids in volume of less than 4%, Brinkmann's formula complemented Einstein's model as follows:

$$\mu_{nf} = \frac{\mu_f}{(1 - \varphi)^{2.5}} \qquad\qquad (\text{ I.14})$$

However, particle collisions are ignored in this connection, which shows a nonlinear increase in

dynamic viscosity with increasing concentration.

II.4.6.3. Pack and Cho model [139]

Pack and Cho suggested the following formula for Al_2O_3 nanoparticles distributed in water:

$$\mu_{nf} = (533.9\varphi^2 + 39.11\varphi + 1)\mu_f \qquad\qquad (I.15)$$

II.4.6.4. Maiga & al. model [176]

Other correlations with extremely particular applications have been presented in the literature. By comparing this connection with the Brinkman and Einstein models, we find that the two drastically underestimate the measured nanofluid viscosity values.

$$\mu_{nf} = (123\varphi^2 + 7.3\varphi + 1)\mu_f \qquad\qquad (I.16)$$

II.4.6.5. Influence of temperature on dynamic viscosity

By increasing the volume fraction of nanoparticles in a carrier fluid, its thermal conductivity is increased, which is interesting for heat transfer. However, by increasing (φ), the viscosity of the nanofluid obtained is necessarily increased, which leads to an increase in pressure drops in the heat exchangers and would require a greater loss of energy to set this coolant in motion.

As the dynamic viscosity increases, the ability of the fluid to flow decreases. The viscosity of liquids generally tends to decrease when the temperature of the latter increases. For this, there are semi-empirical correlations based on experimental results used to calculate the dynamic viscosity of water **[177]** and a nanofluid (Al_2O_3-H_2O) **[178]**.

II.5. Conclusion

In this chapter, types of nanofluids and their preparation methods were reported, and many models were written to calculate the thermophysical properties of various nanofluids. It was difficult to compare different experimental studies on nanofluids because each was performed on nanoparticles of different sizes and shapes. Different theoretical perspectives have evolved to comprehend the cause and importance of this rise in the thermal conductivity of nanofluids. However, none of them succeeded in adequately describing all the experimentally obtained behaviors..
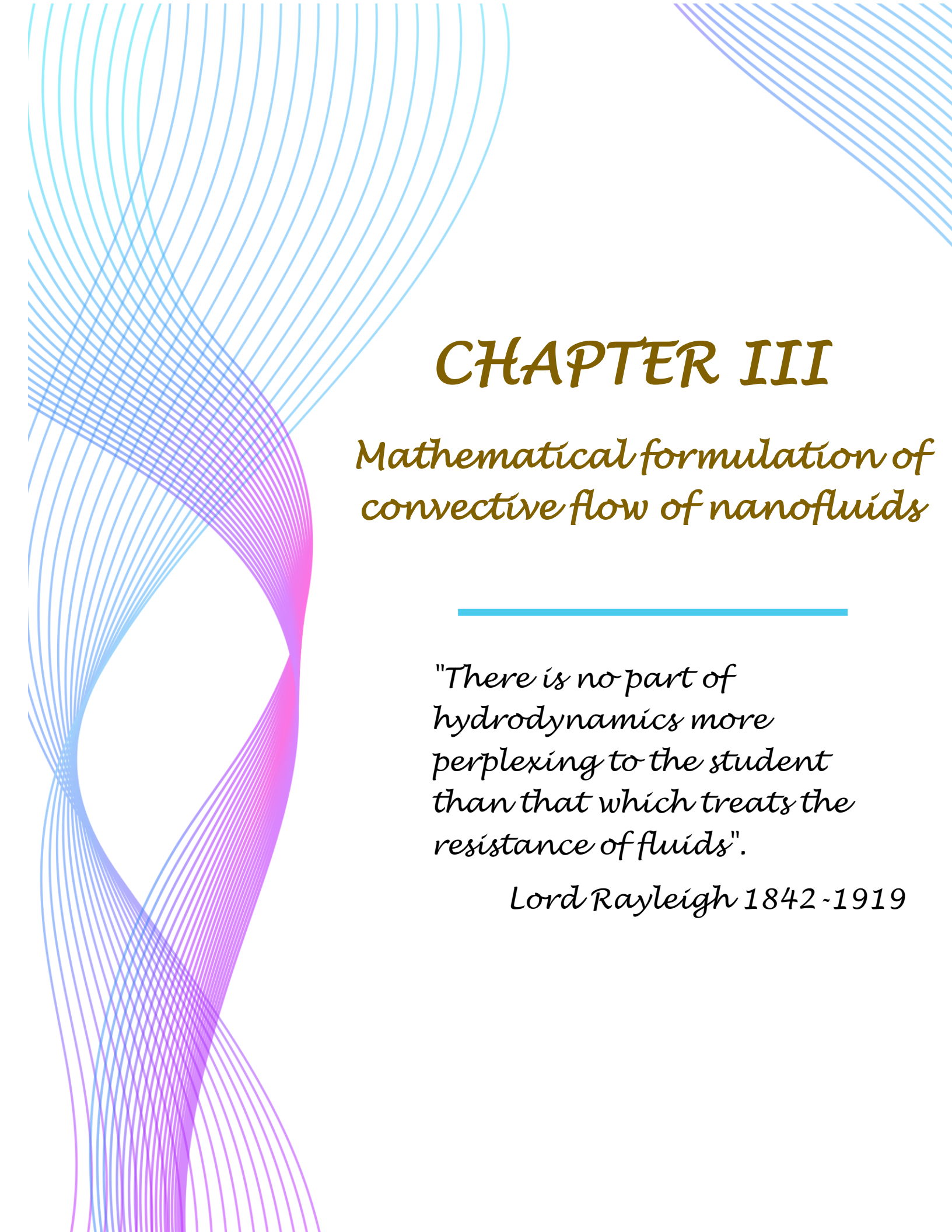
CHAPTER III

Mathematical formulation of convective flow of nanofluids

"There is no part of hydrodynamics more perplexing to the student than that which treats the resistance of fluids".

Lord Rayleigh 1842 -1919

CHAPTER III

Mathematical formulation of convective flow of nanofluids

III.1. Introduction

There are different types of heat transport methods, including conduction, convection, and radiation. The heat exchanges between a surface and a flowing fluid at various temperatures are referred to as convection. Several numerical and experimental techniques are available today to study convection, but numerical simulation is still the most practical and affordable approach compared to experimental techniques. The various heat transfer processes and how they are connected may be understood by numerical modeling. To formally define natural and forced convective, it is essential to specify the relationship between the pressure, temperature, and velocity fields as determined by the mass, momentum, and energy equations.

This chapter aims to evaluate the behavior of a laminar flow; this part is devoted to the modeling and the setting in equations of the problem (continuity, momentum, energy) with the boundary conditions and reveals the dimensionless reference numbers and the thermophysical properties of nanoparticles and base fluids used in the numerical simulation.

III.2. General equations

Convection mathematical model is based on equations that integrate numerous characteristics such as pressure, temperature, and velocity. These are variations on the general equations stated below (continuity, momentum, and energy).

III.2.1. Equation of continuity

The principle of conservation of the mass, during a flow, is expressed mathematically and represented as follows:

$$\frac{\partial \rho}{\partial t} + div(\rho v) = 0 \qquad\qquad (\text{II.1})$$

Assuming that the density is constant, the following equation is simplified:

$$\frac{\partial u}{\partial x} + \frac{\partial v}{\partial y} = 0 \qquad\qquad (\text{II.2})$$

III.2.2. Momentum equations

The principle of conservation of the quantity of movement makes it possible to establish the relations between the characteristics of the fluid and its movement and the cause, which produces it. The rate of change of momentum delimited in the volume may be equivalent to the total of all outside forces acting on it. For an incompressible Newtonian fluid, the Navier-Stokes equations for mixed convection in 2D are written in the following form:

- Momentum equation along the axis (x):

$$u\frac{\partial u}{\partial x} + v\frac{\partial u}{\partial y} = -\frac{1}{\rho}\frac{\partial p}{\partial x} + v\left(\frac{\partial^2 u}{\partial x^2} + \frac{\partial^2 u}{\partial y^2}\right) \qquad (\text{II.3})$$

- Momentum equation along the axis (y):

$$u\frac{\partial v}{\partial x} + v\frac{\partial v}{\partial y} = -\frac{1}{\rho}\frac{\partial p}{\partial y} + v\left(\frac{\partial^2 v}{\partial x^2} + \frac{\partial^2 v}{\partial y^2}\right) + (\rho\beta)g(T\text{-}T_c) \qquad (\text{II.4})$$

III.2.3. Equation of energy conservation

It is a local expression of the first law of thermodynamics, which translates that the variation with respect to time of the total energy per unit volume. This principle connects different terms:

$$\frac{\partial T}{\partial t} + u\frac{\partial T}{\partial x} + v\frac{\partial T}{\partial y} = \alpha\left(\frac{\partial^2 T}{\partial x^2} + \frac{\partial^2 T}{\partial y^2}\right) \qquad (\text{II.5})$$

III.2.4. Boussinesq approximation

The Boussinesq approximation **[179]** was first presented by **Oberbeck [180]**. Lorenz used it (1881) to establish a correlation in natural convection. Since then, works dealing with natural convection in fluids within the framework of the so-called Oberbeck-Boussinesq hypothesis have been the subject of a great bibliography in recent years.

The Oberbeck-Boussinesq approximation states that the various thermophysical properties of the fluid are independent of temperature and pressure. Moreover, the fluid is supposed to be incompressible but also dilatable, the density of the fluid is supposed to be constant, equal to its average value (ρ_f), in all the formalism except for the term of thrust ($\rho\vec{g}$). Where its first order

expansion gives the density concerning temperature:

$$\rho = \rho_f \left[1 - \beta(T - T_f) \right] \tag{II.6}$$

Many issues involving natural and mixed convection may be solved using this first-order expansion since the temperature differential inside the fluid never exceeds 10 degrees. The thermal expansion coefficient of a fluid is defined as:

$$\beta = -\frac{1}{\rho}\left(\frac{\partial \rho}{\partial T}\right)_p \tag{II.7}$$

III.3. Thermophysical characteristics of nanofluids used in the investigated application

The thermal conductivity of the nanofluid has been calculated using the model of **Maxwell [148]** as Equation (II.9). The dynamic viscosity of the nanofluid is computed as Equation (II.14) in accordance with the model of **Brinkmann [175]**. The density, the specific heat capacity, and the coefficient of thermal expansion of the nanofluid are computed using the Equations (II.2), (II.6) and (II.8) **[139, 145, 146]**. The thermal properties of water, nanofluid (H_2O–Ethylene Glycol) and nanoparticles are provided in the following table.

Table III.1: Thermophysical characteristics of nanoparticles and base fluid at 25 °C.

	ρ (kg/m³)	C_p (J/kg.K)	k (W/m.K)	μ (kg/m.s)	β (1/K)
Water **(H_2O)**	997.1	4179	0.613	0.001002	21×10^{-5}
50%:50% mixture **H_2O–Ethylene Glycol**	1056	3288	0.425	0.003748	0.000341×10^{-5}
Copper **(Cu)**	8954	383	400	/	1.67×10^{-5}
Silver **(Ag)**	10500	235	429	/	1.89×10^{-5}
Magnesium oxide **(MgO)**	3560	955	45	/	1.13×10^{-5}
Titanium dioxide **(TiO_2)**	4250	686.2	8.9538	/	0.9×10^{-5}
Aluminum oxide **(Al_2O_3)**	3970	765	40	/	0.85×10^{-5}

III.4. Description of the model and simplifying assumptions

Our thesis is devoted to studying mixed convection in a cavity with length (L) and height (H), as shown in Figure III.1. The Aspect Ratio is defined as (AR = H/L) for the cavity, which can be filled with nanofluids containing different concentrations of nanoparticles (or volume fractions). The thermal characteristics of the base fluid and nanoparticles at a reference temperature of 25 °C are reported in Table III.1. The Boussinesq approximation is also believed to be valid for buoyancy force.
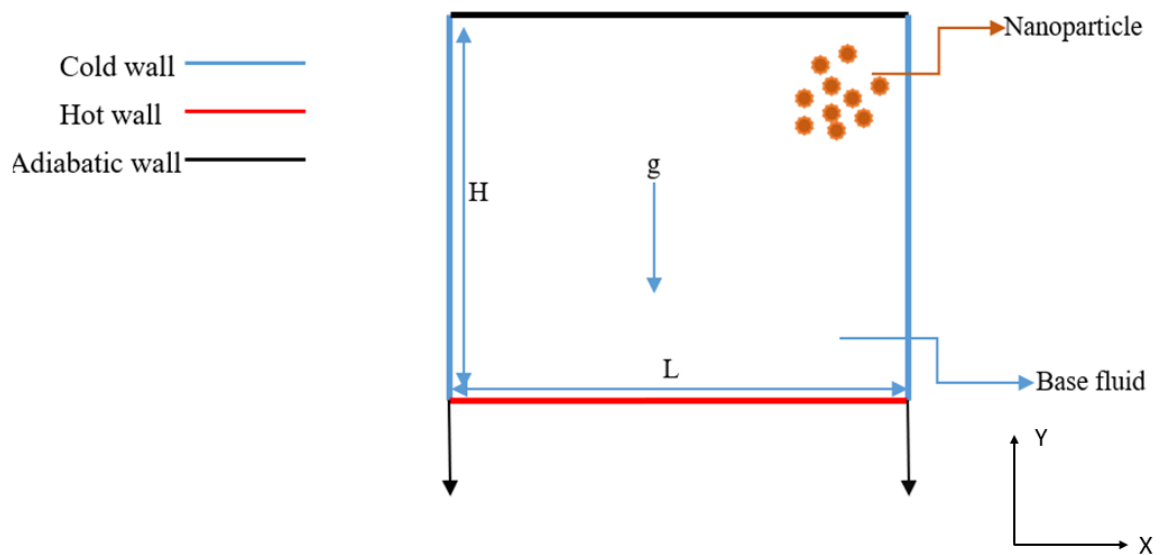
Figure III.1: Problem geometry.

III.4.1. Boundary conditions

In this application, the boundary conditions are:

- Two velocities were taken into account for left and right vertical walls; the velocities and temperature are constant :
    - ✓ The left and right walls move down.
    - ✓ Temperature of the left and right walls is constant ($T = T_c$).
- The top wall was thermally insulated.
- The function of the hot temperature applied to the bottom wall is taken into account:
    - ✓ Sinusoidal temperature:

$$T = T_c + \lambda \cdot (T_h - T_c) \cdot (1 - \cos(2\pi X))$$ (II.8)

III.4.2. Equations of the problem

The following equations governing 2D steady-state mixed convection can be written in dimensionless form after using the Boussinesq approximation and ignoring viscous dissipation. The following dimensionless parameters are used to transform the main equations into their dimensionless form.

$$X = \frac{x}{L}, Y = \frac{y}{L}, U = \frac{u}{U_0}, V = \frac{v}{U_0}, \theta = \frac{(T-T_c)}{(T_h-T_c)}, P = \frac{p}{\rho_{nf} U_0^2}$$

The resulting dimensionless equations are listed below:

$$\frac{\partial U}{\partial X} + \frac{\partial V}{\partial Y} = 0 \qquad \qquad (II.9)$$

$$U \frac{\partial U}{\partial X} + V \frac{\partial U}{\partial Y} = -\frac{\partial P}{\partial X} + \frac{1}{Re} \frac{\mu_{eff}}{v_f \rho_{nf}} \left(\frac{\partial^2 U}{\partial X^2} + \frac{\partial^2 U}{\partial Y^2} \right) \qquad (II.10)$$

$$U \frac{\partial V}{\partial X} + V \frac{\partial V}{\partial Y} =$$

$$-\frac{\partial P}{\partial Y} + \frac{1}{Re} \frac{\mu_{eff}}{v_f \rho_{nf}} \left(\frac{\partial^2 U}{\partial X^2} + \frac{\partial^2 U}{\partial Y^2} \right) + \frac{\rho \beta_{nf}}{\rho_{nf} \beta_f} Ri\theta \qquad (II.11)$$

$$U \frac{\partial \theta}{\partial X} + V \frac{\partial \theta}{\partial Y} = \frac{\alpha_{nf}}{\alpha_f} \frac{1}{Pr\, Re} \left(\frac{\partial^2 \theta}{\partial X^2} + \frac{\partial^2 \theta}{\partial Y^2} \right) \qquad (II.12)$$

The following table shows the results of solving the equations above (in their dimensionless version) using the boundary above conditions.

Table III.2: Solving the equations in dimensionless version using boundary conditions.

	Hydrodynamic conditions	Thermal conditions
Application	• For left and right walls, move down: $X = 0;\ 0 < Y < 1;\ U = 0;\ V = -1$ $X = 1;\ 0 < Y < 1;\ U = 0;\ V = -1$ $Y = 1;\ 0 < X < 1;\ U = 0;\ V = 0$	• Left and right walls $\theta = 0$ • Top wall $\partial\theta / \partial Y = 0$ • Bottom wall : $\theta = \lambda(\,1-cos(\,2\pi X\,)\,)$

III.4.3. Heat transfer

The convective heat transfer rate is defined by the dimensionless Nüsselt number (Nu), which plays a unique function. This value is dimensionless and shows the ratio between pure diffusion heat flux and convection heat flow. Then, this number is defined by:

$$Nu = \frac{Q_{conv}}{Q_{cond}} \qquad (\text{II.13})$$

➢ Newton's law gives the convective flux:

$$Q_{conv} = h\,S(T_p - T_f) \qquad (\text{II.14})$$

➢ Fourier's law gives the conductive flux:

$$Q_{cond} = k\,S\frac{(T_p - T_f)}{L_c} \qquad (\text{II.15})$$

From the above equation, the convective exchange coefficient is given as follows:

$$h = \frac{k\,N_u}{L_c} \qquad (\text{II.16})$$

The local Nüsselt number is defined by:

$$Nu(X) = \frac{k_{nf}}{k_f}\frac{\partial\theta}{\partial Y}\bigg|_{wall} \qquad (\text{II.17})$$

The calculation of the average Nüsselt number at the hot wall is given by the formula:

$$Nu_{avg} = \int_0^1 Nu(X)\,dX \qquad (\text{II.18})$$

III.5. CFD code for numerical resolution

Computational fluid dynamics (CFD) is the use of computer simulations to learn about systems with heat transfer, fluid movement, and related phenomena including chemical reactions. CFD is based on sophisticated computers that can simulate and provide adequate and acceptable results. The use of CFD in simulation has grown widespread, particularly in the industrial sector.

Although this method is less costly than experimental approaches and works with rather difficult issues; there are significant drawbacks, including the possibility of uncertainty due to insufficient calculating data per cell and the associated interpolation mistakes for big models. However, they are practical and may be used to validate numerical findings. Experimental techniques are often costly, difficult to execute and take time to solve the issue. Other analytical techniques depend on assumptions. However, they are constrained and unsuited to complicated phenomena.

III.5.1. Numerical methods and types of mesh

The discretization of the equations presented in this chapter, translating the phenomenon of mixed convection, is the operation of transforming these differential equations into a system of algebraic equations. Several methods of discretization of partial differential equations are currently used, such as the method of Finite Volumes, Finite Differences and Finite Elements, Lattice Boltzmann method, and Network Simulation method.

A mesh of nodes is used to divide up the domain; each node has a volume element (volume of control) constructed around it. While the vector values (temperature and pressure) are retained in the mesh node, the scalar numbers (u, v, and w) are kept in the center of the connecting segments. The momentum equations related with the velocity components and the general transport equation associated with the numerical variables have been incorporated into the control volume. The volume under primary control is erased in the direction (X) relative to the longitudinal component under control (u).The control volumes of the transverse components (v) and (w) are adjusted in the Y and Z directions, respectively.

A "staggered grid" is a kind of mesh that allows for improved numerical stability of the solution, precise evaluation of pressure gradients, and more accurate approximation of convective fluxes. The staggered grid for the three composites is shown in Figure III.2. The "Fluent" software code in its version 19.2 deals with several types of structured, unstructured, or hybrid meshes. A structured mesh generally comprises quadrilateral meshes in two dimensions (2D or surface mesh) and hexahedral meshes in three dimensions (3D or volume mesh). In contrast, an unstructured mesh will be composed of quadrilateral or triangular meshes in 2D and hexahedral or tetrahedral in 3D. In a hybrid configuration, the meshes close to the walls are quadrilaterals in 2D and hexahedra in 3D, and the meshes of the rest of the domain are triangles in 2D and tetrahedra in 3D. It is necessary to have the smallest possible meshes in the near wall to model the flows at this location properly;

this particularity is all the more important in a turbulent regime called (inflation). In 3D, the meshes that connect the hexahedrons and the tetrahedrons are prisms or pyramids. Figure III.3 represents the different types of mesh used by our code.

a)   b)   c)
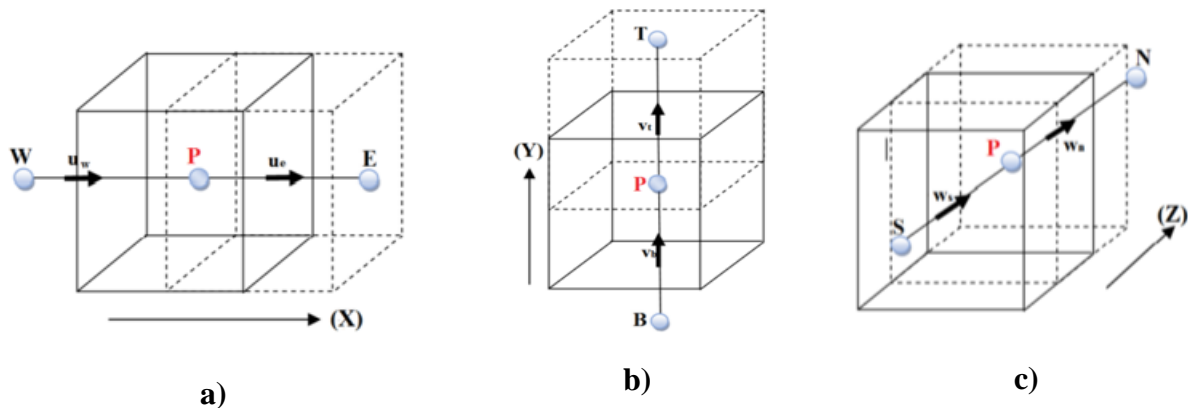
Figure III.2: Staggered grid for: a) under control (u), b) control volumes of the transverse components (v), and c) of (w).

Structured mesh   Unstructured mesh   Hybrid mesh

Structured mesh   Structured mesh by blocs
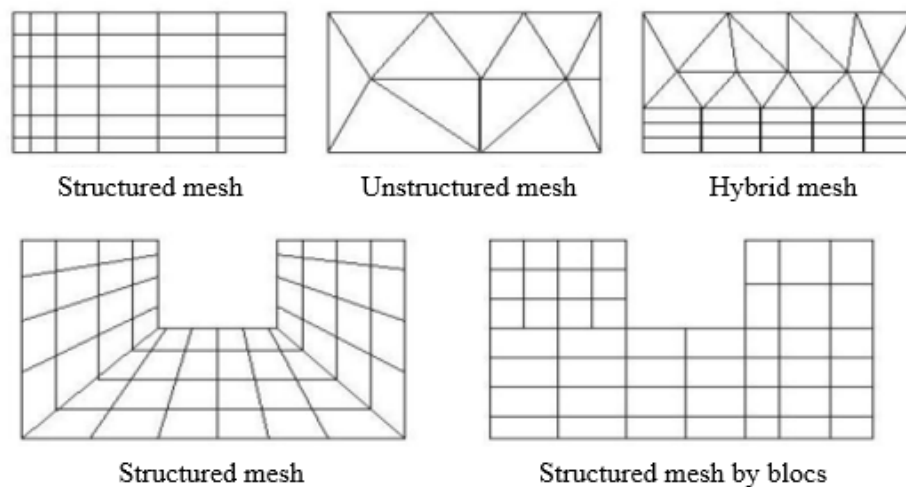
Figure III.3: Types of mesh used by "Fluent" **[181]**.

III.5.2. Choice of the mesh

The ANSYS Geometry Workbench allows the user to construct the geometry of the computational domain and subdivide it into small control volumes or computational cells. All of these elementary volumes constitute the mesh. The definition of the appropriate boundary conditions, at the level of the cells, which coincide or touch the boundary of the computational

domain, is also done at this level. The program Fluent uses the Finite Volume Method (FVM) to handle heat transport and fluid mechanics issues. The functions gathered by ANSYS Workbench include defining the problem geometry, inspecting the mesh, defining the boundaries (different sorts of boundary conditions), and defining the computation domains (fluid or solid) **[182]**.

III.5.3. Mesh convergence

In CFD modeling, to ensure that the solution provided by the solver after convergence is realistic, it must be independent of the mesh density, the solution should be insensitive to the grid size show in Figure III.4. To check for convergence in the mesh, one must record the changing values of a variable, such as the Nüsselt number, with the progressively refined mesh.
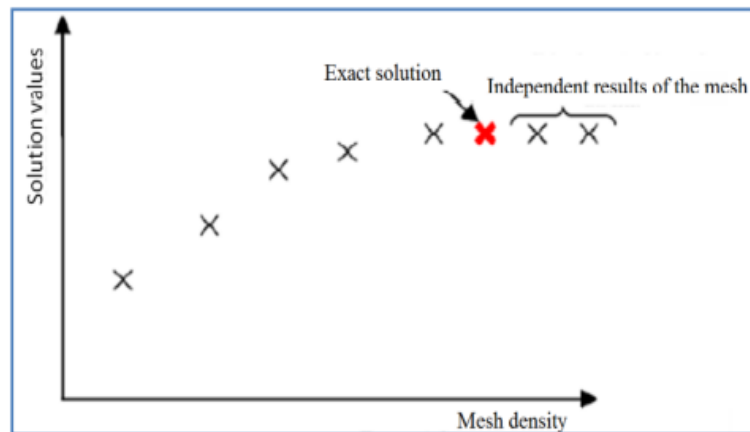
Figure III.4: Test of mesh convergence **[182]**.

In this study, we have chosen quadrilateral grids where Figure III.5 (a-c) illustrates the selected meshes form for three cases related to the Aspect Ratios.

a)

b)

c)
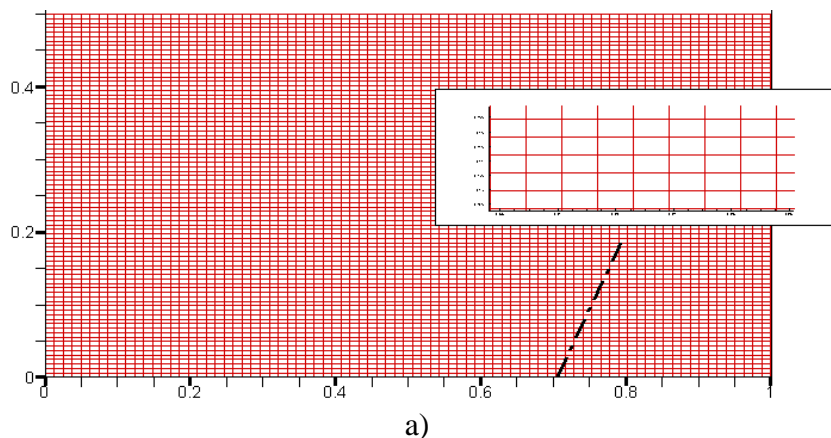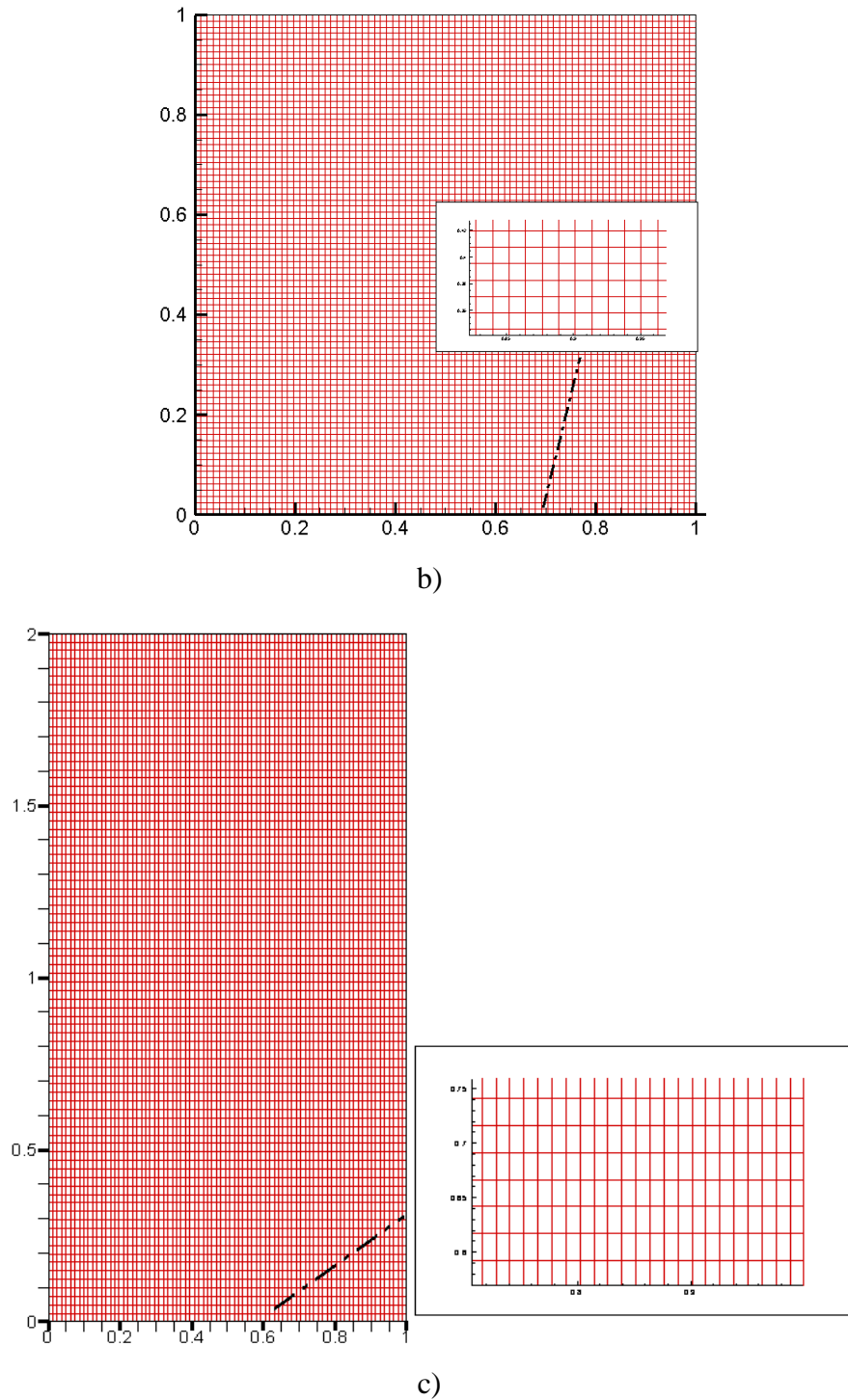
Figure III.5: Grid of mesh for: a) AR=0.5, b) AR=1, and c) AR=2.

The FVM-based Fluent software and the SIMPLE algorithm for velocity-pressure coupling are used in this study to tackle the challenges. The stages in the computation that are detailed below are appropriate for the steady flow regime. In general, we differentiate between **[182]**:

- Transport equation integration.

- Discrimination.

- Connection of pressure and velocity.

- Convergence.

III.5.4. Discretization of equations

To solve equations system needed to simulate fluid flow, our code uses the Finite Volume Method; in reality, a physical issue is resolved in three steps:

- Division of the computational domain into control volumes via a mesh.

- Integration of the equations on each control volume in order to transform them into algebraic equations.

- Resolution of the equations thus discretized.

These equations are put in the following general form:

$$\underbrace{\frac{\partial}{\partial t}(\rho\phi)}_{A}+\underbrace{\sum_{j=1}\frac{\partial}{\partial x_j}(\rho u_j\phi)}_{B}=\underbrace{\sum_{j=1}\frac{\partial}{\partial x_i}(\Gamma_\phi\frac{\partial\phi}{\partial x_j})}_{C}+\underset{D}{S_\phi} \qquad (\text{II.19})$$

In the stationary two-dimensional situation, the transport equation is formulated as follows for each variable (ϕ):

$$\frac{\partial}{\partial x}(\rho u\phi)+\frac{\partial}{\partial y}(\rho v\phi)=\frac{\partial}{\partial x}(\Gamma\frac{\partial\phi}{\partial x})+\frac{\partial}{\partial y}(\Gamma\frac{\partial\phi}{\partial y})+S_\phi \qquad (\text{II.20})$$

According to the FVM, this last equation is discretized, and the maintained equation system is solved for each consecutive value (ϕ), as shown in the reference **[183]**.

Table III.3: Different terms of the transport equations.

Equation	Value of ϕ	Diffusion coefficient Γ	Source term S_ϕ
Continuity	1	0	0
Quantity of movement axe x	U	$\mu_{nf}/\rho_{nf}\alpha_f$	$-\partial P/\partial X$
Quantity of movement axe y	V	$\mu_{nf}/\rho_{nf}\alpha_f$	$-\partial P/\partial Y$
Energy	θ	α_{nf}/α_f	0

Numerically solving CFD problems requires an iterative process. To appreciate the convergence of the iterative process, convergence criteria must be considered. Thus, the convergence of the iterative process is determined by the concept of residual. After the discretization step, the conservation equation of a given variable (ϕ) on a cell with center (P) can be expressed as bellow **[182]**:

$$a_p \phi_p = \sum_{nb} a_{nb} \phi_{nb} + b \qquad (\text{II}.21)$$

The (nb) indicates the indices of nearby cells; depending on the mesh structure, there are more or less nearby cells. The iterative implicit method is used to solve the linear system of equations that arise as a result of the coefficients (a_P, a_{nb}) and the individual cells (Gauss-Seidel).

In its two discretization systems, Fluent suggests:

- First-order upwind scheme: this approach causes numerical diffusion but allows for stability in the computations.

- Second-order upwind scheme: although it might cause the computation to diverge, this approach can be used to reduce numerical diffusion.

The convergence condition or the halting requirement must be met for the computation to stop. Fluent enables users to evaluate the level of convergence at each iteration by computing the residuals R for each variable (velocity components, energy, pressure ...).

This residue is explained by:

$$R_\phi = \frac{\sum \left| \sum_{nb} a_{nb0} \phi_{nb} + b - a_p \phi_p \right|}{F_{in,\phi}} \qquad (\text{II}.22)$$

These expressions of the residues are valid for all quantities except the pressure; in the case of this quantity, the residue is determined from the continuity equation:

$$R^C = \sum_{Domain} \left| \textit{material creation rate in the field} \right| \qquad (\text{II}.23)$$

III.5.5. Under-relaxation values

The relaxation factors assist in solving nonlinear equations. It is feasible to include a sub-relaxation to lessen the oscillations of the solution and the changes of the variables from one iteration to the next. Although suggestions for each variable are often based on empirical

information, there are no universal rules governing the optimal values of the sub-relaxation coefficients. In our study, the values of under-relaxation are shown in the following table.

Table III.4: Under-relaxation values.

	Pressure	**Quantity of movement**	**Energy**	**Density**
Laminar model	0.3	0.7	1	1

III.5.6. Choice of pressure velocity coupling method

Three algorithms are available in the calculation software:

- SIMPLE: the strongest.
- SIMPLEC: it gives faster convergence for simple problems.
- PISO: it is useful for unsteady flow problems.

The algorithm chosen in our study is the SIMPLE algorithm **[184]**. At the initialization of the calculation, a pressure field fixed a priori is introduced into the momentum balance equation, making it possible to calculate a first velocity field. The combination of mass balance and momentum equations makes it possible to correct these first pressure and velocity fields. The other transport equations are then solved, and the corrected pressure field is used to initialize the calculation at the next iteration. This succession of operations is repeated until the convergence criteria are reached.

The discretization of a diffusion transport equation on a control volume by the FVM involves the velocities values at the volume interfaces (UE, UW, UN, US). It is, therefore, interesting to calculate these velocities directly on the interfaces (without having to perform interpolations). On the other hand, discretizing the continuity equation and the pressure gradient with linear interpolation can induce large errors because a "checkerboard" pressure or velocity distribution is seen as a uniform field.

To circumvent these difficulties, we prefer to use staggered grids. The main grid is built on which the pressure, temperature and concentration are calculated. Two grids shifted to the right and to the top, respectively, are used to calculate the horizontal and vertical velocities.

The SIMPLE algorithm, an acronym for "Semi Implicit Method for Pressure Linked-Equations" makes it possible to solve the system of discrete equations. This algorithm stipulates the existence

of a relationship between the corrected velocities and the corrected pressures in order to verify the mass conservation equation.

The representative diagram of this iterative process is the following:
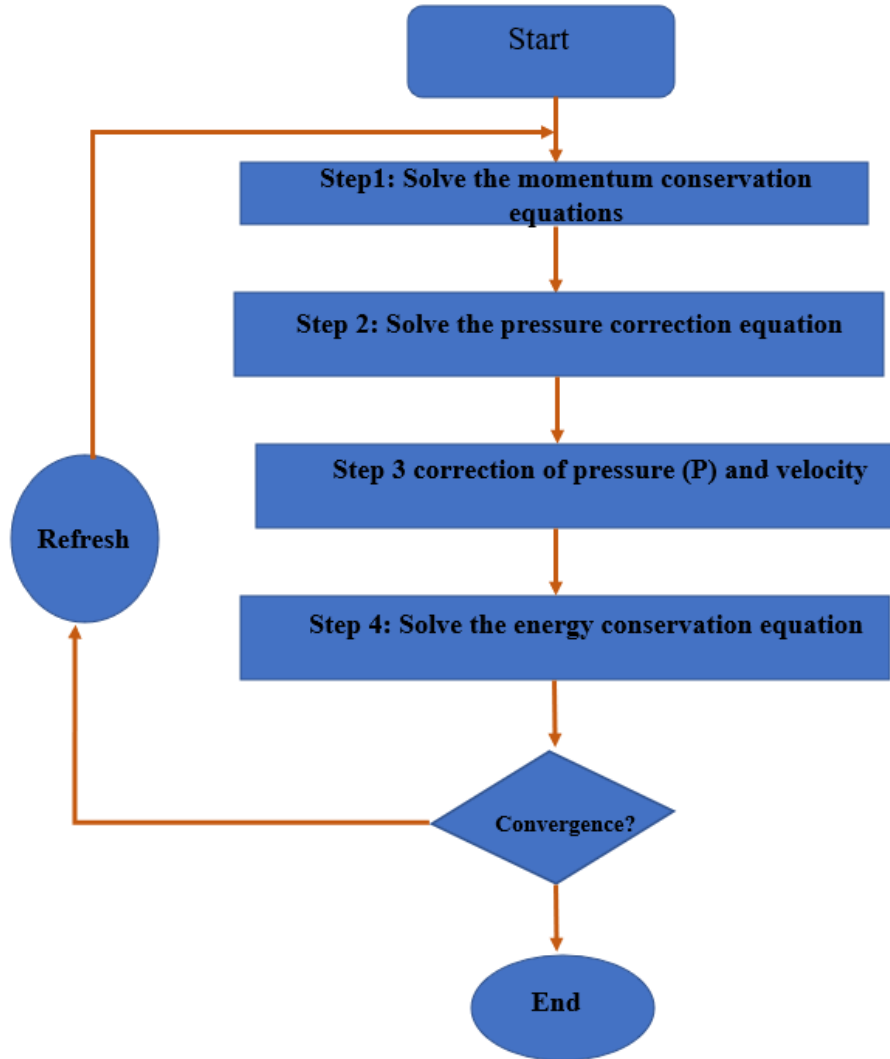
Figure III.6: Representative diagram of the SIMPLE algorithm.

III.5.7. Different methods for numerical modeling

Fluent is a simulation program that requires an understanding of fundamental theoretical concepts to complete the primary phases of its use. These concepts pertain specifically to defining the key equations that regulate the flow. The methodology and simulation approach are described by the organigram in Figure III.7. It begins with the production of geometric models, the use of a mesh generator, the solution of the equations, followed by analysis and display.
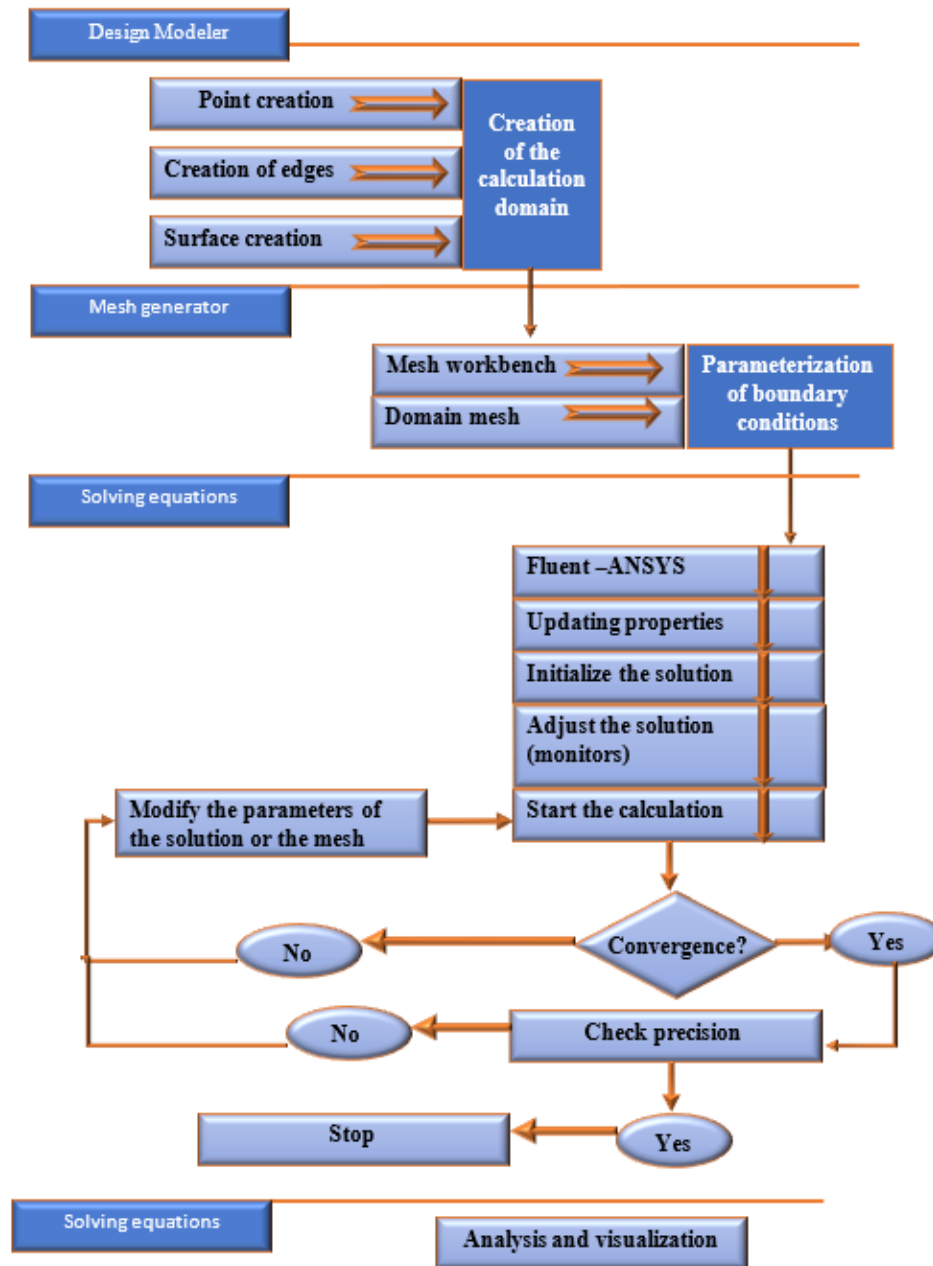
Figure.III.7: Calculation chart.

III.6. Conclusion

The chapter discussed the modeling and set of equations for the problem of laminar flow. The continuity, momentum, and energy equations were used, along with boundary conditions. The dimensionless reference numbers and the thermophysical properties of nanoparticles and base

fluids were also revealed. This information can be used to simulate laminar flow and to study the effects of different parameters on the flow. On the other hand, a clear approach has been presented for the methods to be followed in solving the equations governing the phenomenon in the simulation program and the mechanism it follows, starting from the design to the export of all results.
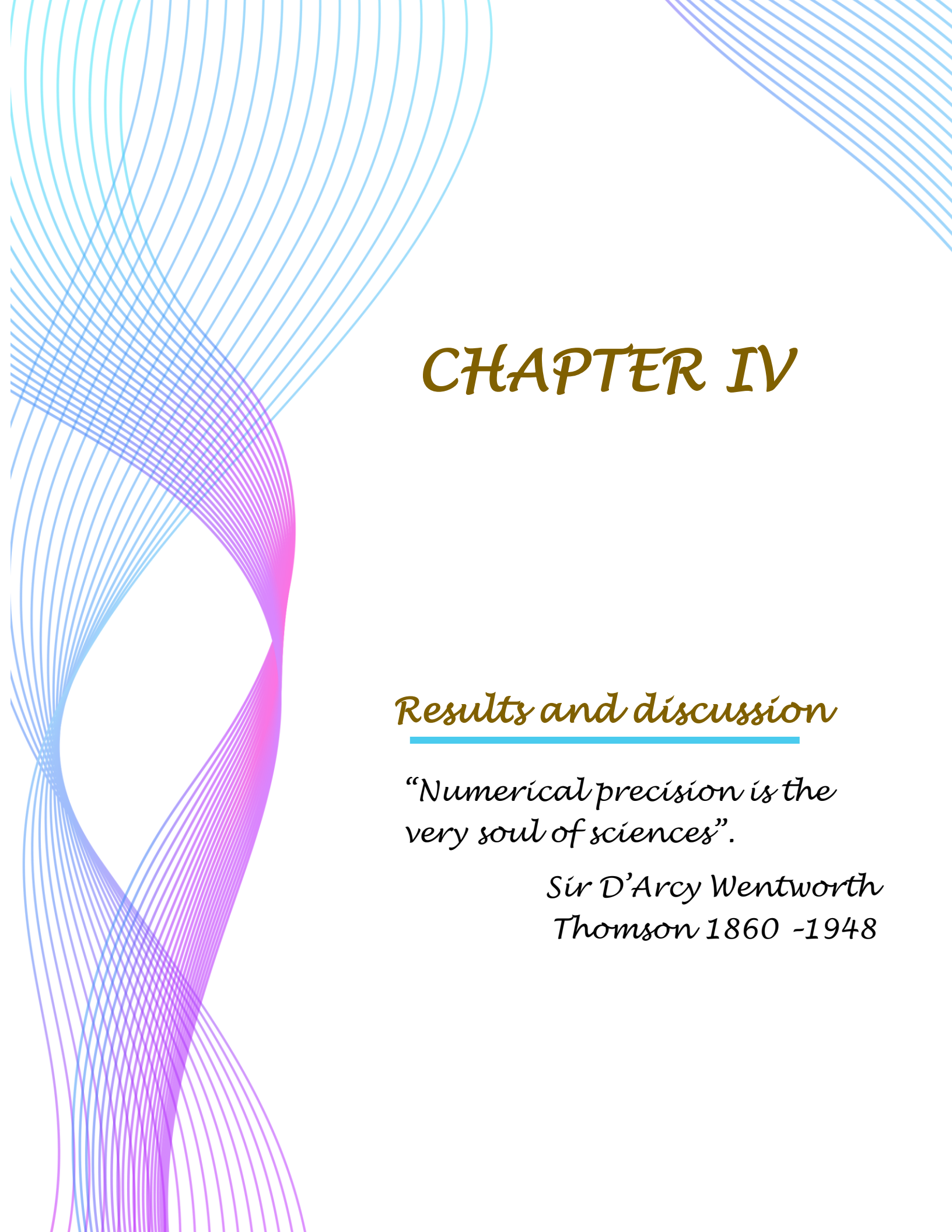
CHAPTER IV

Results and discussion

"Numerical precision is the very soul of sciences".

Sir D'Arcy Wentworth Thomson 1860 -1948

CHAPTER IV

Results and discussion

IV.1. Introduction

This chapter aims to present the numerical simulation results for a two-dimensional model. Hence, the main objective is to show the CFD computer code "Fluent" ability to model the mixed convection flow in a cavity filled with several fluids and to determine the current lines and isotherms, as well as the Nüsselt number for the different volume fraction of nanoparticles, Aspect Ratios, Richardson number, Grashof number, and the temperature amplitude.

IV.2. Influence of mesh on numerical solutions

The grid independence test with target fluid (water) is seen in Figure IV.1. For the case of $Gr = 10^4$ and $R i= 0.1$, the test determined the average Nüsselt number on the bottom wall for several mesh node; it was found that a grid size of 81×81 guarantees a grid-independent solution.
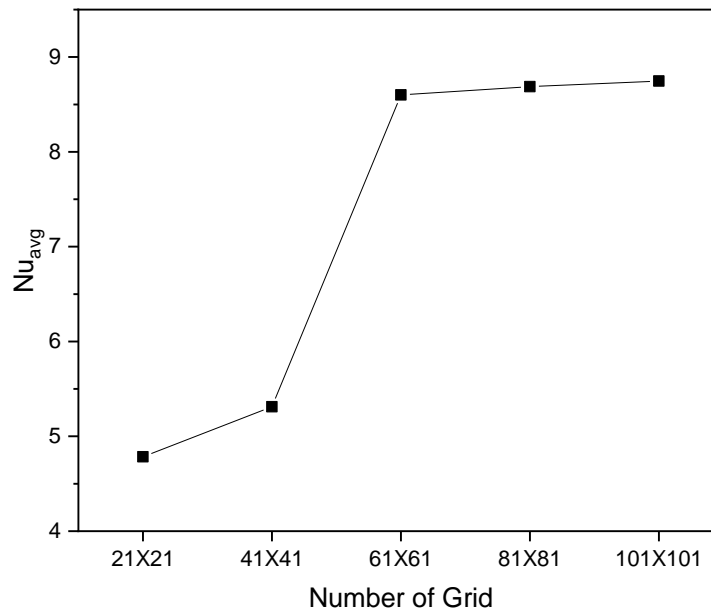
Figure IV.1: Grid study.

IV.3. Validation of the calculation code

The validity of the current numerical solution is established by comparing it to the simulation solution of the average Nüsselt number for different Ra and Re in the case of the square

cavity, differentially heated and filled with air, discovered by **[185-189]** and **[85, 190-194]**, as depicted in Tables IV.1 and IV.2, respectively.

Table IV.1: Comparison of the average Nüsselt results of the present study with previous work at Pr = 0.71.

Ra	Ref. [185]	Ref. [186]	Ref. [187]	Ref. [188]	Ref. [189]	Present study	Error %
10^3	1.118	1.117	-	1.078	1.117	1.053	2.335
10^4	2.245	2.244	2.245	2.244	2.241	2.119	5.57
10^5	4.522	4.520	4.521	4.520	4.510	4.517	0.066
10^6	8.826	8.781	8.8	8.781	8.829	9.18	4.54

Table IV.2: Comparison of the average Nüsselt results of the present study with those of previous work at Gr = 100.

Re	Ref [190]	Ref [191]	Ref [192]	Ref [193]	Ref [85]	Ref [194]	Present study	Error %
1	-	-	-	1.00033	1.01013	1.00033	1.00725	0.692
10^2	1.94	2.02	2.10	2.03116	2.09084	2.04935	2.02525	1.176
400	3.84	4.04	3.85	4.02462	4.16106	4.09826	4.05837	0.973
500	-	-	-	4.52671	4.66369	4.6179	4.56894	1.06
10^3	6.33	6.42	6.33	6.48423	6.55162	6.70345	6.54927	2.3

For various Ra numbers in a square cavity, the presently used computational model of mixed convection is evaluated with a target fluid (water), and excellent agreement is observed compared to the results of **Talebi & al. [67]** and **Bora & al. [80]** as shown in Figure IV.2.a. Another validation was done by comparing the average Nüsselt number for the nanofluid Cu-H_2O with **Talebi & al. [67]** as shown in Figure IV.2.b.

Figures IV.3.a and IV.3.b depict the findings of a comparison between the velocities and temperatures within the square cavity and those found in a study by **T. S. Cheng [195]** with Re = 1500 and Gr = 2.25×10^6 in a top-cooled moving wall and a bottom-heated cavity, respectively. Figures IV.3.c and IV.3.d show two cases for validation by results for Re = 400 and Gr = 100 with the numerical results of **Iwatsu & al. [190]**, **Khanafer and Chamkha [196]**, and **A. J. Chamkha and E. Abu-Nada[69]**. The first case compares the temperature at the cavity mid-section (x = 0.5), and the second case compares the U-velocity at x = 0.5.
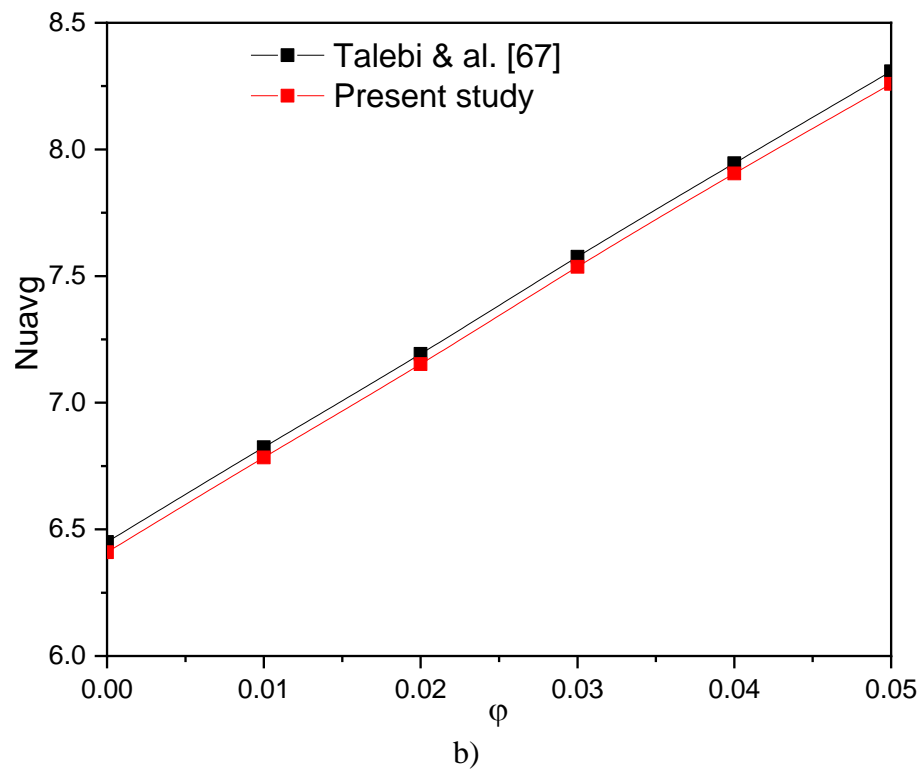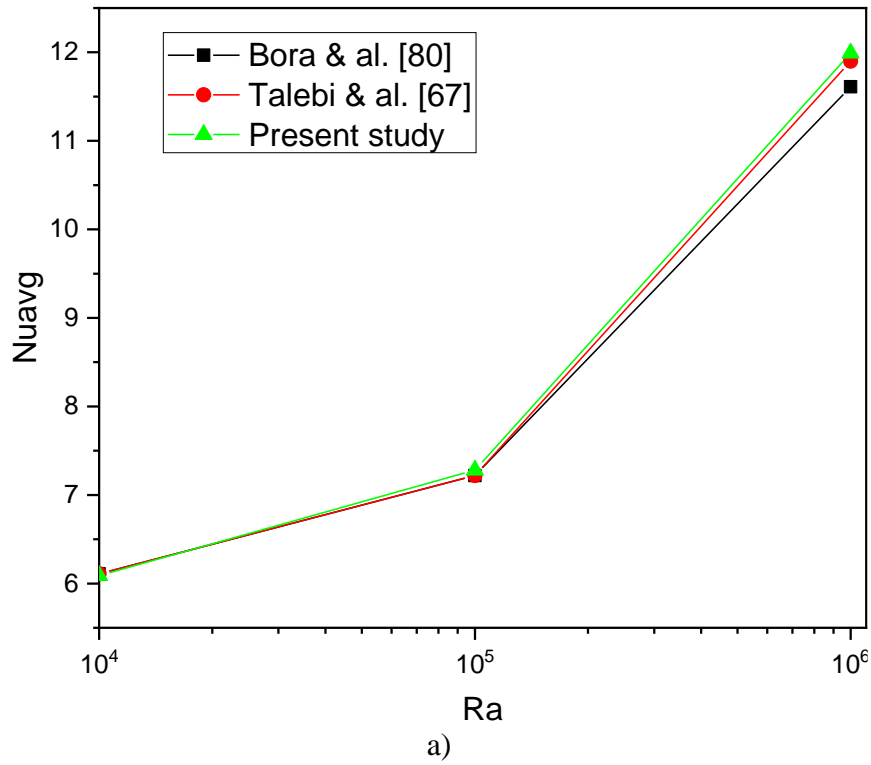
Figure IV.2: Comparing the average Nüsselt number of the present study with those of previous work, a) **Talebi & al. [67]** and **Bora & al. [80]**, b) **Talebi & al. [67]**.
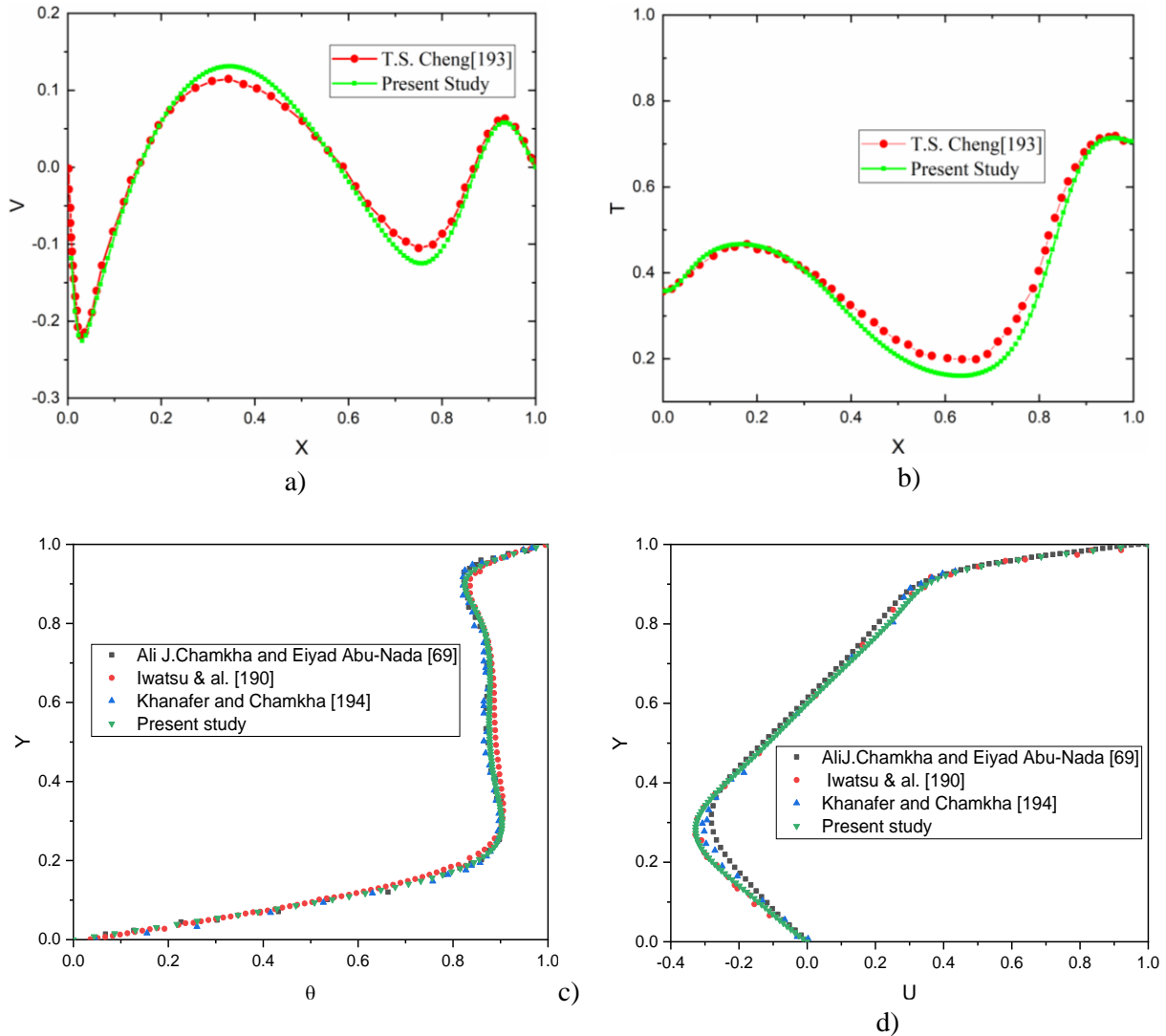
Figure IV.3. Comparison of (a) V-velocity and (b) temperature with **T. S. Cheng [195]** for Re = 1500 and Gr = 2.25×10^6, (c) temperature at mid-section of the cavity (x = 0.5), and (d) U-velocity at (x = 0.5) with **Iwatsu & al. [190]**, **Khanafer** and **Chamkha [196]**, and **A. J. Chamkha and E. Abu-Nada [69]** for Re = 400 and Gr = 100.

IV.4. Distribution of current lines and isothermal lines

Heat transfer via mixed convection in a double lid-driven cavity filled with pure water and Ag-H_2O is modeled and its sensitivity to thermal boundary conditions is investigated. In which the two parallel vertical walls are falling at a fixed speed. A sinusoidal temperature heats the bottom wall; the top wall is considered adiabatic, and the other walls are kept at a cold temperature. After the numerical approach has been confirmed by solving the test case. The results were presented for

Gr = 10^4, five different AR (0.25 - 2), a range of Ri (10^{-1} - 10^2) and the volume fraction for nanoparticles ranging in (0 - 8%). Figure IV.4 represents the streamlines and temperature profile inside the cavity at AR = 0.25 for different Ri and (φ) equal respectively to 0 and 8%.
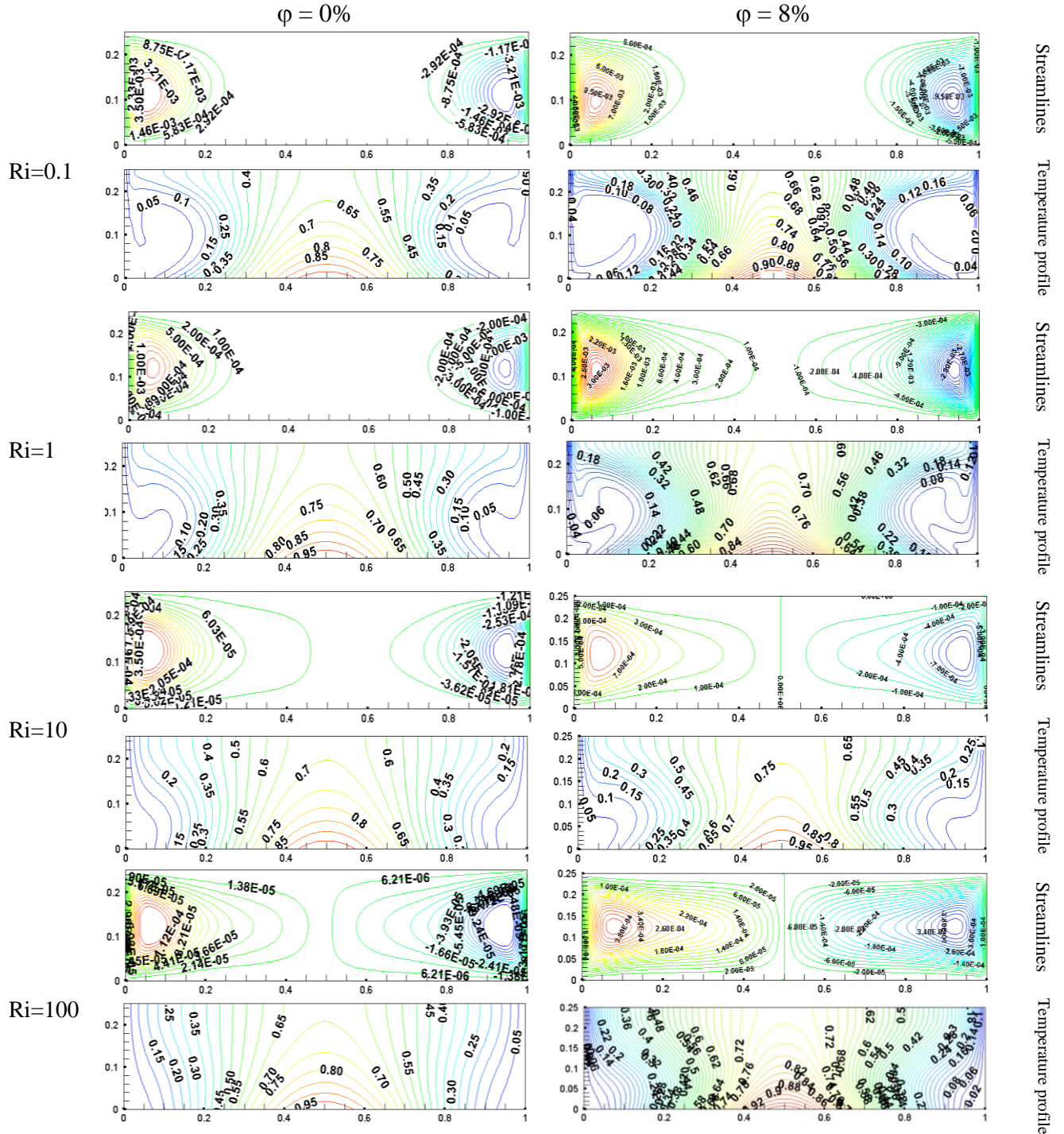
Figure IV.4: Streamlines and temperature profile for a cavity with AR=0.25.

As it is clear in the last figure that the current lines form two vortices inside the gap where the two vortices expand with the increase in Ri. As for the change in temperature, the flow increases at the bottom wall with an increase of nanoparticles compared to the base fluid wall. As can be seen in the same figure, the fluid flows into the cavity at Ri = 100 and is regulated by natural convection.

Inside the cavity, the streamlines and temperature profile are shown for two nanoparticle volume fractions and different Richardson numbers in Figure IV.5. Two vortices form in the cavity when the nanofluids move through it. At Ri = 0.1, the heat flow and its influence may predominate the resultant flow, and the symmetric behavior can be attributed to the insignificant buoyancy force. The influence of natural convection on heat transmission and fluid flow is shown by increasing the number of Richardson while keeping the size of nanoparticles constant. In addition, the flux value increases significantly due to the increase in volume fraction of nanoparticle by 8%.

Figure IV.5 depicts a temperature profile where the forced convection system dominates boundary layers of the cavity wall. Until the cavity obtains an even heat distribution of the temperature lines, the Richardson number determines that the center of the cells will move to the middle of the bottom wall. As can be seen in the same figure, the fluid flows into the cavity at Ri = 100 and is regulated by natural convection.
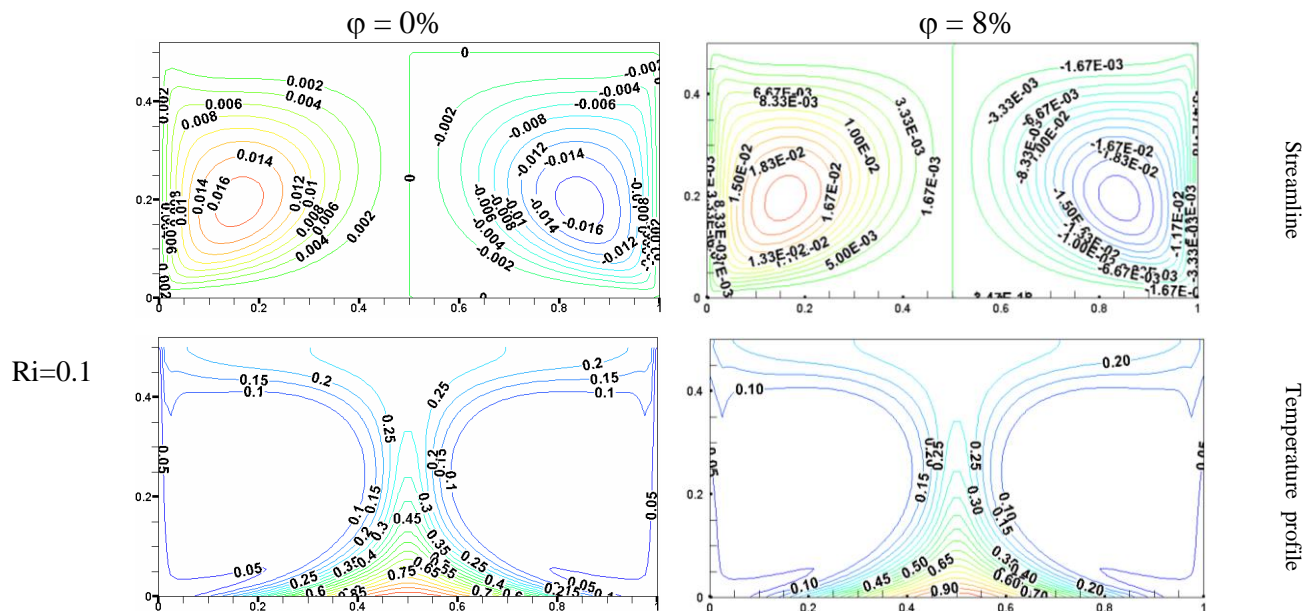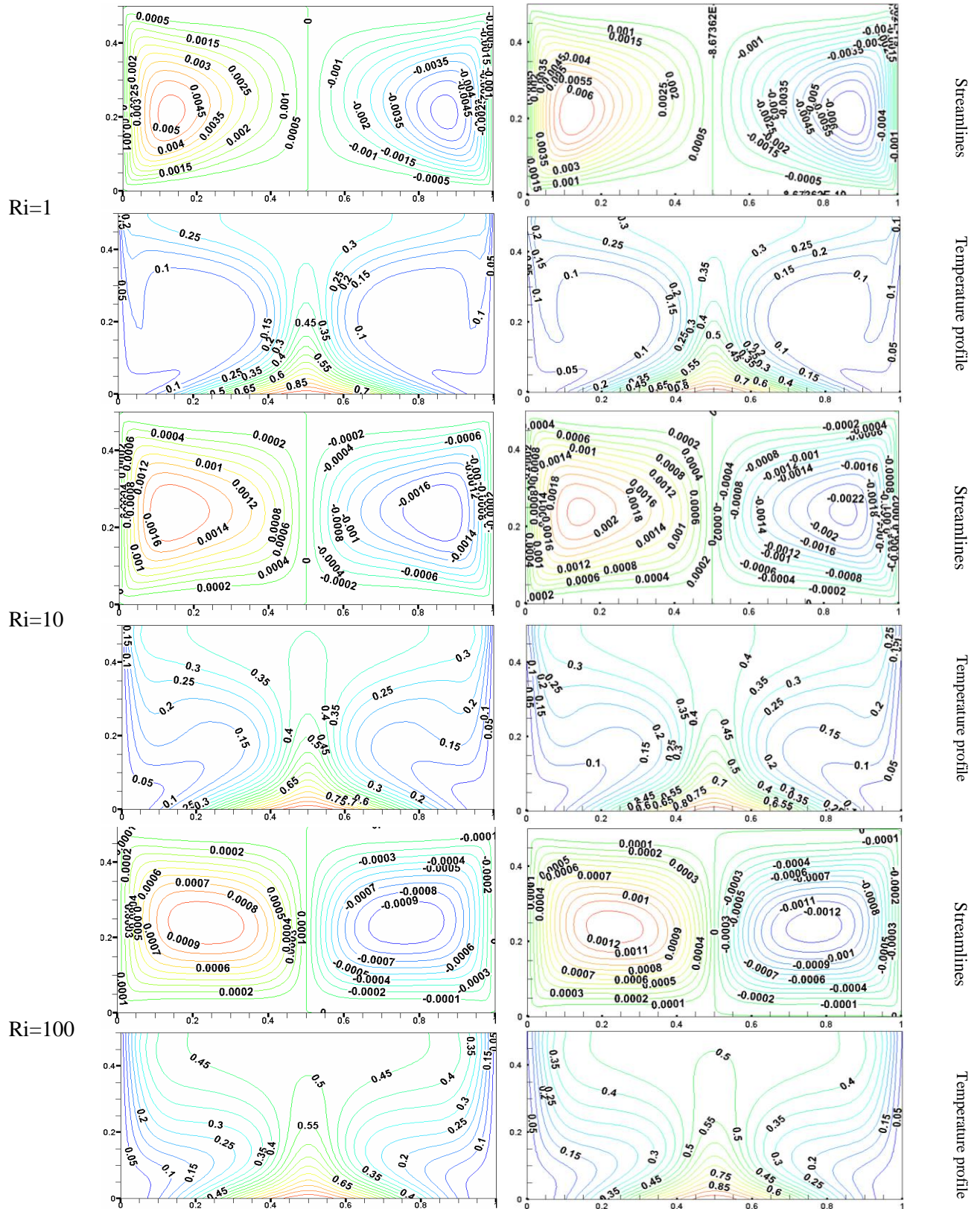
Figure IV.5: Streamlines and temperature profile for a cavity with AR=0.5.

Figure IV.6 shows the current and heat lines of the gap at AR = 0.75.
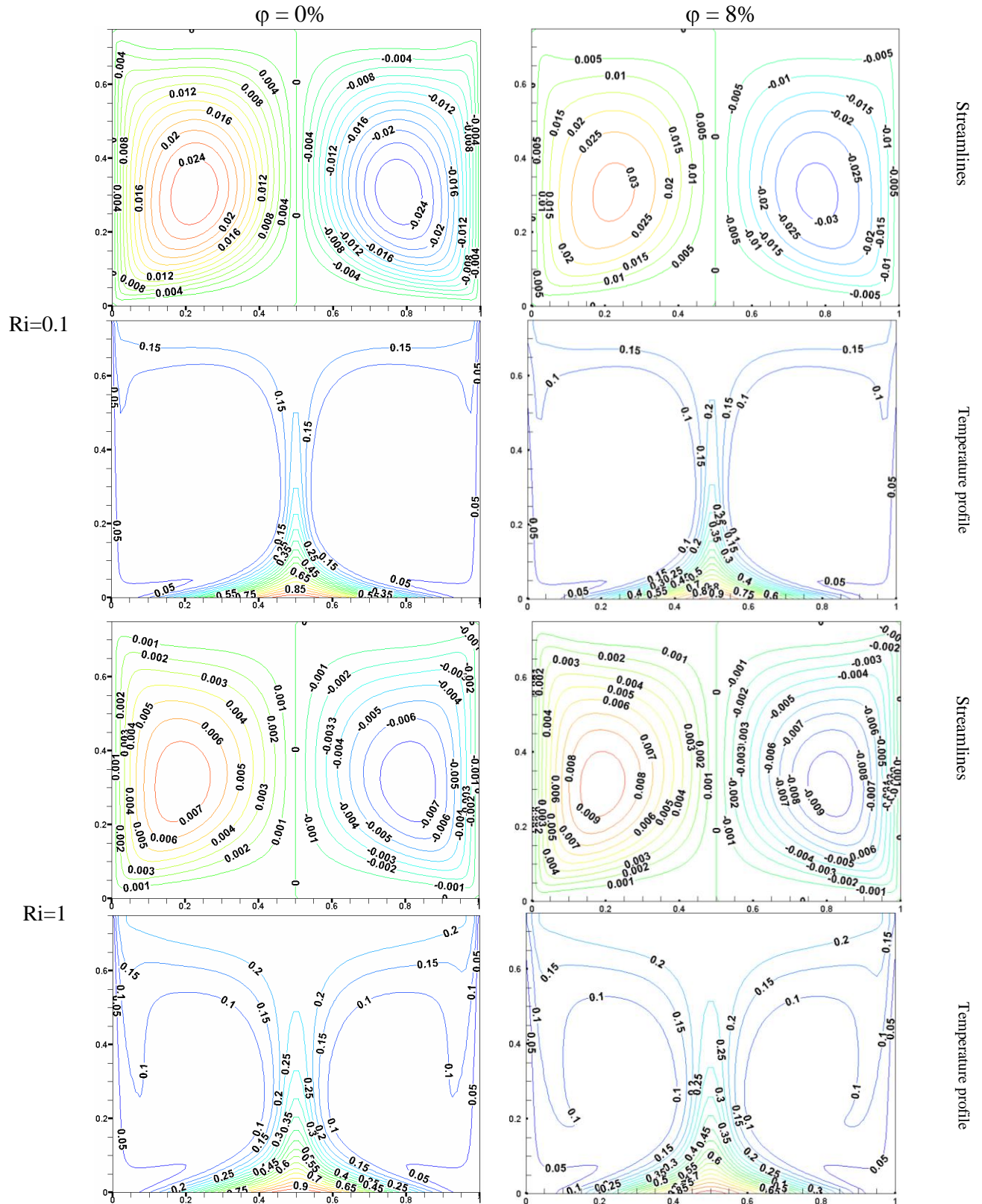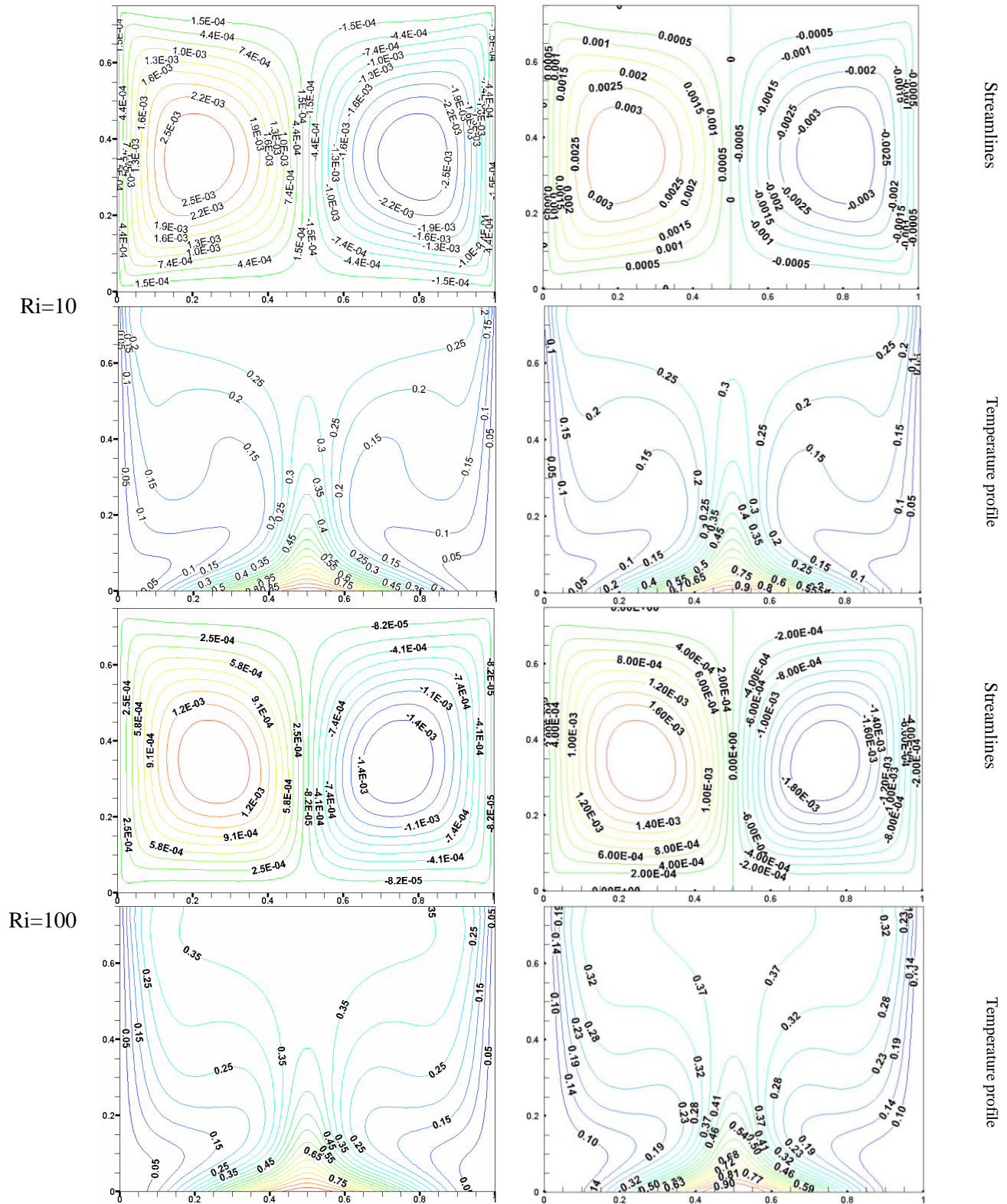
Figure IV.6: Streamlines and temperature profile for a cavity with AR=0.75.

As it is clear from the last figure that as the width ratio increases, the vortices formed in the middle of the gap gradually increase to take the shape of a circle. At Ri = 0.01, forced convection predominates indicating that there are substantial vertical temperature differences. On the other hand, heat dispersion would be less near the horizontal walls. The AR of the cavity grows from 0.25 to 0.75 without significantly changing the cavity temperature distribution. However, heat transmission in the cavity starts when the mixed thermal mode reaches Ri = 1, and the thermal boundary layers vanish. The mode is dominated by natural convection when Ri = 100.

The streamlines and temperature profile of the cavity at AR=1 are shown in the following figure.

Ri=1

Ri=10

Streamlines

Temperature profile

Streamlines

Figure IV.7: Streamlines and temperature profile for a cavity with AR=1.

Rising the concentration of nanoparticles of varying sizes significantly advances the flow, and the size of the vortices depicted in the figure is larger than those of different AR. This is because the asymptotes stimulated by natural convection decrease in strength and size as the nanoparticles get bigger and the dynamic viscosity increases. Figure IV.7 demonstrates that the flow is downward along the relocating side walls before becoming horizontal in the center zone. While the circulation near the cavity's center is more significant in relation to the enclosure's boundary due to the condition of non-slip, it rises gradually until it collides with the upper thermal insulated wall, transforming it into the horizontal walls, where the greater the number of Richardson produces higher temperatures.

The streamlines and temperature profile are shown in Figure IV.8 for an AR=2. It can be noted that the increase in AR, produces an irregular pattern due to the movement of the walls verticality, and the heat transfer by natural convection becomes more dominant than the conduction, which is greatly influenced by the decrease in the boundary layer at the level of the wall hot. This justifies the flow towards each wall where the size of the nanoparticles plays an important role in heating/cooling the package, which leads to an increase in heat transfer.

Temperature profile

Streamlines

Ri=0.1

Ri=1

Temperature profile

Streamlines

Ri=10

Ri=100

Ri=100

Figure IV.8: Streamlines and temperature profile for a cavity with AR=2.

IV.5. Evolutions of average number of Nüsselt

IV.5.1. Influence of Richardson number on the average Nüsselt number

Figure IV.9 presents the bottom (hot) wall average Nüsselt number for Ag-H_2O nanofluid with various Ri, AR and (φ).

b)

c)

d)
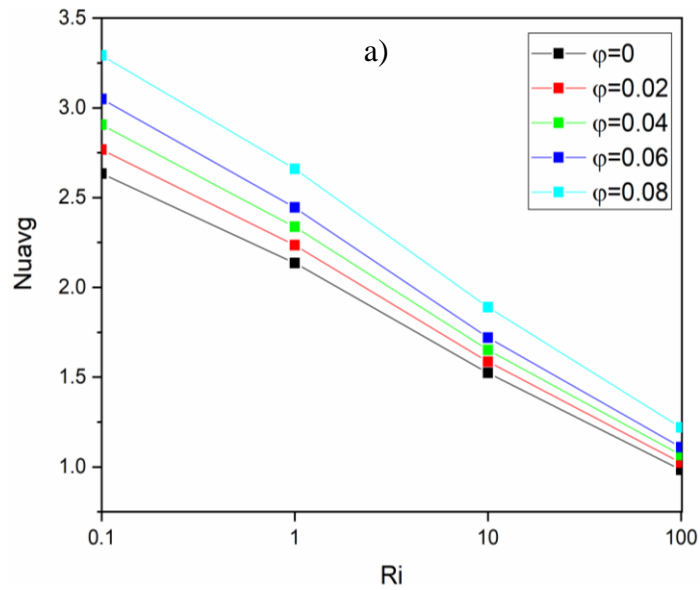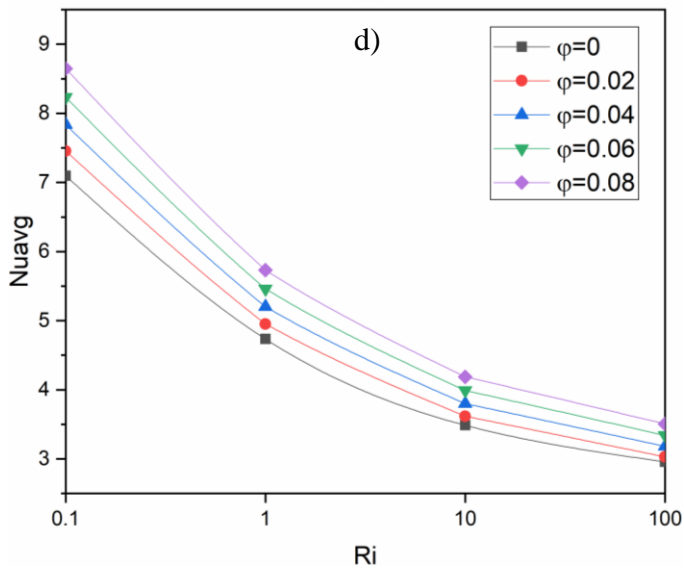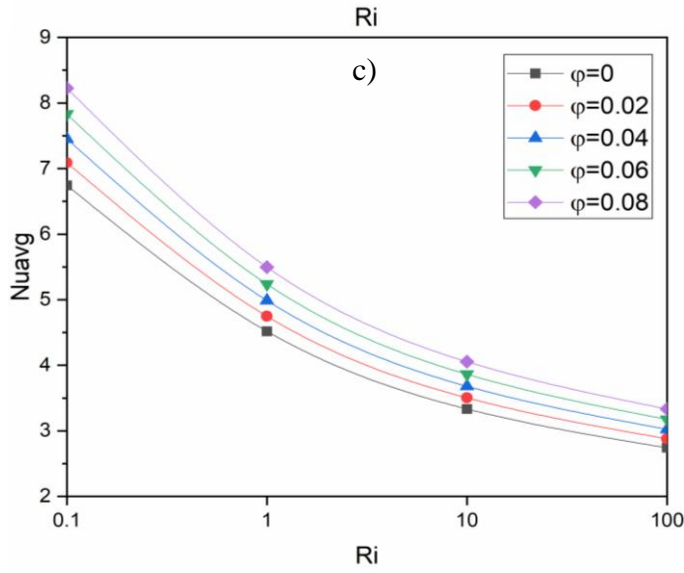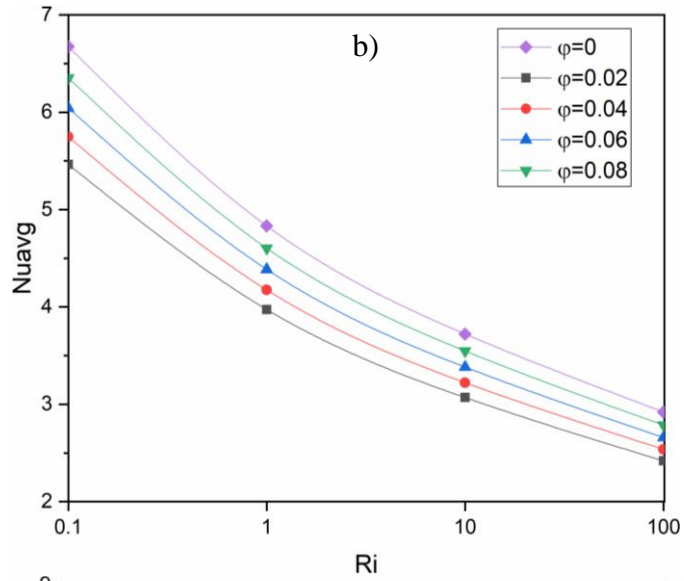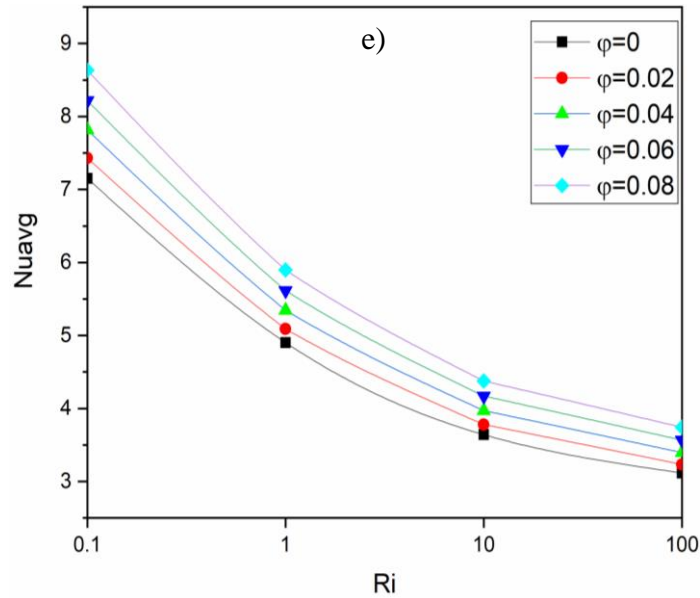
Figure IV.9: Average Nüsselt number at the bottom for various Aspect Ratio, (a) AR=0.25, (b) AR=0.5, (c) AR=0.75, (d) AR=1, (e) AR=2.

The difference can be observed between the pure fluid and the nanofluids, as the increase in the volume fraction of nanoparticles increases the thermal conductivity and thus increases the average Nüsselt number, which is inversely related to the Ri. This is due to the high speed of the moving vertical walls and, therefore, higher shear strength.

IV.5.2. Influence of Aspect Ratio on the average Nüsselt number

Figure IV.10 allows us to better compare Nu_{avg} with AR for each Ri.

a)
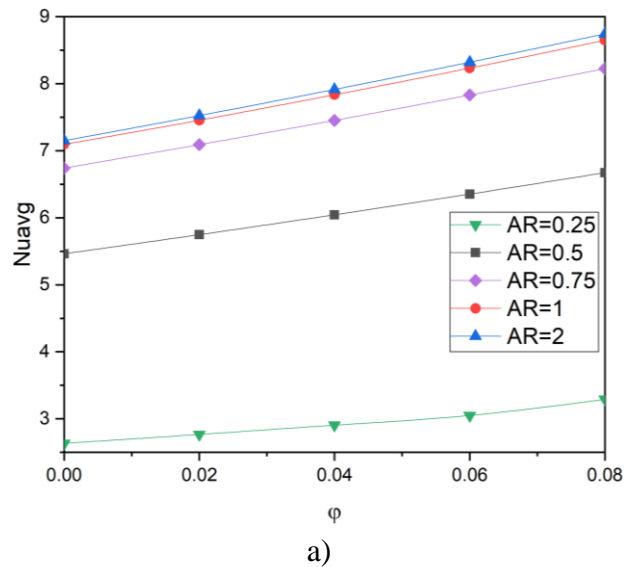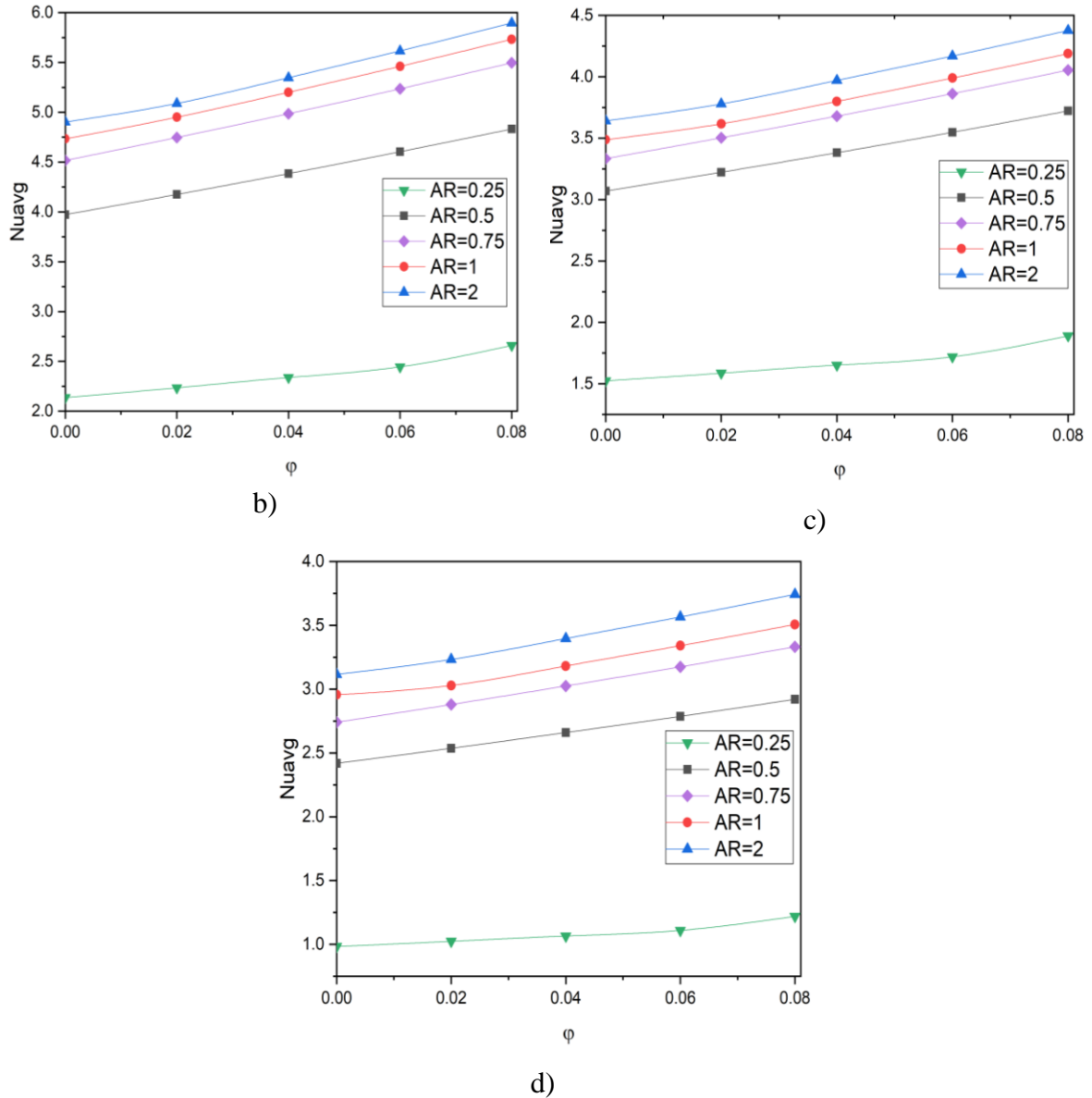
Figure IV.10: Average Nüsselt number at the bottom for various Richardson numbers, (a) Ri=0.1, (b) Ri=1, (c) Ri=10, (d) Ri=100.

We can notice that the rise in the volume fraction nanoparticles increases the rate of heat transfer and also with the increase in the Aspect Ratio the Nu_{avg} number increases; that is, the maximum heat transfer occurs at AR = 2 and minimum at AR = 0.25.

IV.5.3. Influence of nanoparticles on the average Nüsselt number

Figure IV.11.a shows the average Nüsselt number at Ri=0.1, AR=1 and Gr=10^4 for different (φ) and nanoparticles with cylindrical form.

a)

b)
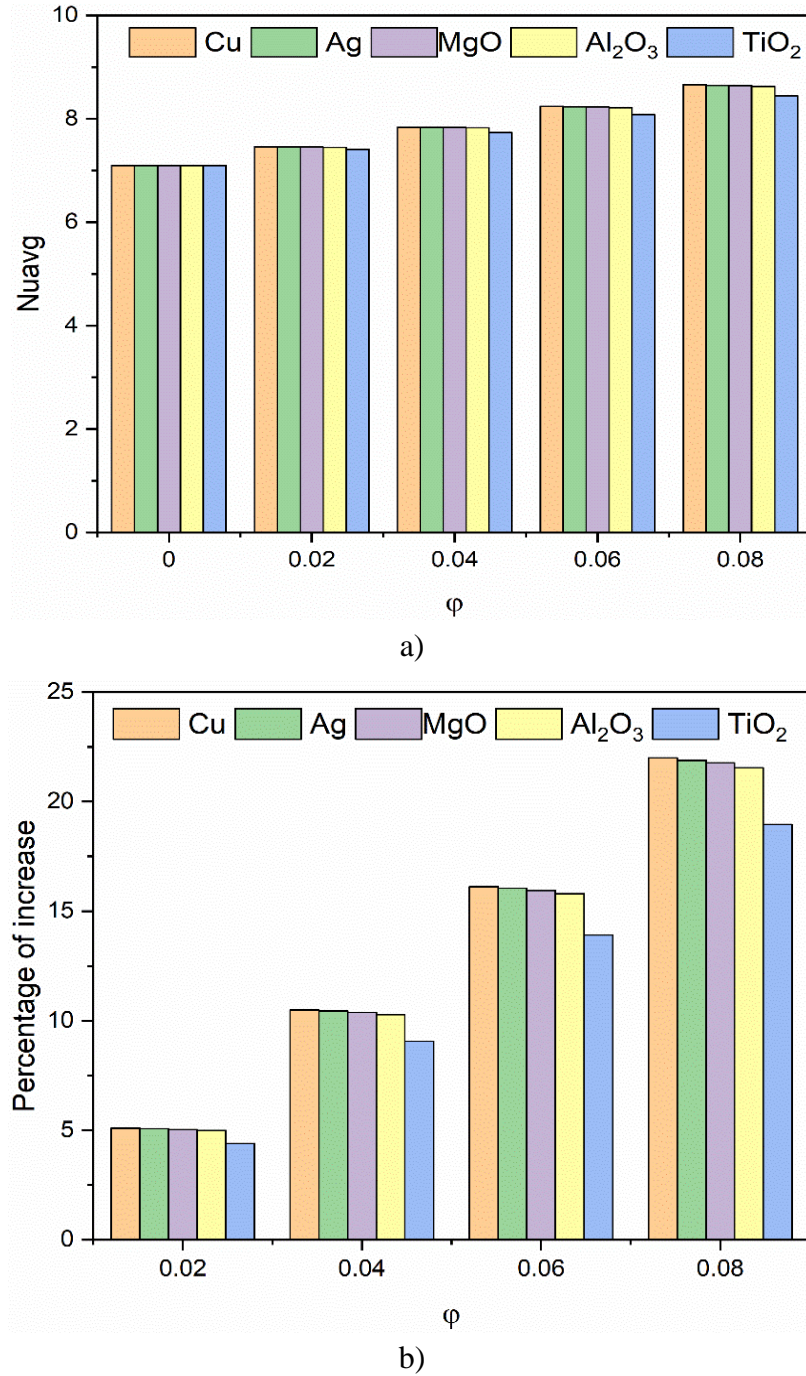
Figure IV.11: Average Nüsselt number at the bottom for various nanoparticles at Ri=0.1 and AR=1, (a) average Nüsselt number, (b) percentage of increase.

Figure IV.11.b reports the percentage of increase of all nanoparticles in heat transfer. The average Nüsselt number is greatest for copper nanoparticles and least for titanium oxide nanoparticles; this reason is due to the thermophysical properties of all particles. In addition, the nanoparticles

composed of titanium oxide TiO_2 had the lowest heat transfer rate where the ratio was close to the transfer of nanoparticles copper Cu and silver Ag.

IV.5.4. Effect of base fluid on the average Nüsselt number

Figure IV.12.a shows the average Nüsselt number for (Ag-H_2O/EG) nanofluid for different (φ) and Ri at AR = 1 and Gr = 10^4; as the average Nüsselt number increases with increasing (φ) and decreases with increasing Ri. Figure IV.12.b represents the average Nüsselt number for two nanofluids (Ag-H_2O/EG) and (ag-H_2O) for Ri = 0.1 and AR = 1; it appears from the figure that the nanofluid (Ag-H_2O/EG) increased in the heat transfer rate compared to the Ag-H_2O nanofluid, and this is due to the basic physical properties of the first nanofluid.

a)   b)
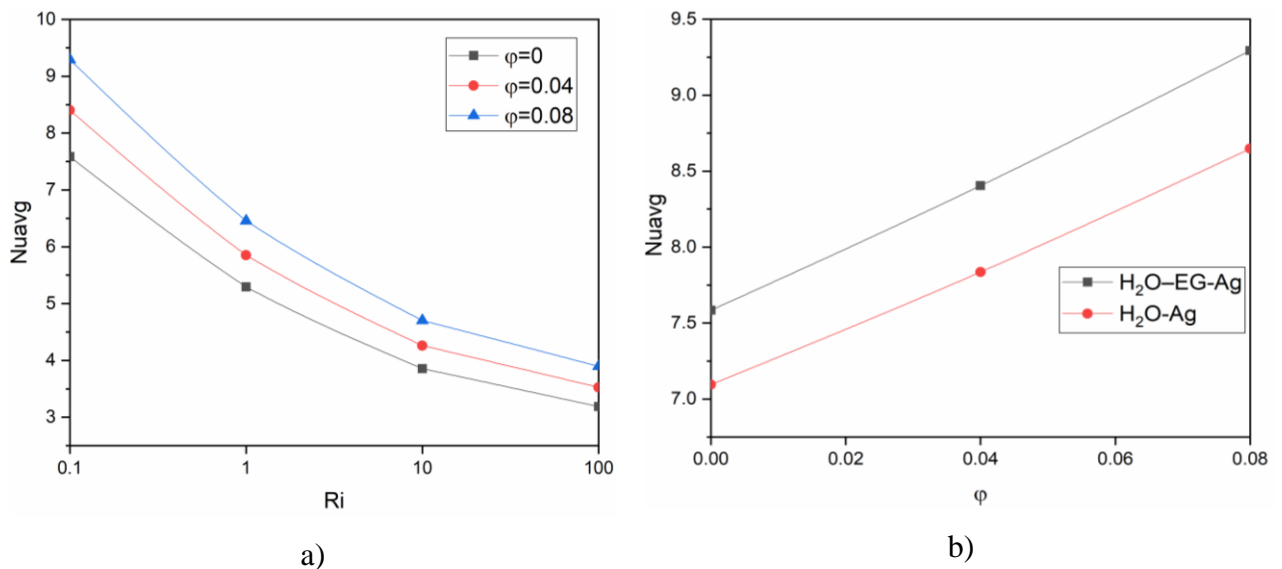
Figure IV.12: Average Nüsselt number at the bottom for various nanofluid at AR=1, (a) average Nüsselt number for (H_2O/EG-Ag), (b) comparison of the Nüsselt number of nanofluid H_2O/EG-Ag and nanofluid (H_2O-Ag).

IV.5.5. Effect of Grashof number on the average Nüsselt number

Figure IV.13 shows the effect of the Grashof number on the average Nüsselt number for Ag-H_2O nanofluid and different Richardson numbers at AR = 1 and φ = 0.04. It can be seen from the figure that the average Nüsselt number increases with the increase in the Grashof number, and this reason is due to the increase in the acceleration of the movement of the nanofluid and thus the increase in the transfer of natural convection.
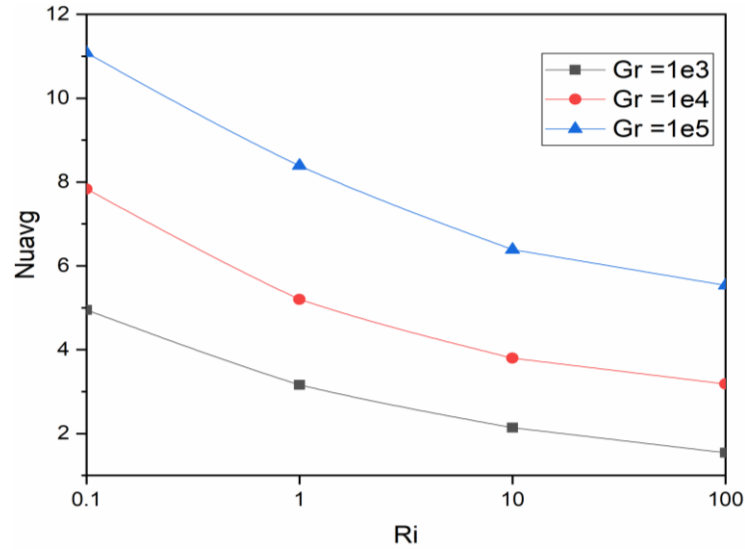
Figure IV.13: Average Nüsselt number at the bottom wall for various Gr at AR=1 and φ=0.04.

IV.5.6. Effect of sinusoidal thermal amplitude on the average Nüsselt number

The following figure shows the average Nüsselt number for different thermal sinusoidal amplitudes and Richardson numbers at AR = 1, φ = 0.04 and Gr = 10^4.
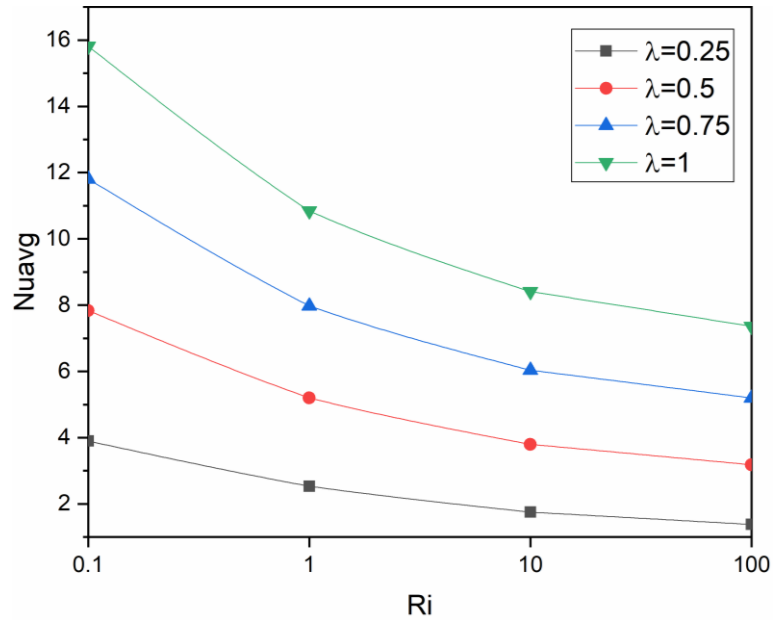
Figure IV.14: Average Nüsselt number at the bottom wall for various thermal sinusoidal amplitudes at AR=1, φ=0.04 and Gr=10^4.

The average Nüsselt number increases with an increase in thermal sinusoidal amplitudes due to an increase in the hot temperature of the bottom wall.

IV.5.7. Effect of direction of velocity in double-lid driven on the average Nüsselt number

The following figure shows the average Nüsselt number for the direction of double-lid driven in the cavity for different (φ) at Ri = 0.1, AR = 1 and Gr = 10^4. Where it is noted from the figure that the average Nüsselt number increases with the movement of the vertical walls downward and this is due to the fluid flow with Archimedes force
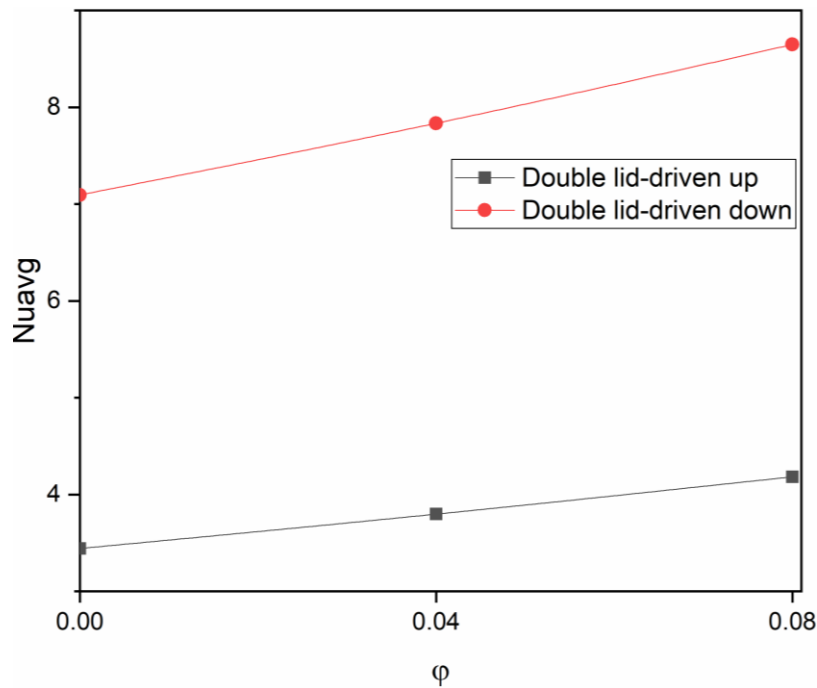
Figure IV.15: Average Nüsselt number at the bottom wall for direction of velocity in double-lid driven at Ri=0.1, AR=1 and Gr=10^4.

IV.6. Conclusion

This chapter deals with numerical simulations for various Aspect Ratios, volume fractions of nanoparticles, nanofluids, Richardson numbers, Grashof numbers, and thermal amplitudes. Initially, a study was presented for the stability of the mesh; this last was considered stable if the residuals of the governing equations converged to a small value. Then, results validation with

previous literature was performed. This helped to ensure that the numerical simulations were accurate and reliable.

The effect of streamlines and temperature profiles inside the cavity was also clarified to visualize the flow and heat transfer. It was found that the addition of nanoparticles in the base fluid improves heat transfer, and that copper nanoparticles have relatively the highest heat transfer rate. Also, the Aspect Ratio plays an important role in heat transfer to reduce energy consumption. The results can be used to design and optimize heat transfer systems.
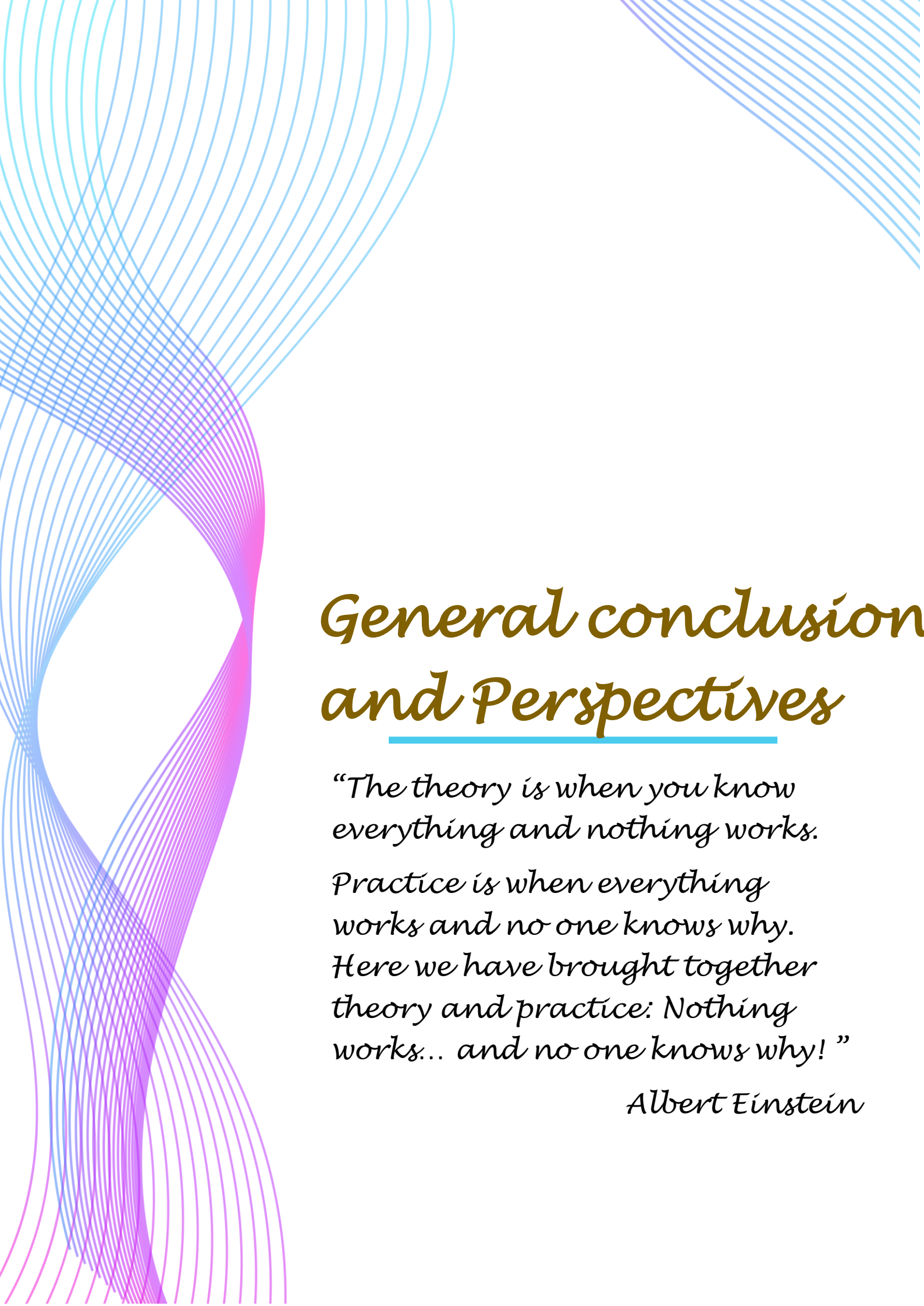
General conclusion and Perspectives

"The theory is when you know everything and nothing works.

Practice is when everything works and no one knows why. Here we have brought together theory and practice: Nothing works… and no one knows why!"

Albert Einstein
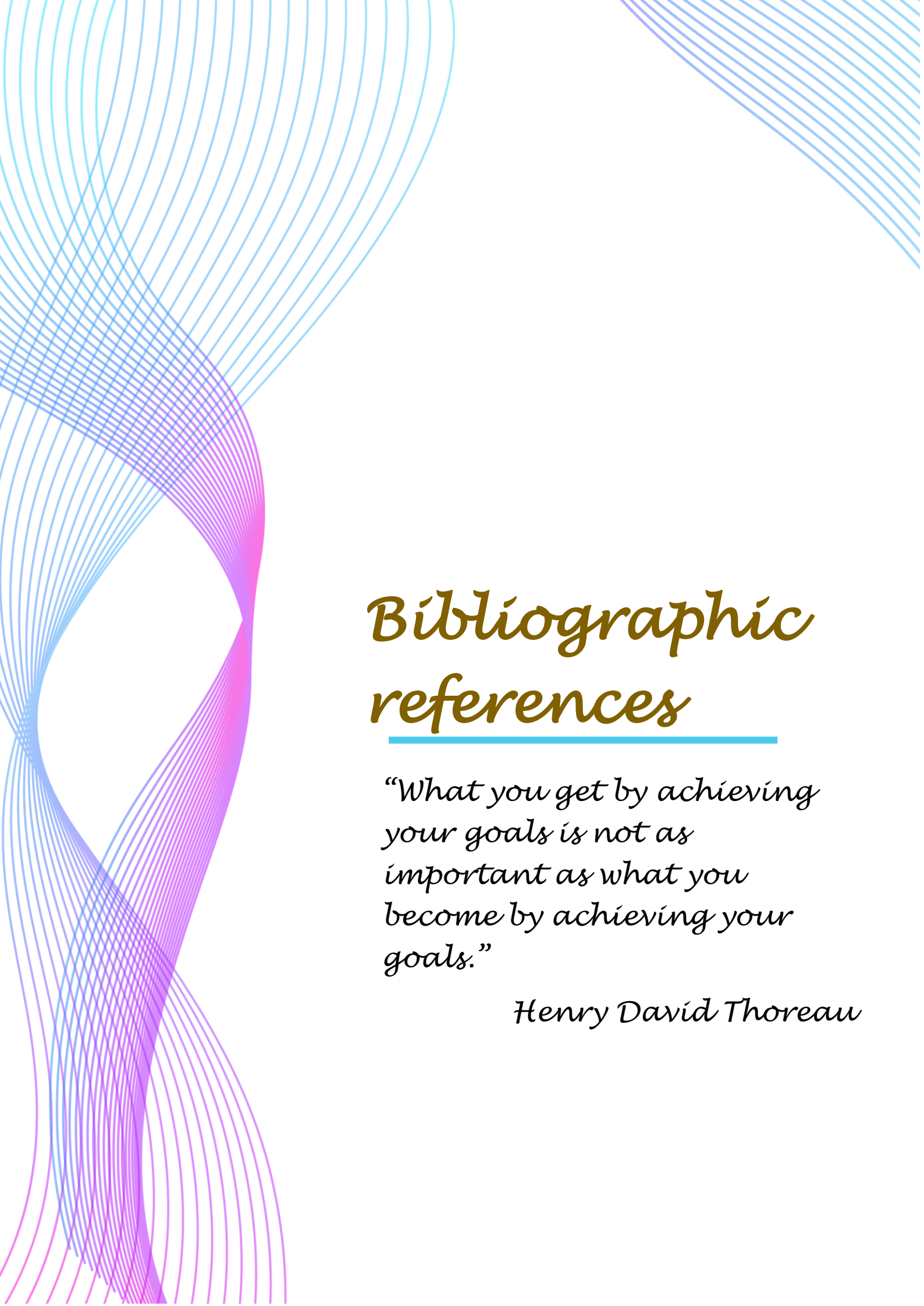
Bibliographic references

"What you get by achieving your goals is not as important as what you become by achieving your goals."

Henry David Thoreau

1. Okonkwo, E.C., et al., *An updated review of nanofluids in various heat transfer devices.* Journal of Thermal Analysis and Calorimetry, 2021. **145**(6): p. 2817-2872.
2. Choi, S.U. and J.A. Eastman, *Enhancing thermal conductivity of fluids with nanoparticles*. 1995, Argonne National Lab., IL (United States).
3. Choi, S., et al., *Anomalous thermal conductivity enhancement in nanotube suspensions.* Applied physics letters, 2001. **79**(14): p. 2252-2254.
4. Eastman, J.A., et al., *Anomalously increased effective thermal conductivities of ethylene glycol-based nanofluids containing copper nanoparticles.* Applied physics letters, 2001. **78**(6): p. 718-720.
5. Sundar, L.S., et al., *Thermal conductivity and viscosity of stabilized ethylene glycol and water mixture Al2O3 nanofluids for heat transfer applications: An experimental study.* International Communications in Heat and Mass Transfer, 2014. **56**: p. 86-95.
6. Esfe, M.H., et al., *Experimental evaluation, new correlation proposing and ANN modeling of thermal properties of EG based hybrid nanofluid containing ZnO-DWCNT nanoparticles for internal combustion engines applications.* Applied Thermal Engineering, 2018. **133**: p. 452-463.
7. Hemmat Esfe, M., S. Esfandeh, and M. Rejvani, *Modeling of thermal conductivity of MWCNT-SiO2 (30: 70%)/EG hybrid nanofluid, sensitivity analyzing and cost performance for industrial applications.* Journal of Thermal Analysis and Calorimetry, 2018. **131**(2): p. 1437-1447.
8. Esfe, M.H., et al., *Development of a new correlation and post processing of heat transfer coefficient and pressure drop of functionalized COOH MWCNT nanofluid by artificial neural network.* Current Nanoscience, 2018. **14**(2): p. 104-112.
9. Esfe, M.H., A. Alirezaie, and M. Rejvani, *TTTd alterations gradient of thermal conductivity increases with the rise of volume fraction of up to 1%, and emmmy then, the sensitivity decreases. Generally, the current study is a combination of empirical studies along.* Appl Therm Eng, 2017. **111**: p. 1202-1210.
10. Rostamian, S.H., et al., *An inspection of thermal conductivity of CuO-SWCNTs hybrid nanofluid versus temperature and concentration using experimental data, ANN modeling and new correlation.* Journal of Molecular Liquids, 2017. **231**: p. 364-369.
11. Alirezaie, A., et al., *Price-performance evaluation of thermal conductivity enhancement of nanofluids with different particle sizes.* Applied Thermal Engineering, 2018. **128**: p. 373-380.
12. Hemmat Esfe, M., et al., *ANN modeling, cost performance and sensitivity analyzing of thermal conductivity of DWCNT–SiO2/EG hybrid nanofluid for higher heat transfer.* Journal of Thermal Analysis and Calorimetry, 2018. **131**(3): p. 2381-2393.
13. Esfe, M.H., M.K. Amiri, and A. Alirezaie, *Thermal conductivity of a hybrid nanofluid.* J Therm Anal Calorim, 2018. **134**(2): p. 1113-1122.
14. Mekroussi, S., et al., *Mixed convection in complicated cavity with non-uniform heating on both sidewalls.* Int J Heat Technol, 2017. **35**(4): p. 1023-1033.
15. Mekroussi, S., et al., *Analysis of mixed convection in an inclined lid-driven cavity with a wavy wall.* Journal of Mechanical Science and Technology, 2013. **27**(7): p. 2181-2190.
16. Kadari, A., N.-E. Sad Chemloul, and S. Mekroussi, *Numerical Investigation of Laminar Natural Convection in a Square Cavity With Wavy Wall and Horizontal Fin Attached to the Hot Wall.* Journal of Heat Transfer, 2018. **140**(7).
17. Sheikholeslami, M., et al., *Numerical mesoscopic method for transportation of H2O-based nanofluid through a porous channel considering Lorentz forces.* International Journal of Modern Physics C, 2019. **30**(02n03): p. 1950007.

18. Guan, Q., et al., *Modeling of nanofluid-fluid two-phase flow and heat transfer.* International Journal of Computational Methods, 2018. **15**(08): p. 1850072.

19. Ghalambaz, M., et al., *Thermal energy storage optimization using composite foam-nano enhanced phase change materials.* Journal of Energy Storage, 2023. **63**: p. 107001.

20. Biswas, N., et al., *Hybridized nanofluidic convection in umbrella-shaped porous thermal systems with identical heating and cooling surfaces.* International Journal of Numerical Methods for Heat & Fluid Flow, 2023.

21. Tian, C., et al., *Experimental study on mixed convection in an asymmetrically heated, inclined, narrow, rectangular channel.* International Journal of Heat and Mass Transfer, 2018. **116**: p. 1074-1084.

22. Szabo, P.S. and W.-G. Früh, *The transition from natural convection to thermomagnetic convection of a magnetic fluid in a non-uniform magnetic field.* Journal of Magnetism and Magnetic Materials, 2018. **447**: p. 116-123.

23. Miroshnichenko, I. and M. Sheremet, *Turbulent natural convection heat transfer in rectangular enclosures using experimental and numerical approaches: A review.* Renewable and Sustainable Energy Reviews, 2018. **82**: p. 40-59.

24. Bianco, V., F. Scarpa, and L.A. Tagliafico, *Numerical analysis of the Al2O3-water nanofluid forced laminar convection in an asymmetric heated channel for application in flat plate PV/T collector.* Renewable Energy, 2018. **116**: p. 9-21.

25. Saleh, M.S., et al., *A numerical investigation of the effect of sinusoidal temperature on mixed convection flow in a cavity filled with a nanofluid with moving vertical walls.* Heat Transfer.

26. Saleh, M.S., et al., *Effect of rotating cylinder on nanofluid heat transfer in a bifurcating grooved channel equipped with porous layers.* International Journal of Modern Physics B, 2023: p. 2350289.

27. Chadi, K., et al., *Impact of geometric shape of cavity on heat exchange using Cu-Al2O3-H2O hybrid nanofluid.* Waves in Random and Complex Media, 2022: p. 1-18.

28. Hachichi, F., et al., *Obstacle's effects and their location inside the square cavity on the thermal performance of Cu–Al2O3/H2O hybrid nanofluid.* Heat Transfer.

29. Beldjani, C., et al., *Efficiency improvement of air-cooled photovoltaic modules utilizing copper heat dissipators.* DESALINATION AND WATER TREATMENT, 2022. **279**: p. 140-146.

30. MEKROUSSI, S., *Simulation du transfert convectif dans une couche limite turbulente en présence d'obstacle décollé de la paroi*. 2008, Tiaret.

31. Saidi, L., et al., *A Numerical Investigation of the Free Flow in a Square Porous Cavity with Non-Uniform Heating on the Lower Wall.* Engineering, Technology & Applied Science Research, 2022. **12**(1): p. 7982-7987.

32. Sheremet, M.A. and I. Pop, *Mixed convection in a lid-driven square cavity filled by a nanofluid: Buongiorno's mathematical model.* Applied Mathematics and Computation, 2015. **266**: p. 792-808.

33. Öztop, H.F., et al., *Mixed convection of MHD flow in nanofluid filled and partially heated wavy walled lid-driven enclosure.* International Communications in Heat and Mass Transfer, 2017. **86**: p. 42-51.

34. Billah, M., et al., *Unsteady buoyancy-driven heat transfer enhancement of nanofluids in an inclined triangular enclosure.* International communications in heat and mass transfer, 2013. **49**: p. 115-127.

35. Ghasemi, B. and S. Aminossadati, *Mixed convection in a lid-driven triangular enclosure filled with nanofluids.* International Communications in Heat and Mass Transfer, 2010. **37**(8): p. 1142-1148.

36. Sheikholeslami, M. and A.J. Chamkha, *Flow and convective heat transfer of a ferro-nanofluid in a double-sided lid-driven cavity with a wavy wall in the presence of a variable magnetic field.* Numerical Heat Transfer, Part A: Applications, 2016. **69**(10): p. 1186-1200.

37. Mehrali, M., et al., *Heat transfer and entropy generation analysis of hybrid graphene/Fe3O4 ferro-nanofluid flow under the influence of a magnetic field.* Powder technology, 2017. **308**: p. 149-157.

38. Dehkordi, R.B., et al., *Molecular dynamics simulation of ferro-nanofluid flow in a microchannel in the presence of external electric field: Effects of Fe3O4 nanoparticles.* International Communications in Heat and Mass Transfer, 2020. **116**: p. 104653.

39. Gürdal, M., et al., *Numerical investigation on turbulent flow and heat transfer characteristics of ferro-nanofluid flowing in dimpled tube under magnetic field effect.* Applied Thermal Engineering, 2022. **200**: p. 117655.

40. Karthikeyan, S., A. Prathima, and M. Periyasamy, *Characteristics studies on Stoechospermum marginatum, brown marine algae with Al2O3 nanofluid.* Materials Today: Proceedings, 2020. **33**: p. 3746-3750.

41. Duan, Z., et al., *Milling force and surface morphology of 45 steel under different Al2O3 nanofluid concentrations.* The International Journal of Advanced Manufacturing Technology, 2020. **107**(3): p. 1277-1296.

42. Bozorg, M.V., et al., *CFD study of heat transfer and fluid flow in a parabolic trough solar receiver with internal annular porous structure and synthetic oil–Al2O3 nanofluid.* Renewable Energy, 2020. **145**: p. 2598-2614.

43. Sharafeldin, M., et al., *Evacuated tube solar collector performance using copper nanofluid: Energy and environmental analysis.* Applied Thermal Engineering, 2019. **162**: p. 114205.

44. Yan, S.-R., et al., *Molecular dynamics simulation of Water-Copper nanofluid flow in a three-dimensional nanochannel with different types of surface roughness geometry for energy economic management.* Journal of Molecular Liquids, 2020. **311**: p. 113222.

45. Abu-Hamdeh, N.H., et al., *The thermal properties of water-copper nanofluid in the presence of surfactant molecules using molecular dynamics simulation.* Journal of Molecular Liquids, 2021. **325**: p. 115149.

46. Toghraie, D., et al., *Molecular dynamics simulation of Couette and Poiseuille Water-Copper nanofluid flows in rough and smooth nanochannels with different roughness configurations.* Chemical Physics, 2019. **527**: p. 110505.

47. Kumar, R., et al., *Influence of Al2O3 and TiO2 nanofluid on hard turning performance.* The International Journal of Advanced Manufacturing Technology, 2020. **106**(5): p. 2265-2280.

48. Sreedevi, P., P.S. Reddy, and M. Sheremet, *A comparative study of Al2O3 and TiO2 nanofluid flow over a wedge with non-linear thermal radiation.* International Journal of Numerical Methods for Heat & Fluid Flow, 2019.

49. Du, S., J. Sun, and P. Wu, *Preparation, characterization and lubrication performances of graphene oxide-TiO2 nanofluid in rolling strips.* Carbon, 2018. **140**: p. 338-351.

50. Zhang, C., et al., *Optimization of the electricity/heat production of a PV/T system based on spectral splitting with Ag nanofluid.* Renewable Energy, 2021. **180**: p. 30-39.

51. Mir, S., et al., *A comprehensive study of two-phase flow and heat transfer of water/Ag nanofluid in an elliptical curved minichannel.* Chinese Journal of Chemical Engineering, 2020. **28**(2): p. 383-402.

52. Rozati, S.A., et al., *Natural convection heat transfer of water/Ag nanofluid inside an elliptical enclosure with different attack angles.* Mathematical Methods in the Applied Sciences, 2020.

53.   Tong, Y., et al., *Energy and exergy comparison of a flat-plate solar collector using water, Al2O3 nanofluid, and CuO nanofluid.* Applied Thermal Engineering, 2019. **159**: p. 113959.

54.   Shang, Y., et al., *The computational study of microchannel thickness effects on H2O/CuO nanofluid flow with molecular dynamics simulations.* Journal of Molecular Liquids, 2022. **345**: p. 118240.

55.   Toghraie, D., et al., *The effect of using water/CuO nanofluid and L-shaped porous ribs on the performance evaluation criterion of microchannels.* Journal of Thermal Analysis and Calorimetry, 2019. **135**(1): p. 145-159.

56.   Arefmanesh, A. and M. Mahmoodi, *Effects of uncertainties of viscosity models for Al2O3–water nanofluid on mixed convection numerical simulations.* International journal of Thermal sciences, 2011. **50**(9): p. 1706-1719.

57.   Rosdzimin, A., S. Zuhairi, and C. Azwadi, *Simulation of mixed convective heat transfer using lattice Boltzmann method.* Int. J. of Automotive and Mechanical Engineering, 2010. **2**: p. 130-143.

58.   Nemati, H., et al., *Lattice Boltzmann simulation of nanofluid in lid-driven cavity.* International Communications in Heat and Mass Transfer, 2010. **37**(10): p. 1528-1534.

59.   Sheikhzadeh, G., et al., *Numerical study of mixed convection flows in a lid-driven enclosure filled with nanofluid using variable properties.* Results in Physics, 2012. **2**: p. 5-13.

60.   Boutra, A., K. Ragui, and Y.K. Benkahla, *Numerical study of mixed convection heat transfer in a lid-driven cavity filled with a nanofluid.* Mechanics & Industry, 2015. **16**(5): p. 505.

61.   Öğüt, E.B. and K. Kahveci, *Mixed convection heat transfer of ethylene glycol and water mixture based Al2O3 nanofluids: effect of thermal conductivity models.* Journal of Molecular Liquids, 2016. **224**: p. 338-345.

62.   Boulahia, Z., A. Wakif, and R. Sehaqui, *Mixed convection heat transfer of Cu-water nanofluid in a lid driven square cavity with several heated triangular cylinders.* Int. J. Innov. Appl. Stud., 2016. **17**: p. 82-89.

63.   Mastiani, M., M.M. Kim, and A. Nematollahi, *Density maximum effects on mixed convection in a square lid-driven enclosure filled with Cu-water nanofluids.* Advanced Powder Technology, 2017. **28**(1): p. 197-214.

64.   Zeghbid, I. and R. Bessaïh, *Mixed convection in a lid-driven square cavity with heat sources using nanofluids.* Fluid Dynamics & Materials Processing, 13 (4), 2017: p. 251-273.

65.   Munshi, M.J.H., N. Jahan, and G. Mostafa, *Mixed convection heat transfer of nanofluid in a lid-driven porous medium square enclosure with pairs of heat source-sinks.* American Journal of Engineering Research (AJER), 2019. **8**(6): p. 59-70.

66.   Serna, J., F. Velasco, and A.S. Meca, *Application of network simulation method to viscous flows: The nanofluid heated lid cavity under pulsating flow.* Computers & Fluids, 2014. **91**: p. 10-20.

67.   Talebi, F., A.H. Mahmoudi, and M. Shahi, *Numerical study of mixed convection flows in a square lid-driven cavity utilizing nanofluid.* International Communications in Heat and Mass Transfer, 2010. **37**(1): p. 79-90.

68.   Sebdani, S.M., M. Mahmoodi, and S.M. Hashemi, *Effect of nanofluid variable properties on mixed convection in a square cavity.* International Journal of Thermal Sciences, 2012. **52**: p. 112-126.

69.   Chamkha, A.J. and E. Abu-Nada, *Mixed convection flow in single-and double-lid driven square cavities filled with water–Al2O3 nanofluid: Effect of viscosity models.* European Journal of Mechanics-B/Fluids, 2012. **36**: p. 82-96.

70. Mansour, M., et al., *Numerical simulation of mixed convection flows in a square lid-driven cavity partially heated from below using nanofluid.* International Communications in Heat and Mass Transfer, 2010. **37**(10): p. 1504-1512.

71. Shahi, M., A.H. Mahmoudi, and F. Talebi, *Numerical study of mixed convective cooling in a square cavity ventilated and partially heated from the below utilizing nanofluid.* International Communications in Heat and Mass Transfer, 2010. **37**(2): p. 201-213.

72. Garoosi, F., S. Garoosi, and K. Hooman, *Numerical simulation of natural convection and mixed convection of the nanofluid in a square cavity using Buongiorno model.* Powder technology, 2014. **268**: p. 279-292.

73. Hajialigol, N., et al., *Laminar mixed convection of Cu-water nano-fluid in two-sided lid-driven enclosures.* Journal of Nanostructures, 2011. **1**(1): p. 44-53.

74. Said, Z., H. Mohammed, and R. Saidur, *Mixed convection heat transfer of nanofluids in a lid driven square cavity: a parametric study.* International Journal of Mechanical and Materials Engineering, 2013. **8**(1): p. 48-57.

75. Boulahia, Z., A. Wakif, and R. Sehaqui, *Numerical investigation of mixed convection heat transfer of nanofluid in a lid driven square cavity with three triangular heating blocks.* International Journal of Computer Applications, 2016. **143**(6): p. 37-45.

76. Rahman, M., R. Nasrin, and M. Hoque, *Heat-mass transfer of nanofluid in lid-driven enclosure under three convective modes.* GANIT: Journal of Bangladesh Mathematical Society, 2018. **38**: p. 73-83.

77. Selimefendigil, F. and H.F. Öztop, *Mixed convection of nanofluid filled cavity with oscillating lid under the influence of an inclined magnetic field.* Journal of the Taiwan Institute of Chemical Engineers, 2016. **63**: p. 202-215.

78. Oztop, H.F. and I. Dagtekin, *Mixed convection in two-sided lid-driven differentially heated square cavity.* International Journal of Heat and mass transfer, 2004. **47**(8-9): p. 1761-1769.

79. Sharma, B., B. Kumar, and R.N. Barman, *Numerical investigation of Cu-water nanofluid in a differentially heated square cavity with conducting solid square cylinder at center.* Journal homepage: http://iieta. org/Journals/IJHT, 2018. **36**(2): p. 714-722.

80. Bora, M.K., et al., *Numerical investigation of Ag-H2O nanofluid in a lid driven square cavity with different shaped conducting and insulating cylinders placed at centre.* Journal homepage: http://iieta. org/journals/ijht, 2019. **37**(3): p. 831-838.

81. Muhammad, N., S. Nadeem, and A. Issakhov, *Finite volume method for mixed convection flow of Ag–ethylene glycol nanofluid flow in a cavity having thin central heater.* Physica A: Statistical Mechanics and its Applications, 2020. **537**: p. 122738.

82. Hussain, S., M. Jamal, and B.P. Geridonmez, *Impact of fins and inclined magnetic field in double lid-driven cavity with Cu–water nanofluid.* International Journal of Thermal Sciences, 2021. **161**: p. 106707.

83. Karim, A., et al., *Influence of the periodicity of sinusoidal boundary condition on the unsteady mixed convection within a square enclosure using an Ag–water nanofluid.* Energies, 2017. **10**(12): p. 2167.

84. Abbou, B., et al., *Effect of aspect ratio and nonuniform temperature on mixed convection in a double lid-driven cavity.* Numerical Heat Transfer, Part A: Applications, 2022: p. 1-11.

85. Abu-Nada, E. and A.J. Chamkha, *Mixed convection flow in a lid-driven inclined square enclosure filled with a nanofluid.* European Journal of Mechanics-B/Fluids, 2010. **29**(6): p. 472-482.

86.   Alinia, M., D. Ganji, and M. Gorji-Bandpy, *Numerical study of mixed convection in an inclined two sided lid driven cavity filled with nanofluid using two-phase mixture model.* International Communications in Heat and Mass Transfer, 2011. **38**(10): p. 1428-1435.

87.   Abbasian Arani, A., J. Amani, and M. Hemmat Esfeh, *Numerical simulation of mixed convection flows in a square double lid-driven cavity partially heated using nanofluid.* Journal of Nanostructures, 2012. **2**(3): p. 301-311.

88.   Fereidoon, A., et al., *Evaluation of mixed convection in inclined square lid-driven cavity filled with Al2O3/water nano-fluid.* Engineering Applications of Computational Fluid Mechanics, 2013. **7**(1): p. 55-65.

89.   Kefayati, G.R., *FDLBM simulation of mixed convection in a lid-driven cavity filled with non-Newtonian nanofluid in the presence of magnetic field.* International Journal of Thermal Sciences, 2015. **95**: p. 29-46.

90.   Jafari, M., et al., *Lattice Boltzmann simulation of mixed convection heat transfer in a corrugated wall cavity utilizing water-based nanofluids.* Heat Transfer—Asian Research, 2012. **41**(8): p. 649-665.

91.   Fattahi, E. and M. Jafari, *Effect of wavy wall on convection heat transfer of water-al2o3 nanofluid in a lid-driven cavity using lattice boltzmann method.* International Journal of Engineering, 2012. **25**(2): p. 165-176.

92.   Parvin, S., M. Alim, and N. Hossain, *Mixed convection in a lid-driven cavity using nanofluid: effect of physical parameters.* Eng e-Trans (ISSN 1823-6379), 2012. **7**(2): p. 86-95.

93.   Nasrin, R., M. Alim, and A.J. Chamkha, *Combined convection flow in triangular wavy chamber filled with water–CuO nanofluid: effect of viscosity models.* International Communications in Heat and Mass Transfer, 2012. **39**(8): p. 1226-1236.

94.   Saha, L.K., M.C. Somadder, and K.S. Uddin, *Mixed convection heat transfer in a lid driven cavity with wavy bottom surface.* American Journal of Applied Mathematics, 2013. **1**(5): p. 92-101.

95.   Garoosi, F., L. Jahanshaloo, and S. Garoosi, *Numerical simulation of mixed convection of the nanofluid in heat exchangers using a Buongiorno model.* Powder Technology, 2015. **269**: p. 296-311.

96.   Hemmat Esfe, M., M. Akbari, and A. Karimipour, *Mixed convection in a lid-driven cavity with an inside hot obstacle filled by an Al2O3–water nanofluid.* Journal of Applied Mechanics and Technical Physics, 2015. **56**(3): p. 443-453.

97.   Oztop, H.F., *Combined convection heat transfer in a porous lid-driven enclosure due to heater with finite length.* International Communications in Heat and Mass Transfer, 2006. **33**(6): p. 772-779.

98.   Elharfi, H., et al., *Mixed convection heat transfer for nanofluids in a lid-driven shallow rectangular cavity uniformly heated and cooled from the vertical sides: The cooperative case.* International Scholarly Research Notices, 2012. **2012**.

99.   Salahi, H., M.A. Sharif, and S. Rasouli, *Laminar mixed convective heat transfer in a shallow inclined lid-driven cavity filled with nanofluid.* Journal of Thermal Science and Engineering Applications, 2015. **7**(4).

100.   Karimipour, A., et al., *Mixed convection of copper–water nanofluid in a shallow inclined lid driven cavity using the lattice Boltzmann method.* Physica A: Statistical Mechanics and Its Applications, 2014. **402**: p. 150-168.

101.   Sheikhzadeh, G., M. Arbaban, and M. Mehrabian, *Laminar natural convection of Cu-water nanofluid in concentric annuli with radial fins attached to the inner cylinder.* Heat and Mass Transfer, 2013. **49**(3): p. 391-403.

102. Karimipour, A., et al., *Periodic mixed convection of a nanofluid in a cavity with top lid sinusoidal motion.* Proceedings of the Institution of Mechanical Engineers, Part C: Journal of Mechanical Engineering Science, 2011. **225**(9): p. 2149-2160.

103. Mahmoodi, M., *Mixed convection inside nanofluid filled rectangular enclosures with moving bottom wall.* Thermal science, 2011. **15**(3): p. 889-903.

104. Kefayati, G.R. and H. Tang, *MHD mixed convection of viscoplastic fluids in different aspect ratios of a lid-driven cavity using LBM.* International Journal of Heat and Mass Transfer, 2018. **124**: p. 344-367.

105. Bidgoli, R.M., et al., *Numerical simulation of mixed convection in two-sided lid driven shallow cavity subjected to nanofluid; impact of velocity ratio at specific richardson number.* Journal of Current Research in Science, 2013. **1**(6): p. 495.

106. Chatterjee, D., S.K. Gupta, and B. Mondal, *Mixed convective transport in a lid-driven cavity containing a nanofluid and a rotating circular cylinder at the center.* International Communications in Heat and Mass Transfer, 2014. **56**: p. 71-78.

107. Valizadeh Ardalan, M., et al., *Analysis of unsteady mixed convection of Cu–water nanofluid in an oscillatory, lid-driven enclosure using lattice Boltzmann method.* Journal of Thermal Analysis and Calorimetry, 2021. **145**(4): p. 2045-2061.

108. Kabir, M.H., M.J.H. Munshi, and N. Parveen. *Numerical study of MHD mixed convection heat transfer of nanofluid in a lid-driven porous rectangular cavity with three square heating blocks*. in *AIP Conference Proceedings*. 2019. AIP Publishing LLC.

109. Billah, M., M. Rahman, and U. Sharif, *Heat transfer enhancement of nanofluids in a lid-driven triangular enclosure having a discrete heater.* Procedia Engineering, 2013. **56**: p. 330-336.

110. Rahman, M., et al., *Numerical investigation of heat transfer enhancement of nanofluids in an inclined lid-driven triangular enclosure.* International communications in heat and mass transfer, 2011. **38**(10): p. 1360-1367.

111. Javaherdeh, K., M. Kalteh, and T. Azarbarzin, *Mixed Convection Heat Transfer of a Nanofluid in a Lid-Driven Triangular Enclosure with Triangular Heat Source.* Journal of Nanofluids, 2014. **3**(2): p. 172-180.

112. Rahman, M., et al., *Laminar mixed convection in inclined triangular enclosures filled with water based Cu nanofluid.* Industrial & engineering chemistry research, 2012. **51**(10): p. 4090-4100.

113. Selimefendigil, F. and H.F. Öztop, *Mixed convection in a partially heated triangular cavity filled with nanofluid having a partially flexible wall and internal heat generation.* Journal of the Taiwan Institute of Chemical Engineers, 2017. **70**: p. 168-178.

114. Zahan, I., R. Nasrin, and M. Alim, *Mixed convective hybrid nanofluid flow in lid-driven undulated cavity: effect of MHD and Joule heating.* Journal of Naval Architecture and Marine Engineering, 2019. **16**(2): p. 109-126.

115. Al-Rashed, A.A., et al., *Effect of a porous medium on flow and mixed convection heat transfer of nanofluids with variable properties in a trapezoidal enclosure.* Journal of Thermal Analysis and Calorimetry, 2020. **139**(1): p. 741-754.

116. Hasib, M.H., M.S. Hossen, and S. Saha, *Effect of tilt angle on pure mixed convection flow in trapezoidal cavities filled with water-Al2O3 nanofluid.* Procedia Engineering, 2015. **105**: p. 388-397.

117. Aghaei, A., et al., *Numerical study of magnetic field on mixed convection and entropy generation of nanofluid in a trapezoidal enclosure.* Journal of Magnetism and Magnetic Materials, 2016. **403**: p. 133-145.

118. Ahmed, S.E., et al., *MHD mixed convection in trapezoidal enclosures filled with micropolar nanofluids.* Nanoscience and Technology: An International Journal, 2018. **9**(4).

119. Cho, C.-C. and C.-L. Chen, *Mixed convection heat transfer performance of water-based nanofluids in lid-driven cavity with wavy surfaces.* International Journal of Thermal Sciences, 2013. **68**: p. 181-190.

120. Mansour, R.B., N. Galanis, and C. Nguyen, *Experimental study of mixed convection with water–Al2O3 nanofluid in inclined tube with uniform wall heat flux.* International Journal of Thermal Sciences, 2011. **50**(3): p. 403-410.

121. Momin, G.G., *Experimental investigation of mixed convection with water-Al2O3 & hybrid nanofluid in inclined tube for laminar flow.* Int. J. Sci. Technol. Res, 2013. **2**(12): p. 195-202.

122. Aberoumand, S. and A. Jafarimoghaddam, *Mixed convection heat transfer of nanofluids inside curved tubes: An experimental study.* Applied Thermal Engineering, 2016. **108**: p. 967-979.

123. Manay, E. and E. Mandev, *Experimental investigation of mixed convection heat transfer of nanofluids in a circular microchannel with different inclination angles.* Journal of Thermal Analysis and Calorimetry, 2019. **135**(2): p. 887-900.

124. Doroodmand, M., E. Goshtasbi Rad, and A. Rostamzadeh, *Experimental investigation of mixed convection heat transfer in vertical tubes by nanofluid: Effects of reynolds number and fluid temperature.* International Journal of Engineering, 2014. **27**(8): p. 1251-1258.

125. Abdulsahi, A. and K. Al-Farhany, *Experimental investigation of mixed convection on a rotating circular cylinder in a cavity filled with nanofluid and porous media.* Al-Qadisiyah Journal for Engineering Sciences, 2020. **13**(2): p. 99-108.

126. Otanicar, T.P., P.E. Phelan, and J.S. Golden, *Optical properties of liquids for direct absorption solar thermal energy systems.* Solar Energy, 2009. **83**(7): p. 969-977.

127. Wang, X.-Q. and A.S. Mujumdar, *Heat transfer characteristics of nanofluids: a review.* International journal of thermal sciences, 2007. **46**(1): p. 1-19.

128. Wang, X.-Q. and A.S. Mujumdar, *A review on nanofluids-part II: experiments and applications.* Brazilian Journal of Chemical Engineering, 2008. **25**: p. 631-648.

129. Yoo, D.-H., K. Hong, and H.-S. Yang, *Study of thermal conductivity of nanofluids for the application of heat transfer fluids.* Thermochimica Acta, 2007. **455**(1-2): p. 66-69.

130. Daniel, M.-C. and D. Astruc, *Gold nanoparticles: assembly, supramolecular chemistry, quantum-size-related properties, and applications toward biology, catalysis, and nanotechnology.* Chemical reviews, 2004. **104**(1): p. 293-346.

131. Chamsa-Ard, W., et al., *Nanofluid types, their synthesis, properties and incorporation in direct solar thermal collectors: A review.* Nanomaterials, 2017. **7**(6): p. 131.

132. Han, Z., *Nanofluids with enhanced thermal transport properties*. 2008.

133. Wang, Y., Z. Iqbal, and S. Mitra, *Rapid, low temperature microwave synthesis of novel carbon nanotube–silicon carbide composite.* Carbon, 2006. **44**(13): p. 2804-2808.

134. Kwon, Y.-K. and P. Kim, *Unusually high thermal conductivity in carbon nanotubes*, in *High Thermal Conductivity Materials*. 2006, Springer. p. 227-265.

135. Jana, S., A. Salehi-Khojin, and W.-H. Zhong, *Enhancement of fluid thermal conductivity by the addition of single and hybrid nano-additives.* Thermochimica acta, 2007. **462**(1-2): p. 45-55.

136. Kong, L., J. Sun, and Y. Bao, *Preparation, characterization and tribological mechanism of nanofluids.* Rsc Advances, 2017. **7**(21): p. 12599-12609.

137. Pop, E., V. Varshney, and A.K. Roy, *Thermal properties of graphene: Fundamentals and applications.* MRS bulletin, 2012. **37**(12): p. 1273-1281.

138. Mashali, F., et al., *Thermo-physical properties of diamond nanofluids: A review.* International Journal of Heat and Mass Transfer, 2019. **129**: p. 1123-1135.

139. Pak, B.C. and Y.I. Cho, *Hydrodynamic and heat transfer study of dispersed fluids with submicron metallic oxide particles.* Experimental Heat Transfer an International Journal, 1998. **11**(2): p. 151-170.

140. Heyhat, M., et al., *Experimental investigation of turbulent flow and convective heat transfer characteristics of alumina water nanofluids in fully developed flow regime.* International Communications in Heat and Mass Transfer, 2012. **39**(8): p. 1272-1278.

141. Ho, C., et al., *Natural convection heat transfer of alumina-water nanofluid in vertical square enclosures: an experimental study.* International Journal of Thermal Sciences, 2010. **49**(8): p. 1345-1353.

142. Teng, T.-P. and Y.-H. Hung, *Estimation and experimental study of the density and specific heat for alumina nanofluid.* Journal of Experimental Nanoscience, 2014. **9**(7): p. 707-718.

143. Vajjha, R., D. Das, and B. Mahagaonkar, *Density measurement of different nanofluids and their comparison with theory.* Petroleum Science and Technology, 2009. **27**(6): p. 612-624.

144. Khanafer, K. and K. Vafai, *A critical synthesis of thermophysical characteristics of nanofluids.* International journal of heat and mass transfer, 2011. **54**(19-20): p. 4410-4428.

145. Xuan, Y. and W. Roetzel, *Conceptions for heat transfer correlation of nanofluids.* International Journal of heat and Mass transfer, 2000. **43**(19): p. 3701-3707.

146. Bejan, A., *Convection heat transfer*. 2013: John wiley & sons.

147. Kim, J., Y.T. Kang, and C.K. Choi, *Analysis of convective instability and heat transfer characteristics of nanofluids.* Physics of fluids, 2004. **16**(7): p. 2395-2401.

148. Maxwell, J.C., *A treatise on electricity and magnetism*. Vol. 1. 1873: Clarendon press.

149. Hamilton, R.L. and O. Crosser, *Thermal conductivity of heterogeneous two-component systems.* Industrial & Engineering chemistry fundamentals, 1962. **1**(3): p. 187-191.

150. Yu, W. and S. Choi, *The role of interfacial layers in the enhanced thermal conductivity of nanofluids: a renovated Maxwell model.* Journal of nanoparticle research, 2003. **5**(1): p. 167-171.

151. Bruggeman, V.D., *Berechnung verschiedener physikalischer Konstanten von heterogenen Substanzen. I. Dielektrizitätskonstanten und Leitfähigkeiten der Mischkörper aus isotropen Substanzen.* Annalen der physik, 1935. **416**(7): p. 636-664.

152. Gupte, S.K., S.G. Advani, and P. Huq, *Role of micro-convection due to non-affine motion of particles in a mono-disperse suspension.* International journal of heat and mass transfer, 1995. **38**(16): p. 2945-2958.

153. Avsec, J. and M. Oblak, *The calculation of thermal conductivity, viscosity and thermodynamic properties for nanofluids on the basis of statistical nanomechanics.* International Journal of Heat and Mass Transfer, 2007. **50**(21-22): p. 4331-4341.

154. Evans, W., J. Fish, and P. Keblinski, *Role of Brownian motion hydrodynamics on nanofluid thermal conductivity.* Applied physics letters, 2006. **88**(9): p. 093116.

155. Pil Jang, S. and S.U. Choi, *Effects of various parameters on nanofluid thermal conductivity.* 2007.

156. Esfe, M.H., et al., *An experimental study on thermal conductivity of MgO nanoparticles suspended in a binary mixture of water and ethylene glycol.* International Communications in Heat and Mass Transfer, 2015. **67**: p. 173-175.

157. Li, X., et al., *Stability and enhanced thermal conductivity of ethylene glycol-based SiC nanofluids.* International Journal of Heat and Mass Transfer, 2015. **89**: p. 613-619.

158.   Patel, H.E., T. Sundararajan, and S.K. Das, *An experimental investigation into the thermal conductivity enhancement in oxide and metallic nanofluids.* Journal of Nanoparticle Research, 2010. **12**(3): p. 1015-1031.

159.   Chon, C.H., et al., *Empirical correlation finding the role of temperature and particle size for nanofluid (Al 2 O 3) thermal conductivity enhancement.* Applied Physics Letters, 2005. **87**(15): p. 153107.

160.   Paul, G., T. Pal, and I. Manna, *Thermo-physical property measurement of nano-gold dispersed water based nanofluids prepared by chemical precipitation technique.* Journal of colloid and interface science, 2010. **349**(1): p. 434-437.

161.   Simpson, S., et al., *Nanofluid thermal conductivity and effective parameters.* Applied Sciences, 2018. **9**(1): p. 87.

162.   Choi, S., et al., *Anomalous thermal conductivity enhancement in nanotube suspensions.* Applied physics letters, 2001. **79**(14): p. 2252-2254.

163.   Ali, F.M., et al., *The effect of volume fraction concentration on the thermal conductivity and thermal diffusivity of nanofluids: numerical and experimental.* Review of Scientific Instruments, 2010. **81**(7): p. 074901.

164.   Hemmat Esfe, M., et al., *Evaluation of thermal conductivity of COOH-functionalized MWCNTs/water via temperature and solid volume fraction by using experimental data and ANN methods.* Journal of Thermal Analysis and Calorimetry, 2015. **121**(3): p. 1273-1278.

165.   Kim, S.H., S.R. Choi, and D. Kim, *Thermal conductivity of metal-oxide nanofluids: particle size dependence and effect of laser irradiation.* 2007.

166.   Xie, H.-q., et al., *Thermal conductivity of suspensions containing nanosized SiC particles.* International Journal of Thermophysics, 2002. **23**(2): p. 571-580.

167.   Xie, H., et al., *Thermal conductivity enhancement of suspensions containing nanosized alumina particles.* Journal of applied physics, 2002. **91**(7): p. 4568-4572.

168.   Wang, X., X. Xu, and S.U. Choi, *Thermal conductivity of nanoparticle-fluid mixture.* Journal of thermophysics and heat transfer, 1999. **13**(4): p. 474-480.

169.   Agarwal, R., et al., *Synthesis, characterization, thermal conductivity and sensitity of CuO nanofluids.* Applied Thermal Engineering, 2016. **102**: p. 1024-1036.

170.   Chopkar, M., et al., *Effect of particle size on thermal conductivity of nanofluid.* Metallurgical and materials transactions A, 2008. **39**(7): p. 1535-1542.

171.   Al-Waeli, A.H., et al., *Influence of the base fluid on the thermo-physical properties of PV/T nanofluids with surfactant.* Case Studies in Thermal Engineering, 2019. **13**: p. 100340.

172.   Kumar Vandrangi, S., et al., *Effect of base fluids on thermo-physical properties of SiO2 nanofluids and development of new correlations.* Mathematical methods in the applied sciences, 2020.

173.   Maheshwary, P., C. Handa, and K. Nemade, *A comprehensive study of effect of concentration, particle size and particle shape on thermal conductivity of titania/water based nanofluid.* Applied Thermal Engineering, 2017. **119**: p. 79-88.

174.   Einstein, A., *Eine neue bestimmung der moleküldimensionen*. 1905, ETH Zurich.

175.   Brinkman, H.C., *The viscosity of concentrated suspensions and solutions.* The Journal of chemical physics, 1952. **20**(4): p. 571-571.

176.   Maiga, S.E.B., et al., *Heat transfer enhancement by using nanofluids in forced convection flows.* International journal of heat and fluid flow, 2005. **26**(4): p. 530-546.

177.   Hagen, K.D., *Heat transfer with applications*. 1999: Prentice Hall.

178. Nguyen, C., et al., *Temperature and particle-size dependent viscosity data for water-based nanofluids–hysteresis phenomenon.* International journal of heat and fluid flow, 2007. **28**(6): p. 1492-1506.

179. Oberbeck, A., *Über die Wärmeleitung der Flüssigkeiten bei Berücksichtigung der Strömungen infolge von Temperaturdifferenzen.* Annalen der Physik, 1879. **243**(6): p. 271-292.

180. Cengel, Y., *Heat Transfer A Practical Approach, WCB McGraw-Hill.* Ellison, New York, 2003: p. 609.

181. Matsson, J.E., *An introduction to ANSYS fluent 2021*. 2021: SDC Publications.

182. Fedala, D., *Simulation numérique des écoulements internes dans les turbomachines.* Cours du Laboratoire d'Energétique et de Mécanique des Fluides Interne ENSAM, CER de Paris, 2007.

183. Patankar, S.V., *Numerical heat transfer and fluid flow*. 2018: CRC press.

184. Patankar, V., *Numerical Heat Transfer and Fluid Flow, McGraw-Hill Book Company, New York.* 1980.

185. de Vahl Davis, G., *Natural convection of air in a square cavity: a bench mark numerical solution.* International Journal for numerical methods in fluids, 1983. **3**(3): p. 249-264.

186. Peng, Y., C. Shu, and Y. Chew, *A 3D incompressible thermal lattice Boltzmann model and its application to simulate natural convection in a cubic cavity.* Journal of Computational Physics, 2004. **193**(1): p. 260-274.

187. Bilgen, E., *Natural convection in cavities with a thin fin on the hot wall.* International Journal of Heat and Mass Transfer, 2005. **48**(17): p. 3493-3505.

188. Aly, A.M., *Natural convection of Al2O3-water nanofluid filled annulus between a wavy rectangle and a square cavity using Buongiorno's two-phase model.* ZAMM-Journal of Applied Mathematics and Mechanics/Zeitschrift für Angewandte Mathematik und Mechanik, 2020. **100**(9): p. e202000002.

189. Boudjeniba, B., et al., *Transition to chaotic natural convection of Cu-water nanofluid in an inclined square enclosure.* Int. J. Heat Technol, 2019. **37**(2): p. 413-422.

190. Iwatsu, R., J.M. Hyun, and K. Kuwahara, *Mixed convection in a driven cavity with a stable vertical temperature gradient.* International Journal of Heat and Mass Transfer, 1993. **36**(6): p. 1601-1608.

191. Khanafer, K.M., A.M. Al-Amiri, and I. Pop, *Numerical simulation of unsteady mixed convection in a driven cavity using an externally excited sliding lid.* European Journal of Mechanics-B/Fluids, 2007. **26**(5): p. 669-687.

192. Tiwari, R.K. and M.K. Das, *Heat transfer augmentation in a two-sided lid-driven differentially heated square cavity utilizing nanofluids.* International Journal of heat and Mass transfer, 2007. **50**(9-10): p. 2002-2018.

193. Waheed, M., *Mixed convective heat transfer in rectangular enclosures driven by a continuously moving horizontal plate.* International Journal of Heat and Mass Transfer, 2009. **52**(21-22): p. 5055-5063.

194. Gibanov, N.S., et al., *Mixed convection with entropy generation of nanofluid in a lid-driven cavity under the effects of a heat-conducting solid wall and vertical temperature gradient.* European Journal of Mechanics-B/Fluids, 2018. **70**: p. 148-159.

195. Cheng, T., *Characteristics of mixed convection heat transfer in a lid-driven square cavity with various Richardson and Prandtl numbers.* International Journal of Thermal Sciences, 2011. **50**(2): p. 197-205.

196. Khanafer, K.M. and A.J. Chamkha, *Mixed convection flow in a lid-driven enclosure filled with a fluid-saturated porous medium.* International Journal of Heat and Mass Transfer, 1999. **42**(13): p. 2465-2481.

Abstract:

In this thesis, a two-dimensional numerical simulation was performed to study mixed convection in a nanofluid-filled cavity where vertical walls move up and down at a uniform speed, and are kept at a lower temperature. The upper wall has been thermally insulated, and the lower wall is heated according to a sinusoidal evolution.

The Finite Volume Method was used to solve the governing equations of the phenomenon and the thermal conductivity of the nanofluid was calculated by applying Maxwell's model, and the effective dynamic viscosity was determined using the Brinkmann model.

The results were obtained following the modification of several parameters such as the Richardson number ($10^{-1} \sim 10^{2}$), the Aspect Ratio (0.25-2) of the cavity, Grashof number ($10^{3} \sim 10^{5}$), nanofluids with different volume fractions of nanoparticles (0-8%), and thermal amplitudes ranging from (0.25-1).

It was found from the obtained results that the addition of nanoparticles in the base fluid improves heat transfer, and that copper nanoparticles have relatively the highest heat transfer rate. Also, the Aspect Ratio plays an important role in heat transfer to reduce energy consumption.

Keywords: Mixed convection, Cavity, Nanofluid, Nanoparticles, FVM, CFD.

ملخص:

في هذه الأطروحة تم إجراء محاكاة عددية ثنائية الأبعاد لدراسة الحمل الحراري المختلط في تجويف تم ملؤه بالعديد من الموائع النانوية حيث كانت الجدران العمودية تتحرك من الاعلى إلى أسفل بسرعة موحدة ودرجة حرارة أقل، كما تم عزل الجدار العلوي حرارياً. اما الجدار السفلي تم تسخينه تفاضلياً.

تم إستخدام طريقة الحجم المحدود لحل المعادلات الحاكمة للظاهرة وتم حساب الموصلية الحرارية للمائع النانوي بإستخدام نموذج ماكسويل، كما تم حساب اللزوجة الديناميكة الفعالة عن طريق إستخدام نموذج برينكمان.

تم الحصول على النتائج اثر تغيير عدة معلمات مثل: عدد ريتشاردسون (10^{-1}-10^2)، نسبة العرض للارتفاع (0.25-2)، عدد غراشوف (10^3-10^5)، موائع نانوية بعدة أحجام للجسيمات (0-8%)، واتساع حراري يتراوح بين (0.25-1).

حيث تبين من النتائج التي تم الحصول عليها أن إضافة الجسيمات النانوية في المائع الأساسي يحسن من إنتقال الحرارة، كما أن الجسيمات النانوية النحاسية كان لها أعلى نسبة في نقل الحرارة. إن نسبة العرض للارتفاع تلعب دوراً مهما في نقل الحرارة ويمكن إستخدام الموائع النانوية للحد من إستهلاك الطاقة.

كلمات مفتاحية : حمل حراري مختلط، تجويف مربع، مائع نانوي، جسيمات نانوية، طريقة الحجم المحدود (FVM)، CFD.

Résumé :

Dans cette thèse, une simulation numérique bidimensionnelle a été réalisée pour étudier la convection mixte dans une cavité remplie de nanofluides où les parois verticales se déplacent de haut en bas à une vitesse uniforme, et sont maintenues à une température plus basse. La paroi supérieure a été isolée thermiquement, et la paroi inférieure est chauffée selon une évolution sinusoidale.

La Méthode des Volumes Finis a été utilisée pour résoudre les équations gouvernantes du phénomène et la conductivité thermique du nanofluide a été calculée en appliquant le modèle de Maxwell, et la viscosité dynamique effective a été déterminée à l'aide du modèle de Brinkmann.

Les résultats ont été obtenus suite à la modification de plusieurs paramètres tels que le nombre de Richardson (10^{-1}~10^2), le rapport d'aspect (0.25~2) de la cavité, le nombre de Grashof (10^3~10^5), les nanofluides avec différentes fractions volumiques de nanoparticules (0~8%), et les amplitudes thermiques allant de (0.25~1).

Il a été constaté à partir des résultats obtenus que l'ajout de nanoparticules dans le fluide de base améliore le transfert de chaleur, et que les nanoparticules de cuivre avaient relativement le taux de transfert de chaleur le plus élevé. Aussi, le rapport d'aspect joue un rôle important dans le transfert de chaleur pour réduire la consommation d'énergie.

Mots clés : Convection mixte, Cavité, Nanofluide, Nanoparticule, MVF, CFD.